Targeted, Genome-scale Overexpression in Proteobacteria

Authors

Amy B. Banta[1,2], Ashley N. Hall[1,2], Kevin S. Myers[2,3], Ryan D. Ward[1,2,4], Bryce C. Davis[1], Rodrigo A. Cuellar[5], Michael Place[2], Claire C. Freeh[1], Emily E. Bacon[1,5], and Jason M. Peters[1,2,6,7,8]

Affiliations

[1]Pharmaceutical Sciences Division, School of Pharmacy, University of Wisconsin-Madison, Madison, WI, USA. [2]DOE Great Lakes Bioenergy Research Center, University of Wisconsin-Madison, Madison, WI, USA. [3]Wisconsin Energy Institute, University of Wisconsin-Madison, Madison, WI, USA. [4]Laboratory of Genetics, University of Wisconsin-Madison, Madison, WI, USA. [5]Microbiology Doctoral Training Program, University of Wisconsin-Madison, Madison, WI, USA. [6]Department of Bacteriology, University of Wisconsin-Madison, Madison, WI, USA. [7]Department of Medical Microbiology and Immunology, University of Wisconsin-Madison, Madison, WI, USA. [8]Center for Genomic Science Innovation, University of Wisconsin-Madison, Madison, WI, USA. e-mail: jason.peters@wisc.edu

Abstract

Targeted, genome-scale gene perturbation screens using Clustered Regularly Interspaced Short Palindromic Repeats interference (CRISPRi) and activation (CRISPRa) have revolutionized eukaryotic genetics, advancing medical, industrial, and basic research. Although CRISPRi knockdowns have been broadly applied in bacteria, options for genome-scale gene overexpression face key limitations. Here, we develop a facile approach for genome-scale overexpression in bacteria we call, "CRISPRtOE" (CRISPR transposition and OverExpression). We first create a platform for comprehensive gene targeting using CRISPR-associated transposons (CAST) and show that transposition occurs at a higher frequency in non-transcribed DNA. We then demonstrate that CRISPRtOE can upregulate gene expression in Proteobacteria with medical and industrial relevance by integrating synthetic promoters of varying strength upstream of target genes. Finally, we employ CRISPRtOE screening at the genome-scale in the model bacterium *Escherichia coli* and the non-model biofuel producer *Zymomonas mobilis*, recovering known and novel antibiotic and engineering targets. We

envision that CRISPRtOE will be a valuable overexpression tool for antibiotic mode of action, industrial strain optimization, and gene function discovery in bacteria.

Importance

Systematic alteration of bacterial gene expression enables identification of genes relevant to diverse fields of study and practical applications. Although many targeted, genome-scale genetic tools exist for reducing or eliminating gene expression, there are few facile approaches for systematic gene overexpression in bacteria. Here, we develop a targeted overexpression approach for Proteobacteria of medical and industrial importance that precisely inserts strong promoters upstream of genes using CRISPR-associated transposons. We demonstrate that this approach can be used to systematically overexpress genes in both model (*Escherichia coli* K-12) and non-model (*Zymomonas mobilis*) Proteobacteria for the purpose of understanding antibiotic resistance mechanisms and improving strain resilience in biofuel production conditions, respectively.

Introduction

Overexpression (OE) studies have been invaluable for gene phenotyping in medical (1–3), industrial (4), and basic contexts (3, 5). When used at the genome-scale, OE enables systematic functional interrogation of genes that are normally cryptic under screening conditions, mimics natural resistance mechanisms, and complements loss of function approaches by identifying genes with opposite phenotypes when knocked down versus overexpressed (1, 6). Clustered Regularly Interspaced Short Palindromic Repeats activation (CRISPRa) has allowed routine, genome-scale overexpression screening in eukaryotes for drug synergy/antagonism (6) or sensitivity/resistance to toxic plant compounds that reduce bioproduct yields (7). For example, a recent screen in mammalian cells for genes that interact with the anti-cancer drug, rigosertib, leveraged genome-scale CRISPR interference (CRISPRi) knockdowns with CRISPRa OE to identify target pathways (1). OE has also enhanced strain optimization for industrial purposes, such as a genome-wide CRISPRa screen in in *Saccharomyces cerevisiae* for genes involved in resistance to the biofuel production stressor, furfural (7).

Existing genome-scale OE approaches in bacteria have key limitations. Classic OE approaches, such as random integration of promoter-containing transposons to overexpress downstream genes(8), are untargeted and require high-density transposon (Tn) libraries to

resolve phenotypic ambiguities caused by the effects of Tn insertion versus OE. Libraries of Open Reading Frames (ORFs) cloned into multi-copy plasmids (9) are technically targeted approaches, but are tedious and expensive to construct, limiting their utility in non-model bacteria. Further, the use of plasmids presents additional complications, such as the constant requirement for antibiotic selection for plasmid maintenance—complicating screens for antibiotic function—and copy number variation that increases experimental noise (10). Contemporary approaches have sought to mitigate these issues and make genome-scale OE more accessible. For instance, Trackable Multiplex Recombineering (TRMR) is a targeted approach that uses recombinase-aided DNA editing (recombineering) to insert barcoded promoters or ribosome binding variants upstream of genes to achieve OE (11, 12); however, use of this method at the genome-scale is restricted to bacteria with efficient recombineering systems. An innovative new OE technique, “Dub-seq,” uses random genomic fragments cloned into barcoded, multi-copy plasmids (13, 14). Dub-seq reduces upfront barriers to OE library construction, but at the cost of being untargeted, increasing the complication of downstream analysis, and sharing some downsides of other plasmid-based approaches. Moreover, the length of cloned genomic fragments dictates Dub-seq library screening results; smaller fragments may miss genes that only have phenotypes when co-expressed in operons (e.g., protein complex subunits) while longer fragments may make it more difficult to pinpoint individual genes responsible for the selected phenotype.

Although systematic CRISPRa screens are routinely used in eukaryotes (1–3), no genome-scale CRISPRa studies have been reported in bacteria, to our knowledge. CRISPRa in eukaryotes uses a catalytically inactive Cas9 protein (dCas9) and single guide RNAs (sgRNAs) to deliver activator proteins to promoter regions, facilitating activation by opening chromatin (15). In contrast, CRISPRa-based OE in bacteria requires direct interactions between activator proteins and RNA polymerase (RNAP) that dictate strict activator-RNAP spacing and orientation on DNA(16–19). Recent improvements to bacterial CRISPRa using dCas9 variants with reduced PAM stringency or engineered activator proteins (19) partially mitigated the spacing requirements and increased overall activation; however—even in these optimized systems—only 1/3 to 1/2 of targeted endogenous genes could be upregulated, and the extent of OE was unpredictable (18, 19).

Naturally occurring CRISPR-associated transposon (CAST) systems(20) have been engineered to generate targeted insertions in bacterial genomes with high efficiency(21–23). Although several CAST systems have been described (24–26), the Tn*6677* system from *Vibrio cholerae* (VcCAST) is among the best characterized and most precise(27–30). In VcCAST, a

100 nuclease-deficient Type I-F CRISPR system pairs with a Tn*7*-like transposase to achieve guide
101 RNA-directed transposition. Guide RNA spacers direct VcCAST proteins to a complementary
102 protospacer, resulting in transposition of Tn*6677* end-flanked DNA ~49 bp downstream of the
103 protospacer (27–30). Transposon DNA can be inserted in two orientations with respect to the
104 Tn*6677* ends (R-L or L-R) but is highly biased toward the R-L orientation (21, 31). VcCAST is
105 highly precise, with nearly all tested guides showing >95% on-target insertion activity. The utility
106 of CASTs has been demonstrated for high-efficiency genome editing in Proteobacteria (21),
107 systematic disruption of transcription factor genes in *Pseudomonas aeruginosa* (23), and
108 targeting individual strains in a complex microbiome (22), but existing systems remain sub-
109 optimal for genome-scale functional genomics. Moreover, the use of Tn*6677* to deliver
110 regulatory elements—such as promoters—has recently shown promise in the model bacterium,
111 *Escherichia coli* (32). However, key gaps remain in our ability to deploy CAST systems for
112 genome-scale OE studies in diverse bacteria.
113 Here we addressed those gaps by creating a VcCAST system for targeted, genome-
114 scale OE in Proteobacteria we call, "CRISPRtOE" (CRISPR transposition and OverExpression)
115 (Fig. 1). CRISPRtOE precisely delivers a transposon with an outward facing promoter upstream
116 of genes to facilitate OE. We show the utility of CRISPRtOE to upregulate gene expression in
117 medically and industrially-relevant Proteobacterial species. Finally, we demonstrate genome-
118 scale overexpression in model (*E. coli*) and non-model (*Zymomonas mobilis*) Proteobacteria,
119 defining genes required for resistance to antibiotics or biofuel production stressors, respectively.
120

121 **Results**

122 A VcCAST Platform for Genome-scale Functional Genomics

123 We first generated a VcCAST system designed for genome-scale functional genomics we call,
124 "CRISPRt." Like previous VcCAST constructs (21, 22), CRISPRt enables insertion of Tn*6677* at
125 precise genomic positions specified by programmable gRNAs (Fig. 2A and 2B). Superimposed
126 on this are additional properties for facile use of VcCAST at the genome-scale: 1) Tn insertion is
127 selectable such that all transconjugants contain an integrated Tn; 2) *cas* helper and Tn plasmids
128 only replicate in *pir*-containing *E. coli* cells and are non-replicative in recipient bacteria, obviating
129 the need for plasmid curing prior to phenotyping (23); 3) *cas* and Tn components are on
130 separate plasmids, preventing insertion of *cas* genes into the genome in cases of Tn plasmid
131 co-integration and reducing Tn plasmid size which facilitates conjugation and cargo modification
132 by standard cloning procedures (Fig. 2A, 2B, S1A, and S1B). CRISPRt transconjugants

133 obtained from tri-parental matings were recovered at efficiencies consistent with genome-scale
134 library creation (e.g., ~10^{-2} frequency for *E. coli* K-12 MG1655, Fig. S1C). To confirm the
135 precision of CRISPRt, we targeted both endogenous (*lacZ*) and heterologous (*gfp*) reporter
136 genes for disruption in *E. coli* K-12 (Fig. S1D), using phenotypic assays and Illumina short read
137 sequencing of the genomic DNA-Tn*6677* junction (Tn-seq (33)) as readouts (Fig. 2C, S2A, S2B,
138 S2C, S2D, and S2E). As expected, Tn-seq showed a >99.5% on target efficiency for both *lacZ*
139 and *gfp* spacers, Tn insertion within a tight window centered at ~49 downstream of the
140 protospacer, and a strong Tn insertion bias toward the R-L orientation. Tn plasmid co-integration
141 occurred at a very low frequency (~10^{-3} for *E. coli* K-12, Fig. S2F).
142 Although Protospacer Adjacent Motif (PAM) requirements for VcCAST have been well
143 characterized (a "CN" PAM is sufficient (25)), other genomic features that impact guide efficacy
144 are poorly understood. To address this issue, we created a pooled CRISPRt library targeting
145 both strands of an *mScarlet-I* reporter gene integrated into the *E. coli* K-12 genome (46 gRNAs
146 total, Fig. S3A). Surprisingly, we found that transcription had a significant impact on guide
147 efficacy. To measure relative guide efficacy, we compared the abundance of gRNA spacers in
148 our library before and after transposition into *mScarlet-I* (Fig. S3B). Consistent with previous
149 data from smaller sets of spacers(34), we found considerable variability, with a ~27-fold
150 difference in efficacy between the most and least active guides. Looking for patterns that could
151 explain these differences, we noticed a clear, but not absolute bias toward higher efficiency in
152 template strand targeting guides. Other variables, such as distance from the gene start or PAM
153 identity did not show an obvious trend (Fig. S3C and S3D). The strand bias in insertion
154 frequency suggested either replication or transcription could be impacting guide efficacy. We
155 continued to observe a strand bias when the orientation of *mScarlet-I* was flipped relative to the
156 origin of replication (Fig. S4A and S4B), seemingly ruling out replication as a factor and
157 implicating transcription. Indeed, CRISPRt insertion into a non-transcribed *mScarlet-I* gene
158 showed reduced variation in relative guide efficacy (Fig. S5A). To determine the absolute effect
159 of transcription on CRISPRt efficacy, we cloned the three most active guides from our *mScarlet-I*
160 library (T03, T09, and T21) and individually tested their efficiencies in the presence and absence
161 of transcription (Fig. 2E and S5B). We found that transcription of *mScarlet-I* reduced recovery of
162 CRISPRt transconjugants by 6.9 to 19.6-fold, depending on the guide tested. We conclude that
163 CRISPRt has excellent properties for genome-scale functional genomics while retaining the
164 precision of VcCAST and that CRISPRt efficacy is higher when targeting non-transcribed DNA.
165

166 Targeted and Tunable Overexpression in Proteobacteria

167 We sought to modify CRISPRt into a targeted overexpression system by inserting outward-
168 facing promoters into Tn*6677* that increase transcription of downstream genes (CRISPRtOE
169 (Fig. 3A)). We inserted synthetic, constitutive promoters of varying strength that had been
170 shown to function in Gamma- and Alpha-proteobacteria (35, 36) into Tn*6677* with the goal of
171 creating an OE gradient (Fig. S6A and S6B). To quantify the OE activity of CRISPRtOE, we
172 generated a "test" strain with a promoterless *mScarlet-I* reporter gene integrated into the *E. coli*
173 K-12 genome. This cassette contained a well-characterized protospacer upstream of *mScarlet-I*
174 to act as a "landing pad" (LP) for CRISPRtOE transposons (Fig. 3A and S6C). The test strain
175 showed negligible mScarlet-I expression in the absence of an upstream CRISPRtOE insertion
176 (Fig. 3B).
177 CRISPRtOE achieved a gradient of *mScarlet-I* OE across our series of tested promoters
178 (Fig. 3B). CRISPRtOE containing the strong H promoter (P_H) showed a ~177-fold increase in
179 mScarlet-I expression, while weaker promoters (P_V and P_A) showed intermediate increases (~2-
180 30-fold); OE was validated at the RNA level using qPCR (Fig. S7A). CRISPRtOE lacking a
181 promoter (no P) failed to stimulate expression above background, although we note that
182 insertions in the reverse orientation (L-R) were excluded from this analysis due to cryptic
183 promoter activity (Fig. S7B and Table S6). We also observed small variations in OE depending
184 on the precise location of insertion for unknown reasons (Table S6).
185 We next sought to demonstrate CRISPRtOE activity in Proteobacteria with medical and
186 industrial relevance. The non-model Alphaproteobacterium, *Zymomonas mobilis*, is a promising
187 biofuel producer and an intriguing example of a free-living bacterium with a naturally reduced
188 genome (37). To assay CRISPRtOE function in *Z. mobilis*, we again generated a promoterless
189 *mScarlet-I* test strain and measured expression following insertion of CRISPRtOE transposons
190 (Fig. S7C and Table S6). We found that CRISPRtOE could produce a gradient of
191 overexpression in *Z. mobilis* up to ~50-fold. Differences in the fold effects of CRISPRtOE across
192 species likely reflect variation in promoter activity among our constitutive promoter set.
193 We then extended this approach to a panel of eight total species including the Gram-
194 negative ESKAPE pathogens (38) *Klebsiella pneumoniae*, *Acinetobacter baumannii*,
195 *Pseudomonas aeruginosa*, and *Enterobacter cloacae*, as well as the industrially and
196 environmentally relevant strains *Pseudomonas putida* (39) and *Shewanella oneidensis* (40),
197 focusing our strongest promoter (P_H) to reduce experimental complexity (Fig. 3C and Table S6).
198 We found that CRISPRtOE could increase mScarlet-I expression in all tested species with an
199 OE range of 232-fold (*E. cloacae*) to 23-fold (*P. aeruginosa*), possibly due to variations in
200 promoter activity, translation initiation or mScarlet-I folding across species. The CRISPRtOE

201 insertion position in most species was centered at 33 bp upstream of *mScarlet-I*, although *A.*
202 *baumannii* showed a wider range of positions for unknown reasons (Fig. S7D and Table S6). We
203 note that the modular design of CRISPRtOE enables facile swapping of promoter sequences
204 with organism-specific or inducible promoters to customize expression levels depending on the
205 application and that we have constructed CRISPRtOE variants with a variety of antibiotic
206 markers to facilitate its use in resistant environmental or clinical isolates. Recovery of
207 CRISPRtOE transconjugants ranged from ~10^{-2} to 10^{-6} across species (Table S7), with most
208 species showing sufficient insertion efficiency to facilitate construction of genome-scale libraries.
209 We conclude that CRISPRtOE is an effective overexpression strategy for Proteobacteria.
210

211 Pooled CRISPRtOE Recapitulates Known Antibiotic Targets

212 There is an urgent need to develop new therapeutics to stem the rising tide of antibiotic
213 resistance (41). One major bottleneck in the process of translating new antimicrobials to the
214 clinic is determining the mode of action, including identifying the direct target. CRISPRtOE could
215 provide a straightforward avenue to antibiotic target discovery because strains with
216 overexpressed target proteins would outgrow competitor strains in a pooled context. For
217 instance, it has been shown that OE of *folA*, encoding the trimethoprim (TMP) target,
218 Dihydrofolate reductase (DHFR), can substantially increase resistance to TMP (42). Likewise,
219 *murA*, encoding the fosfomycin (FOS) target, UDP-NAG enolpyruvyl transferase (MurA), can
220 provide FOS resistance when overexpressed (43).
221 To validate CRISPRtOE as a tool for phenotyping antibiotic targets, we overexpressed
222 the *folA* and *murA* genes in *E. coli* K-12 using the strong promoter construct (P_H). As a hedge
223 against potential variation in integration or OE efficacy, we tiled the region upstream of both
224 genes with 12 unique spacers per gene and created a negative control library that inserted into
225 the *lacZ* coding region (Fig. S8A). We then performed a pooled growth assay competing either
226 the *folA* or *murA* library against the *lacZ* library in sub-lethal concentrations of TMP or FOS,
227 respectively. Strikingly, we found that all CRISPRtOE gRNAs targeting *folA* and *murA* were
228 effective in increasing antibiotic resistance (Fig. S8B and S8C). Relative to *lacZ* controls, the
229 *folA* library grown in TMP showed a 22-fold median increase in abundance while the *murA*
230 library grown in FOS showed a 52-fold median increase. To further characterize these
231 resistance phenotypes, we performed Minimal Inhibitory Concentration (MIC) strip or broth
232 microdilution assays on individual CRISPRtOE isolates (Fig. S8D, S8E, S8F, and S8G). We
233 observed substantial shifts in MIC (~15-30 fold) for CRISPRtOE insertions at varying distances
234 upstream of *folA* (Fig. S8E and S8F), suggesting that CRISPRtOE phenotypes are robust to

235 insertion distances upstream of target genes. We obtained similar results from measuring the
236 FOS MIC for *murA* CRISPRtOE isolates (Fig. S8G).
237 Strong phenotypes from *folA* and *murA* OE provided an opportunity to test if
238 CRISPRtOE targeting could be multiplexed. Thus, we targeted both *folA* and *murA* for OE in the
239 same cell using two distinct strategies: 1) kanamycin (KAN)- or gentamicin (GEN)-marked
240 transposons containing either a single *folA* or *murA* spacer were used in a quad-parental mating
241 and transconjugants were selected on both KAN and GEN, or 2) a kanamycin-marked Tn*6677*
242 containing a CRISPR array with both *folA* and *murA* spacers was used in a tri-parental mating
243 and transconjugants were selected on KAN (Fig. S9A). We found that 97% of KAN^R/GEN^R
244 transconjugants from the quad-parental mating contained insertions upstream of both *folA* and
245 *murA*, and we confirmed TMP^R/FOS^R phenotypes for four tested isolates (Fig. S9B, S9C, and
246 S9D). In contrast, only 12.5% of transconjugants from the tri-parental mating contained both
247 *folA* and *murA* upstream insertions in the correct orientation; however, all four colonies tested
248 were TMP^R/FOS^R (Fig. S9B, S9C, and S9D). We conclude that CRISPRtOE is effective at
249 targeting endogenous genes, such as antibiotic targets, and can be effectively multiplexed.
250

251 Genome-scale CRISPRtOE Validates Antibiotic Targets and Reveals 252 Resistance Pathways

253 Buoyed by our success with *folA* and *murA*, we expanded the scope of our CRISPRtOE
254 screening approach to the genome-scale (Fig. 4A). We targeted all protein-coding genes in the
255 *E. coli* K-12 genome with ~10 gRNAs designed to integrate transposons within a small window
256 upstream of genes without disrupting downstream coding sequences (~45,000 guides total).
257 Based solely on this design, we predicted that 64% of transposon insertions would occur in
258 intergenic regions and 36% would occur in upstream genes (Fig. S10A and S10B). Thus, we
259 generated two pooled libraries—one with promoter H and one without a defined promoter—to
260 distinguish between phenotypes caused by OE rather than upstream gene disruption.
261 We found that CRISPRtOE effectively targeted regions upstream of genes across the
262 genome. We first used Tn-seq to map transposon locations, then performed a computational
263 analysis to associate insertions in the proper orientation (R-L) with downstream genes. Based
264 on this analysis, an average of ~97% of insertions occurred at locations consistent with the
265 library design, demonstrating high, on target efficiency (Fig. S10C, Table S8). Unfortunately,
266 transposon insertion locations could not be defined using gRNA spacer sequences alone, as a
267 fraction of transconjugant cells likely obtained and expressed multiple gRNAs during the mating

268 procedure. This resulted in transposons that inserted at a site designated by the library design
269 that nonetheless did not match the gRNA spacer found within the inserted transposon
270 ("hijacked" transposons). Although our libraries showed that, on average, ~29% of transposon
271 insertions were hijacked (Fig. S10C, Table S8), we estimate that only ~3.5% of transconjugants
272 in our library contained more than one insertion based on mating experiments that used
273 differentially marked transposons (Fig. S10D). In our Tn-seq analysis, we found that
274 CRISPRtOE insertions occurred in a tight distribution largely within 100 bp of the 5′ ends of
275 genes (Fig. 4B). This is in stark contrast to the nearly flat distribution of Tn*5* insertions, which
276 are known to occur pseudo-randomly (44). For instance, the visual distinction between
277 CRISPRtOE targeted and Tn*5* pseudo-random insertion was readily apparent at the non-
278 essential *lac* locus (Fig. 4C).
279 To test the ability of CRISPRtOE to identify antibiotic-relevant gene phenotypes at the
280 genome-scale, we grew our libraries in the presence or absence of a sublethal concentration of
281 TMP and measured relative strain abundance. Biological replicates showed excellent
282 agreement at the gene level (R^2 ~ 0.92, Fig. S11A), underscoring the high reproducibility of
283 genome-scale CRISPRtOE. The *folA* gene was a clear positive outlier with >1000-fold
284 enrichment in TMP versus untreated (Fig. 5A and 5B), demonstrating the power of our
285 CRISPRtOE screen in recovering antibiotic targets. Substantial *folA* enrichment was only seen
286 in the P_H-containing library and not in the promoterless library, indicating that OE, rather than
287 transposon insertion per se, was responsible for the phenotype (Fig. 5B). Promoter-dependent
288 phenotypes were largely distinct from insertion phenotypes across the entire genome, as
289 relative strain abundances of the P_H and no promoter libraries after TMP treatment were not
290 correlated (R^2 = 0.007, compare Fig. S11B and S11C). Computational subsampling of our
291 libraries suggested that CRISPRtOE library complexity could be reduced, if desired. Gene-level
292 phenotypes remained robust after subsampling the library from ~10 to 4 random guides per
293 gene (R^2 = 0.905, Fig. S12A). Further, we obtained many of the same top hits, including *folA*, if
294 we only considered guides that targeted the first gene in operons (Fig. S13A). Thus, we
295 anticipate that future CRISPRtOE libraries could achieve genome-scale overexpression with far
296 fewer guides per gene.
297 Significant outliers outside of the direct target revealed potential TMP resistance or
298 susceptibility mechanisms (Fig. 5A and 5B). For instance, one of the most resistant outlier
299 genes was *soxS*, encoding an AraC-type transcription activator known to regulate genes
300 involved in antibiotic resistance (45) (Fig. 5B). Indeed, AraC and MarR family transcription factor
301 genes and their regulons were among the most resistant outliers in our screen (e.g., *marR*, *rob*,

302 *marA* and the SoxS/Rob/MarA regulated AcrAB efflux pump (46), Table S9), highlighting the
303 ability of CRISPRtOE to identify resistance gene regulators by amplifying natural activation
304 circuits.

305 Other resistance and susceptibility mechanisms centered on folate metabolism. TMP
306 treatment reduces cellular methionine levels due to the involvement of tetrahydrofolate (the
307 product of DHFR) in methionine synthesis (47). CRISPRtOE of the *metR* gene, which encodes
308 a positive regulator of methionine biosynthesis genes (48), increased TMP resistance (Fig. 5B),
309 possibly in increasing flux through the pathway. In contrast, *metF* OE was highly deleterious in
310 the presence of TMP (Fig. 5A), likely due to depletion of 5,10-methylenetetrahydrofolate pools
311 normally used by the ThyA-DHFR pathway to generate tetrahydrofolate (49). We validated this
312 toxicity by showing that *metF* OE from a multi-copy plasmid reduces the MIC for TMP by ~4-fold
313 (Fig. 5C). Neither *metR* nor *metF* were recovered in previous TMP loss-of-function screens (50,
314 51), demonstrating the utility of CRISPRtOE to identify new players in antibiotic function.
315 Interestingly, CRISPRtOE of *folM*, which is thought to encode a protein with DHFR activity (52),
316 was highly toxic to TMP-treated cells (Fig. 5A, Table S9). Although unintuitive, this result is
317 consistent with other genome-scale phenotyping studies that found that disruption of *folM*
318 increases resistance to TMP (50, 51).

319 Finally, genes involved in cellular polysaccharide synthesis, including Enteric Common
320 Antigen (ECA) biosynthesis genes (e.g., genes in the *rff*/*wec* operon), were functionally enriched
321 among sensitive outliers (FDR = 0.0054, ks test; Table S10A). Previous work has shown that
322 disruption of the ECA pathway also increases TMP sensitivity, possibly by sequestering
323 thymidine pools and leading to "hyper-acting" version of thymine-less death (53). Our work
324 suggests that dysregulation by OE, in addition to disruption, can cause ECA-dependent toxicity
325 in TMP-treated cells. Although ECA genes exist in complex operons that may be disrupted by
326 insertion (Fig. 5D), phenotypes for some ECA genes required the presence of P_H in the
327 transposon (Table S9). We chose to focus our follow up analysis on *rffM* (a.k.a. *wecG*), which is
328 the last gene in the ECA operon and showed a phenotype that was strongly dependent on P_H
329 (Table S9). To validate TMP sensitivity upon *rffM* OE and to rule out *cis* effects from disruption of
330 the ECA operon, we expressed *rffM* from a multi-copy plasmid. Plasmid-based OE of *rffM*
331 reduced the TMP MIC by ~4-fold (Fig. 5E), confirming that OE is the source of toxicity. As ECA
332 is found on the cell surface, we considered that ECA pathway disruption by *rffM* OE might
333 increase susceptibility to a broader set of small molecule inhibitors other than TMP. To test this,
334 we screened our plasmid-based *rffM* OE strain against 24 chemicals using a Biolog Phenotype
335 Array. We found that *rffM* OE increased sensitivity to additional small molecule compounds,

336 such as diamide (a.k.a., tetramethylazodicarboxamide) and rifamycin SV (Fig. 5F and S14A and
337 S14B). Thus, OE of ECA synthesis genes increases susceptibility to TMP and other small
338 molecule inhibitors, although the precise mechanism and scope of affected inhibitors remains
339 unknown.

340 We next expanded our genome-scale proof-of-principle studies by screening our
341 CRISPRtOE library against FOS, finding expected, underexplored, and potentially novel FOS
342 resistance determinants (Fig. 6 and S15 and Table S11). As expected, *murA* was a prominent
343 resistant outlier along with the gene upstream of *murA*, *ibaG* (Fig. 6A and S15A). As OE of *ibaG*
344 and *murA* showed similar fold increases in FOS treated cells, we speculated that the *ibaG*
345 phenotype is due to increased transcription of *murA* rather than a contribution of the *ibaG* gene
346 product to FOS resistance, per se.

347 Among the other top resistance genes, we identified several genes within the *phn*
348 operon (*phnCDEFGHIJKLMNOP*) (Fig. 6A and S15A and Table S11) which is involved in
349 degradation of small molecules containing carbon-phosphate (C-P) bonds known as
350 phosphonates (54). Intriguingly, FOS contains a C-P bond that is central to the molecule and
351 likely critical for its function as an antibiotic. The *phn* operon was previously implicated in FOS
352 resistance in a screen that used randomly inserting transposons that contained promoters (55),
353 but the genetic basis of the OE phenotype was not further characterized. We found that
354 CRISPRtOE insertions upstream, but not downstream of *phnM* allowed for FOS resistance,
355 suggesting that OE of *phnM*, *phnN*, *phnO*, or *phnP* was responsible for the phenotype (Fig. 6B).
356 We first validated *phnC* and *phnM* CRISPRtOE phenotypes outside of the pooled screen
357 context, finding increases in the FOS MIC of ~8- and ~11-fold, respectively (Fig. 6C and S15B).
358 Deletion of *phnMNOP* had no impact on the FOS MIC of otherwise wild-type (WT) cells,
359 demonstrating that the role of *phn* genes in FOS resistance is only apparent through OE (Fig.
360 6D, 6E, and S15C). However, deletion of *phnMNOP* eliminated the increase in FOS resistance
361 caused by *phnC* CRISPRtOE (Fig. 6E and S15D). Reasoning from the insertion data that OE of
362 *phnM* was most likely to be the key player in our FOS resistance phenotype, we overexpressed
363 *phnM* from a multi-copy plasmid and measured FOS MICs. Consistent with our hypothesis, we
364 found that *phnM* OE was sufficient to increase the FOS MIC in otherwise wild-type cells and for
365 a strain lacking *phnMNOP* on the chromosome (Fig. 6E and S15D). Interestingly, plasmid-based
366 *phnM* OE in a *phnC* CRISPRtOE Δ*phnMNOP* background further increased the FOS MIC to
367 ~37-fold over WT (Figures 5E and S15D), suggesting that *phnM* functions alongside other
368 members of the *phn* operon, but also acts as a critical bottleneck to FOS resistance in WT cells.

369 Finally, we investigated the role of *waaY*, which encodes the lipopolysaccharide (LPS)
370 core heptose II kinase (56), in FOS resistance. In the absence of *waaY*, LPS is not
371 phosphorylated on heptose II (56) and cells become sensitized to a number of small molecule
372 inhibitors and antibiotics, but not FOS (45). However, our CRISPRtOE screen suggested that
373 *waaY* OE could provide resistance to FOS (Fig. S15A and S15E). We confirmed that *waaY*
374 increases the FOS MIC when overexpressed in *cis* (via CRISPRtOE) or *trans* (via multi-copy
375 plasmid). Thus, our experiments suggest that cellular levels of *waaY* and by extension, LPS
376 phosphorylation, are insufficient to provide FOS resistance but OE can overcome this deficit. In
377 sum, genome-scale CRISPRtOE recovered known antibiotic targets and resistance
378 mechanisms as well as intriguing new players in resistance.
379

380 Genome-scale CRISPRtOE in a non-model bacterium identifies potential 381 engineering targets

382 We next sought to extend our genome-scale CRISPRtOE approach beyond model bacteria and
383 well-characterized inhibitors. *Zymomonas mobilis* is an Alphaproteobacterium that shows
384 promise in conversion of deconstructed plant material (hydrolysate) into biofuels. Plant
385 hydrolysates contain sugars used by *Z. mobilis* in the production of biofuels, but also a complex
386 mixture of inhibitory compounds that originate from the deconstruction process or from the plant
387 material itself. Only some of these inhibitors are known. In principle, OE screens could identify
388 engineering targets that overcome the growth defects caused by hydrolysate inhibitors and
389 increase biofuel yields. To identify potential engineering targets, we constructed CRISPRtOE
390 libraries containing no promoter or P_H that targeted all protein coding genes in the *Z. mobilis*
391 ZM4 genome (~20,000 guides total) using the same design principles described above for *E.*
392 *coli*. We used Tn-seq to map transposon locations and found high on-target efficiency (Fig.
393 S10C). We then screened our libraries against a concentration of ammonia fiber expansion
394 (AFEX)-treated switchgrass hydrolysate that resulted in ~50% growth inhibition when added to
395 defined medium. We found multiple genes that improved the relative and absolute growth of *Z.*
396 *mobilis* in switchgrass hydrolysate (Fig. 7A and 7B and Table S12). We focused our follow up
397 studies on two intriguing resistant outliers, *fumA*, encoding Fumarase A, and *rpoE*, encoding an
398 extracytoplasmic function (ECF) σ factor (Fig. 7, S16, and S17). Fumarase typically participates
399 in the tricarboxylic acid (TCA) cycle, but *Z. mobilis* has an incomplete TCA pathway lacking key
400 enzymes such as malate dehydrogenase (57). CRISPRtOE and plasmid-based OE of *fumA*
401 outside the pooled context validated the growth advantage of *fumA* over WT, although the

402 absolute magnitude of this advantage was modest (Fig. S16A, S16B, S17A, and S17B).
403 However, CRISPRtOE and plasmid-based OE of *rpoE* in hydrolysate showed a much larger
404 absolute growth effect versus WT (Fig. 7C, 7D, S16C, S16D, S17C, and S17D). As many ECF σ
405 factors are involved in mitigating cell stress, we speculate that *rpoE* OE "pre-induces" a cellular
406 stress response which reduces the long lag phase associated with growth in hydrolysate.
407 However, we caution that very little is known about the RpoE regulon in *Z. mobilis*, and the
408 name "*rpoE*" may be misleading as the *Z. mobilis* protein shows low percent identity with well-
409 characterized RpoE proteins from other bacteria (e.g., *E. coli* K-12 RpoE (58) (b2573) ~23%,
410 *Rhodobacter sphaeroides* RpoE (59) (RSP_2681) ~40%). In sum, we extended genome-scale
411 CRISPRtOE to the non-model bacterium *Z. mobilis* and successfully identified genes that
412 improved growth in complex plant hydrolysate.
413

414 Discussion

415 Functional genomics approaches that are robustly scalable and readily applicable to diverse
416 bacteria are required to bridge the yawning gap between genome sequencing and gene function
417 assessment. Our work provides a targeted, systematic, and practical approach for genome-
418 scale gene overexpression in Proteobacteria and possibly beyond. By modifying VcCAST for
419 use in functional genomics (Fig. 1 and 2) and defining non-transcribed regions of DNA as high-
420 efficiency insertion sites (Fig. S3), we demonstrated targeted and tunable OE in Proteobacteria
421 with medical, industrial, and basic research relevance (Fig. 3). Our genome-scale OE screen for
422 targets and modulators of TMP and FOS efficacy in the model organism *E. coli* highlight the
423 exquisite specificity of CRISPRtOE in recovering genes and pathways that underpin antibiotic
424 function (Fig. 4, 5 and 6). The extension of our genome-scale OE screening approach to the
425 non-model bacterium *Z. mobilis* in a complex inhibitor mixture and the ease of constructing
426 individual CRISPRtOE inhibitor-resistant strains demonstrates the potential utility for industrial
427 strain optimization (Fig. 7). Given the ease of implementing CRISPRtOE in the organisms
428 explored here, we anticipate that our approach will be readily expandable to many other
429 microbes and screening conditions. While our manuscript was under review, another manuscript
430 was published that showed that VcCAST containing promoters could be used to upregulate
431 genes in *E. coli*(32). Our work dramatically expands this approach across multiple
432 Proteobacteria and to the genome scale. We note that the replicative CAST vector used in that
433 study is suboptimal for use at the genome-scale due to a lack of Tn selection, the need to cure
434 the plasmid post-editing, and an inability to replicate in important genera such as *Acinetobacter*.

435 CRISPRtOE is a valuable genetic tool for both basic and applied biology. The targeted
436 aspect of CRISPRtOE can be used to generate focused libraries that limit size (number of
437 gRNAs) and scope (number of targeted genes). Moreover, screen hits can be readily pursued
438 for downstream mechanistic analysis by individually cloning gRNAs used in the screen to easily
439 recreate strains outside of the pooled context, a clear benefit over random transposition
440 approaches such as Tn*5*. Additionally, generating pooled sub-libraries from screen hits enables
441 follow up validation at scale. Importantly, the ability to insert transposons with or without
442 promoters at the same genomic locus will allow researchers to disentangle the effects of Tn
443 insertion versus overexpression, simplifying hit interpretation. Further, combining CRISPRtOE
444 with existing gene perturbation approaches such as CRISPRi could enable screening for
445 overexpression suppressors of essential functions at the genome-scale.
446 Our proof of principle work demonstrating that genome-scale CRISPRtOE can identify
447 resistance genes in *E. coli* K-12 holds promise for extending this approach to clinically relevant
448 pathogens with the goal of improving diagnosis and treatment. Importantly, CRISPRtOE action
449 is similar to clinically relevant antibiotic resistance mechanisms, such as IS element
450 transposition and overexpression of downstream resistance genes (60). CRISPRtOE may also
451 be valuable for optimization of strains for industrial use. Industrial strain optimization often
452 occurs through loss of function (61) or directed evolution experiments (62), followed up by
453 plasmid-based overexpression of mutated pathways. CRISPRtOE streamlines this process in
454 non-model bacteria, particularly by enabling recreation of optimized strain features in different
455 genetic backgrounds by targeted transposition. Finally, CRISPRtOE-optimized strains may be
456 immediately useful in production, as CRISPRtOE leaves no heterologously expressed *cas*
457 genes in the recipient strain.
458 Several open questions remain regarding the mechanisms by which genes found in our
459 CRISPRtOE screens provide resistance to TMP, FOS, and hydrolysate. Do potential alterations
460 in the outer membrane caused by *rffM* OE alter cell permeability to small molecule inhibitors
461 such as TMP? RffM catalyzes the first committed step in the pathway to generate ECA modified
462 LPS (ECA-LPS); thus, *rffM* OE would be predicted to increase the ratio of ECA-LPS to N-acetyl-
463 D-glucosamine modified LPS (GlcNAc-LPS) in *E. coli* K-12 (or O-antigen modified LPS in other
464 *E. coli* strains). Consistent with this the Bernhardt lab recently showed that *rffM* OE dramatically
465 reduced GlcNAc-LPS-specific labeling (63), demonstrating perturbation of the outer membrane.
466 Does PhnM act in concert with other members of the Phn enzymatic machinery to modify and
467 degrade FOS? Phn operon members are thought to degrade phosphonates by the following
468 mechanism: *i*) PhnI along with PhnG, PhnH, and PhnL use ATP and phosphonate compounds

469 as substrates to produce 5-triphosphoribosyl-α-1-phosphonate, which is then *ii*) degraded by
470 PhnM into pyrophosphate and 5-phosphoribosyl-α-1-phosphonate, and finally *iii*) the C-P bond
471 is broken by PhnJ as part of the large Phn(GHIJKL)$_2$ complex (64, 65). PhnM lacks C-P lyase
472 activity and is unlikely to directly degrade FOS; however, it is possible that PhnM-mediated
473 conversion of the triphosphorylated phosphonate substrate into a monophosphorylated form is
474 limiting flux through the pathway. Alternatively, if PhnM is sufficient for FOS resistance, by what
475 mechanism does it act? Does the extent of WaaY-dependent, heptose II phosphorylation of LPS
476 mirror the extent of resistance provided by *waaY* OE? Although WaaY appears to be required
477 for phosphorylation (56), the fraction of modified LPS molecules in WT versus *waaY* OE is
478 unknown. Finally, what target genes are induced upon *rpoE* OE to drive resistance to
479 hydrolysate toxins? Mutations in the transcription machinery often occur during laboratory
480 evolution experiments to optimize growth in complex or pleiotropic conditions (66), suggesting
481 that the expression of multiple genes needs to be altered to satisfy the genetic selection. Future
482 work will map the RpoE regulon in *Z. mobilis*, potentially identifying additional stress resilience
483 factors and permitting a comparison to better characterized ECF σs.
484 CRISPRtOE is not without caveats and there may be scenarios in which it is
485 outperformed by other overexpression or gene manipulation strategies. CRISPRtOE and other
486 engineering approaches that insert promoters will alter expression of downstream genes in
487 operons; these effects could complicate but not necessarily preclude identification of gene-level
488 CRISPRtOE phenotypes. Our view is that expression of downstream genes is often
489 advantageous due to fact that protein complexes are often found in operons (e.g., efflux pump
490 subunits). We expect that "No promoter" CRISPRtOE libraries will largely allow for
491 disambiguation of insertion versus overexpression phenotypes, but there may be rare instances
492 in which the combination of insertion and overexpression causes an unexpected genetic
493 interaction because operons contain functionally related genes. In this scenario, Dub-seq or
494 promoter recombineering strategies would be advantageous, as Dub-seq expresses genes *in*
495 *trans* and recombineering can be used to introduce more subtle *cis* mutations that could avoid
496 perturbing upstream genes. Dub-seq can also introduce heterologous DNA from other species
497 for phenotyping (14), something CRISPRtOE is not designed to accomplish. Although we have
498 only demonstrated genome-scale CRISPRtOE in selected Proteobacteria, we envision that
499 improvements to the technology by ourselves and others will enable broad use of the
500 technology in diverse bacteria.
501

502 **Materials and Methods**

503 **Strains and growth conditions.**
504 Strains are listed in Table S1. Growth and antibiotic selection conditions are summarized in
505 Table S2. *Escherichia coli*, *Acinetobacter baumannii*, *Enterobacter cloacae*, *Klebsiella*
506 *pneumoniae,* and *Pseudomonas aeruginosa* were grown in LB broth, Lennox (BD240230) at
507 37°C (or 30°C for CRISPR-guided transposition) in a flask with shaking at 250 rpm, in a culture
508 tube on a roller drum, in a 96 well deepwell plate with shaking at 900 rpm, or in a Tecan Sunrise
509 plate reader shaking with OD600 measurements every 15 min. *Pseudomonas putida* and
510 *Shewanella oneidensis* were grown in LB in a culture tube on a roller drum or in a 96 well
511 deepwell plate with shaking at 900 rpm at 30°C. *Zymomonas mobilis* was grown in RMG
512 medium (10g yeast extract and 2g KH_2PO_4 monobasic/liter with 2% glucose added after
513 autoclaving) at 30°C statically in a culture tube or deepwell plate. *E. coli* was grown in Mueller
514 Hinton Broth (MHB, BD 275730) for antibiotic minimal inhibitory concentration (MIC) assays.
515 Media was solidified with 1.5-2% agar for growth on plates. Antibiotics were added when
516 necessary: *E. coli* (100 µg/ml carbenicillin (carb), 30 µg/ml kanamycin (kan), or 50 µg/ml
517 spectinomycin (spt)), *A. baumannii* (60 µg/ml kan or 100 µg/ml apramycin (apr)), *E. cloacae* (30
518 µg/ml kan or 50 µg/ml spt), *K. pneumoniae* (60 µg/ml kan or 50 µg/ml spt), *P. aeruginosa* (30
519 µg/ml gentamicin (gen) or 1 mg/ml kan), *P. putida* (150 µg/ml apr or 60 µg/ml kan), *S.*
520 *oneidensis* (60 µg/ml kan or 30 µg/ml gen), and *Z. mobilis* (200 µg/ml gen or 100 µg/ml spt).
521 Diaminopimelic acid (DAP) was added at 300 µM to support growth of *dap- E. coli* strains.
522 Strains were preserved in 15% glycerol at -80°C.
523
524 **General molecular biology techniques.**
525 Plasmids are listed in Table S3A and a summary of plasmids for utilizing the CRISPRt and
526 CRISPtOE systems and constructing mScarlet-I reporter strains is in Table S3B.
527 Oligonucleotides are listed in Table S4A (individual) and Tables S4B-E (pooled). *pir*-dependent
528 plasmids were propagated in *E. coli* strain BW25141 (sJMP146) or its derivative sJMP3053.
529 Plasmids were purified using the GeneJet Plasmid Miniprep kit (Thermo K0503), the QIAprep
530 Spin Miniprep Kit (Qiagen 27106), or the Purelink HiPure Plasmid Midiprep kit (Invitrogen
531 K210005). Plasmids were digested with restriction enzymes from New England Biolabs (NEB,
532 Ipswich, MA). Ligations used T4 DNA ligase (NEB M0202) and fragment assembly used
533 NEBuilder Hifi (NEB E2621). Genomic DNA was extracted with the DNeasy Blood & Tissue Kit
534 (Qiagen 69504) or the GeneJet genomic DNA purification kit (Thermo K0721). DNA fragments
535 were amplified by PCR using Q5 DNA polymerase (NEB M0491, for cloning) or One*Taq* DNA
536 Polymerase (NEB M0480, for analysis). PCR products were spin-purified using the Monarch

537 PCR & DNA Cleanup Kit (NEB T1030) or the DNA Clean & Concentrator-5 kit (Zymo Research,
538 Irvine, CA, D4013). Reactions were purified with 1.8X Mag-Bind TotalPure NGS magnetic beads
539 (Omega) on a magnetic rack (Alpaqua). DNA was quantified spectrophometrically using a
540 NanoDrop Lite or fluorometrically using a Qubit with the HS or BR DNA kit (Thermo). Plasmids
541 were transformed into electrocompetent *E. coli* cells using a 0.1 cm cuvette (Fisher FB101) and
542 a BioRad Gene Pulser Xcell on the Bacterial 1 *E. coli* preset protocol (25 µF, 200 ohm, 1800 V)
543 as described in detail previously(67). Oligonucleotides were synthesized by Integrated DNA
544 Technologies (Coralville, IA) or Agilent (SurePrint Oligonucleotide library) (Santa Clara, CA).
545 Sequencing was performed by Functional Biosciences (Madison, WI), Plasmidsaurus (Eugene,
546 OR), Azenta (South Plainfield, NJ), or the University of Wisconsin-Madison Biotechnology
547 Center Next Generation Sequencing Core (UWBC NGS core, Madison, WI).
548
549 ***E. coli* Δ*lac* strain construction.**
550 An *E. coli* MG1655 strain with a *lac* operon deletion (Δ*lac*, Lac$^-$) was constructed by λ-Red-
551 mediated recombination as previously described(68). Briefly, *E. coli* MG1655 (sJMP163)
552 harboring the plasmid pSIM6 (pJMP170) encoding the λ-Red proteins was transformed with a
553 linear DNA fragment encoding an FRT-*kan*-FRT cassette which was amplified by PCR from
554 plasmid pJMP3099 using primers oJMP912 and oJMP913 which also have 40 nt homology to
555 the chromosomal insertion site**)** resulting in strain sJMP3267. The allele was transferred from
556 sJMP3267 to *E. coli* MG1655 (sJMP163) by P1–*vir*-mediated transduction, as previously
557 described(69), resulting in strain sJMP3269. The *kan* gene was removed by transformation with
558 plasmid pCP20 (pJMP3008), encoding a constitutively expressed FLP recombinase, as
559 previously described(70), resulting in strain sJMP3272. Full deletion of the *lac* operon in
560 sJMP3272 was confirmed by PCR with flanking primers (oJMP914 and oJMP915) followed by
561 Sanger sequencing.
562
563 **Construction of chromosomal fluorescent reporters (insertion into the *att*$_{Tn7}$ site).**
564 Fluorescent reporter cassettes are located in a Tn*7* transposon located on an R6K ori (*pir*
565 dependent) plasmid. The transposons were transferred to the *att*$_{Tn7}$ site ~50 bp downstream of
566 *glmS* of a recipient bacterial chromosome by co-conjugation of the Tn*7* transposon donor strain
567 and a second donor strain harboring a plasmid expressing Tn*7* transposase(71). Donor strains
568 encode conjugation machinery, encode *pir*, and are DAP dependent. Briefly, a donor strain with
569 the transposon plasmid, a second donor with the transposase expression plasmid, and the
570 recipient strain were resuspended from plates to an OD_{600}=9 and mixed in equal proportions

571 (100 µl each). Cells were harvested by centrifugation at 5000 rcf for 2 min (except *A. baumannii*
572 at 9000 rcf) and placed on a nitrocellulose filter (Millipore HAWP01300) on an LB plate (except
573 *Z. mobilis* on RMG) and incubated at 30°C (*Z. mobilis* and *P. putida*) or 37°C (all other
574 organisms) for 2-18h. Cells from the filter were resuspended in 300 µl media, serially diluted,
575 and plated with antibiotic selection for the transposon (see growth and selection conditions
576 above) and without DAP to select against the donor strains, and incubated at 30 or 37°C until
577 colonies formed.
578 A transposon containing a GFP expression cassette was derived from a Mobile-CRISPRi
579 plasmid(67) by assembling the AscI-EcoRI fragment of pJMP2824 and annealed
580 oligonucleotides oJMP1420 and oJMP1421 to create pJMP6957. The GFP encoding gene of
581 pJMP6957 was replaced by an mScarlet-I encoding gene derived from Addgene plasmid 85069
582 (pJMP7001) to create pJMP10180 which has an *mScarlet-I* cassette (BbsI sites removed and
583 *mScarlet* converted to *mScarlet-I*) with the T7A1 constitutive promoter in the Tn*7* transposon. A
584 promoterless *mScarlet-I* reporter with the CRISPRt *LZ1* protospacer was derived from
585 pJMP6957, pJMP10180, and synthetic DNA oJMP1599 to create pJMP10206 (see Table S3A
586 for details).
587
588 **Construction of CRISPRt/CRISPRtOE system.**
589 The CRISPRt/CRISPRtOE donor plasmids were derived from pSpinR (pSL1765)(21), Mobile-
590 CRISPRi plasmids(71), and synthetic DNA. Cloning details are located in Table S3A for the
591 individual plasmids. In summary, (1) a functional antibiotic resistance cassette was added to the
592 transposon (pJMP747) and the BsaI cloning site in the gRNA cassette was altered (pJMP10009
593 and pJMP10011). A two plasmid R6K ori (*pir*-dependent) system for selectable CRISPR-guided
594 transposition was created by combining (1) the TnsABC-TniQ-Cas876 expression cassette from
595 pSpinR with the amp^R, R6K ori, mobilizable backbone from Mobile-CRISPRi (pJMP2782) to
596 create pCRISPRt-H (pJMP10233) and (2) the transposon and guide RNA cassette from
597 pJMP10011 with the same backbone (from pJMP2782) to create pCt-T (pJMP10237 and
598 derivatives) which was further minimized, optimized, and altered by adding transcription
599 terminators and moving the guide RNA cassette inside the transposon to produce pCRISPRt-T-
600 gent (pJMP10395) and pCRISPRt-T-kan (pJMP10397). CRISPRtOE plasmids with either no
601 promoter or various strength promoters (pCtOE-noP, pCtOE-P_A, pCtOE-P_H, pCtOE-P_V) were
602 derived from these plasmids by inserting a transcription terminator and promoter cassette
603 derived from synthetic DNA (oJMP2000 plus oJMP2001-2004) into the above plasmids to
604 produce plasmids oJMP10471-10479. Apramycin resistant derivatives of some of these

605 plasmids were created by digesting pJMP10397 and pJMP10478 with XhoI and assembling with
606 a piece of synthetic DNA (oJMP1946) encoding an apramycin resistance gene.
607
608 **CRISPRtOE Guide Design.**
609 Guide RNAs were designed using custom Python scripts
610 (https://github.com/ryandward/CRISPRt_gRNA and https://github.com/ryandward/seq_hunter).
611 The *E. coli* K-12 RefSeq genome assembly, in GenBank file format, was downloaded from the
612 NCBI database (Accession Number: GCF_000005845.2), using the seq_hunter.py script. All
613 genomic locations with a suitable "CN" PAM sequence were identified using the
614 CRISPRt_gRNA.py script. Potential spacers of 32 nucleotides in length were evaluated using
615 awk, and ten were selected based on the following criteria: 1) Unique occurrence in the
616 genome, 2) occurrence on the same strand as the downstream gene, 3) at least 95 nucleotides
617 upstream from the gene annotation**.**
618
619 **CRISPRt/CRISPRtOE individual guide and guide library construction.**
620 Guide sequences (Table S5A-C) were cloned into the BsaI-cloning site of the pCRISPRt-
621 T/pCtOE plasmids. For cloning individual spacer sequences, two 36-nucleotide (nt)
622 oligonucleotides (oligos) were annealed so that they encode the desired sequence flanked by
623 sticky ends compatible to the vector BsaI site, whereas for cloning pooled libraries, DNA
624 fragments encoding spacers were amplified from a pool of oligos and digested with BsaI prior to
625 ligation.
626 To prepare the pCRISPRt-T/pCtOE vectors for cloning, plasmid DNA was extracted from a 100
627 ml culture using a midiprep kit, 2-10 µg plasmid DNA was digested with BsaI-HF-v2 (NEB
628 R3733) in a 100 µl reaction for 4 h at 37°C and then spin-purified.
629 For cloning individual guides, pairs of oligonucleotides (2 µM each) were mixed in a 50 µl total
630 volume of 1X NEB CutSmart buffer, heated at 95°C, 5 min and then cooled to room temperature
631 ~20 min to anneal, and then diluted 1:40 in dH_2O prior to ligation. Ligation reactions (10 µl)
632 contained 1X T4 DNA ligase buffer (NEB), additional DTT (10 mM final) and ATP (0.1 mM final),
633 and 0.5 µl T4 DNA ligase in addition to 50 ng BsaI-digested/spin-purified vector and 2 µl of 1:40
634 diluted annealed oligos. Ligations were incubated at 25°C for 2 h and ligase was heat
635 inactivated for 20 min at 65°C. 1-2 µl ligation was used for electroporation into 50 µl *E. coli*
636 strain BW25141 (sJMP146). Transformations were serially diluted and plated with selection on
637 carb to obtain isolated colonies. After confirmation of sequence, individual plasmids were

638 transformed into *E. coli* mating strain WM6026 (sJMP424 or sJMP3257) with selection on carb
639 and DAP.
640 For cloning pooled libraries, fragments were amplified from 90 nt pooled oligos (IDT oPools or
641 Agilent SurePrint pools) using the following conditions per 100 µl reaction (reaction size was
642 adjusted ~100-600 µl depending on size of library): 20 µl Q5 buffer, 3 µl GC enhancer, 2 µl
643 10mM each dNTPs, 5 µl each 10 µM forward and reverse primers, 2 µl 10 nM pooled oligo
644 library, 1 µl Q5 DNA polymerase, and 186 µl H_2O with the following thermocycling parameters:
645 98°C, 30s; 15-19 cycles of: 98°C, 15s; 56°C, 15s; 72°C, 15s; 72°C, 10 min; 10°C, hold (cycles
646 were adjusted to obtain sufficient PCR product without overamplifying/biasing the library). PCR
647 products (90 bp) were spin-purified, and 300 ng was digested with BsaI-HF-v2 (NEB R3733) in
648 a 100 µl reaction for 2 h at 37°C (no heat kill, reaction size was adjusted proportionally
649 depending on the size of the library). Size and digestion of PCR products were confirmed on a
650 4% agarose E-Gel (Thermo). The BsaI-digested PCR product without further purification
651 (3ng/µl) was ligated into BsaI-digested, spin-purified plasmid as described above except 10 µl of
652 the digested PCR product was ligated with 500 ng cut plasmid in a 100 µl reaction and ligations
653 were incubated at 16°C for 14 h. Library ligations were purified by spot dialysis on a
654 nitrocellulose filter (Millipore VSWP02500) against 0.1 mM Tris, pH 8 buffer for 20 min prior to
655 transformation by electroporation into *E. coli* mating strain WM6026 (sJMP424 or sJMP3257).
656 To obtain sufficient transformants for large libraries, electrocompetent cells were made 5X more
657 concentrated in the final step of the preparation(67) and multiple transformations were carried
658 out depending on the size of the library. Transformations were plated with selection on LB with
659 carb and DAP at a density of ~30,000-50,000 colonies/150 mm petri plate. Cells (>30X more
660 colonies the number of guides, e.g. >1.35 million CFU for the 45,000 guide libraries) were
661 scraped from plates and resuspended in LB + 15% glycerol, density was adjusted to OD_{600}=9,
662 and aliquots were frozen at -80°C.
663
664 **Transfer of the CRISPRt/CRISPRtOE system to the bacterial chromosome.**
665 CRISPRt and CRISPRtOE strains were constructed by triparental mating of two *E. coli* donor
666 strains—one with the pCRISPRt-H plasmid encoding Cas678-TniQ-TnsABC and another with
667 the pCRISPRt-T or pCtOE plasmid containing the transposon with the guide RNA and antibiotic
668 resistance—and a recipient strain. See Table S2 for a summary of growth media and conditions
669 and antibiotic concentrations. All conjugations and selection post-conjugation were carried out at
670 30°C regardless of the normal incubation temperature for the organism. Isolated donor and
671 recipient strains were struck out on plates with the appropriate media and antibiotic (if relevant)

concentrations. Colonies were resuspended from plates into the growth medium used for the recipient to a density of OD_{600}=9. Equal amounts of donors and recipient were mixed together (along with the appropriate no recipient, no CRISPRt-H donor, or no CRISPRt-T donor controls), cells were pelleted by centrifugation at 5000 x *g* (except *A. baumannii* at 9000 x *g*), placed on a nitrocellulose filter (Millipore HAWP01300) on an LB plate (except an RMG plate for *Z. mobilis*), and incubated 12-18 h at 30°C. Cells from the filter were resuspended in 300 µl media, serially diluted, and plated with antibiotic selection for the transposon (see growth and selection conditions above) and without DAP to select against the donor strains, and incubated at 30°C until colonies formed (1-3 days). A typical mating was 100 µl each strain and plating 100 µl undiluted, and 10^{-1} through 10^{-4} dilutions to obtain isolated colonies. For library construction, conjugations were scaled up and plated with selection at a density of ~30,000-50,000 colonies/150 mm petri plate. Cells (>30X more colonies the number of guides, e.g. >1.35 million CFU for the 45,000 guide libraries) were scraped from plates and resuspended in LB + 15% glycerol, density was adjusted to OD_{600}=10-15, and aliquots were frozen at -80°C.

Analysis of phenotype of *E. coli lacZ* and *gfp*-targeting CRISPRt.

For *gfp* targeted CRISPRt, fluorescence level (GFP) of 80 individual colonies was determined. Cultures were grown in 300 µl media in 96 well deepwell plates from a single colony to saturation. Cells were centrifuged at 4,000 x *g* for 10 min and cell pellets were resuspended in 300 µl 1X PBS. 150 µl was transferred to a 96-well black, clear bottom microplate (Corning 3631) and cell density (OD_{600}) and fluorescence (excitation 475 nm, emission 510 nm) were measured in a fluorescence microplate reader (Tecan Infinite Mplex). Fluorescence values were normalized to cell density.

For *lacZ* targeted CRISPRt, the color of 80 individual colonies was determined by patching on LB agar plates containing X-gal (20 µg/ml). Blue indicates the presence of an intact *lacZ* due to metabolism of the X-gal by LacZ (betagalactosidase) and white indicates disruption of *lacZ*.

Analysis of individual CRISPRtOE isolates from various Proteobacteria.

<u>Phenotype determination</u>. Fluorescence levels (mScarlet-I) of 12 CRISPRtOE isolates of all 8 species were determined. Cultures of isolates were grown in 300 µl media in 96 well deepwell plates from a single colony to saturation. Cultures were serially diluted to 1:10,000 (1:100 twice) into fresh media and grown again to saturation (~13 doublings). Cells were centrifuged at 4,000 x *g* for 10 min. Cell pellets were resuspended in 300µl 1X PBS and 150 µl was transferred to a 96-well black, clear bottom microplate (Corning 3631). Cell density (OD600) and fluorescence

706 (excitation 584 nm, emission 607 nms) were measured in a fluorescence microplate reader
707 (Tecan Infinite Mplex). Fluorescence values were normalized to cell density. The assay was
708 repeated three times for *E. coli* and *Z. mobilis* and twice for all other strains.
709 Genotype determination. Insertion positions of 12 CRISPRtOE isolates of all 8 species were
710 determined. Cultures of isolates were grown in 300 µl media in 96 well deepwell plates, serially
711 diluted 1:100 in dH_2O, heated to 90°C for 3 min prior to use as a template for PCR. Fragments
712 (~2000 bp) were amplified by PCR with a forward primer in the transposon (oJMP490) and a set
713 of indexed (4 nt barcode) reverse primers in the *mScarlet-I* coding sequence (oJMP2118-2129)
714 in a 25 µl reaction containing: 5 µl OneTaq buffer, 0.5 µl 10mM each dNTPs, 0.5 µl each 10 µM
715 forward and reverse primers, 2 µl diluted culture, 0.25 µl OneTaq DNA polymerase, and 16.25 µl
716 H_2O with the following touchdown PCR program: 94°C, 3 min then 10 cycles of 94°C, 30s,
717 65°C, 30s (-1°C/cycle), 68°C, 2.5 min, then 25 cycles of 94°C, 30s, 55°C, 30s, 68°C, 2.5 min,
718 then 68°C, 5 min in a BioRad T100 thermalcycler. Sets of indexed PCRs for each organism
719 were pooled, spin purified and sequenced by Oxford nanopore long read amplicon sequencing
720 by Plasmidsaurus. Sequencing data was demultiplexed using a custom Python script
721 (SplitSamplesSeq.py) and insertion position relative to the *mScarlet-I* ATG start codon was
722 determined.
723
724 **mScarlet-I expression analysis**
725 Overnight cultures were diluted 1:1000 into 25ml LB in a 125ml flask in triplicate and incubated
726 at 37ºC, shaking until cultures reached mid-log phase (OD600 ~0.4). Three 3ml culture was
727 treated by vortexing in 375µl cold 5% phenol in ethanol for 10s. Cells were harvested by
728 centrifugation for 10min at 4000xg, flash frozen in a dry ice ethanol bath after decanting
729 supernatant, and stored at -80ºC. Cells were lysed by resuspending in 200µl RNase-free TE
730 buffer, pH8 containing 1µl Ready-Lyse lysozyme (Lucigen R1804M) for 5 min at RT and 1min at
731 55ºC. RNA was extracted with the Monarch Total RNA miniprep kit according to the
732 manufacturer's protocol (includes on column gDNA removal and DNase I treatment). An
733 additional DNA removal step was performed using the DNA-free removal kit (Invitrogen
734 AM1906) according to the manufacturer's protocol. RNA was quantified using a nanodrop
735 spectrophotometer and Qubit fluorometer (Thermo). cDNA was synthesized using Superscript III
736 Reverse Transcriptase (Invitrogen 18080093) using ~3µg total RNA and gene-specific primers
737 at 55ºC for 30min according to the manufacturer's protocol. qPCR was performed using a
738 Roche Lightcycler 480 and Lightcycler 480 SYBR Green I Mastermix (Roche 04707516001) in a
739 20µl reaction containing 10µl 2X mastermix, 1µl each forward and reverse primer (10µM), and

740 2µl cDNA with preincubation at 95°C 10min and amplification at 95°C 10s, 55°C 15s, 72°C 10s
741 for 40 cycles. Fold changes in mScarlet-I gene expression were calculated using the double
742 delta Ct method (72) with *rho* expression for normalization. Two technical replicates are shown
743 each of with the standard deviation of three biological replicates.
744
745 **CRISPRtOE strain construction efficiency**
746 The CRISPRtOE system was transferred to the recipient chromosome by tri-parental
747 conjugation followed by CAST transposition. The reported values are the combined efficiency of
748 conjugation and transposition with the LZ1 guide into a recipient harboring the LP-mScarlet-I
749 reporter. Equal amounts (100µl culture normalized to OD600=9 in media) of recipient, CRISPRt-
750 H donor, and CRISPRt-T donor were mixed and incubated for 16h at 30°C on a nitrocellulose
751 filter on a non-selective plate (RMG for *Z. mobilis*, LB for all other organisms). Cells were
752 resuspended off the filter by vortexing, diluted serially (1:10) in media in triplicate, and 10µl was
753 spotted on selective and non-selective plates and incubated at 30°C. Growth on selective
754 versus non-selective plates was compared to determine efficiency.
755
756 **Multiplex CRISPRtOE strain construction**
757 Strains with two CRISPRtOE insertions were constructed using the same conjugation
758 methodology as for single CRISPRtOE insertions except for method 1, two transposon donor
759 strains with different antibiotic resistance cassettes were used. Insertion position of isolates was
760 confirmed by PCR with one primer in the transposon and a second in the target gene and
761 precise location was determined by sequencing the PCR product. Increased antibiotic
762 resistence of the CRISPRtOE isolates was confirmed by disc diffusion assays. MICs of single
763 isolates from each method were determined using MIC test strips (Lsiofilchem).
764
765 **CRISPRtOE library growth experiments.**
766 Competition experiment growth. The *E. coli* CRISPRtOE *murA* and *folA* libraries were mixed in
767 equal volume with the LP-*lacZ* library: 50 µl frozen stock (OD_{600} = 10) of each library (*murA* +
768 LP-*lacZ* and *folA* + LP-*lacZ*) into 100 ml LB (starting OD_{600} = 0.01) in a 500 ml flask and
769 incubated shaking at 37°C until OD_{600} = 0.2 (~2.5 h) (timepoint = T0) to revive the cells. These
770 cultures were diluted to OD_{600} = 0.02 into 4 ml LB plus antibiotic fosfomycin (0.4 µg/ml, for the
771 *murA* + LP-*lacZ* libraries) or trimethoprim (0.1 µg/ml, for the *folA* + LP-*lacZ* libraries) or no
772 antibiotic control in 14 ml snap cap culture tubes (Corning 352059) in duplicate and incubated
773 with shaking for 18 h at 37°C (T1). These cultures were serially diluted back to OD_{600} = 0.01 into

774 fresh tubes containing the same media and incubated again with shaking for 18 h at 37°C (T2)
775 for a total of ~10-15 doublings. Cells were pelleted from 15 ml of culture in duplicate at each
776 time point T0 and 1ml of culture at timepoints T1 and T2 and stored at -20°C.
777 Whole genome experiment growth. The *E. coli* CRISPRtOE whole genome libraries with no
778 promoter (sJMP10704) or promoter H (sJMP10705) were revived by dilution of 100 µl frozen
779 stock (OD_{600} = 15) into 100 ml LB (starting OD_{600} = 0.015) and incubation in 500 ml flasks
780 shaking at 37°C until OD_{600} = 0.2 (~2.5 h) (timepoint = T0). These cultures were diluted to OD_{600}
781 = 0.02 into 4 ml LB plus antibiotic trimethoprim (0.1 µg/ml) or no antibiotic control in 14 ml snap
782 cap culture tubes (Corning 352059) in duplicate and incubated with shaking for 18 h at 37°C
783 (T1). These cultures were serially diluted back to OD_{600} = 0.01 into fresh tubes containing the
784 same media and incubated again with shaking for 18 h at 37°C (T2) for a total of ~10-15
785 doublings. Cells were pelleted from 15 ml of culture in duplicate at time point T0 and 1ml of
786 culture at timepoints T1 and T2 and stored at -20°C.
787
788 **Analysis of individual CRISPRtOE isolates from library competition experiment.**
789 Insertion positions of 8 CRISPRtOE isolates from the *folA* and *murA* libraries were determined.
790 Cultures of isolates were grown in 3 ml media from an isolated colony, serially diluted 1:100 in
791 dH_2O, heated to 90°C for 3 min prior to use as a template for PCR. Fragments (~600 bp) were
792 amplified by PCR with a forward primer in the transposon (oJMP61) and a reverse primer in the
793 *folA* or *murA* coding sequence (oJMP2349 and oJMP2348, respectively) in a 50 µl reaction
794 containing: 10 µl OneTaq buffer, 1.0 µl 10mM each dNTPs, 1.0 µl each 10 µM forward and
795 reverse primers, 2 µl diluted culture, 0.5 µl OneTaq DNA polymerase, and 16.25 µl H_2O with the
796 following touchdown PCR program: 94°C, 3 min then 10 cycles of 94°C, 30s, 65°C, 30s (-
797 1°C/cycle), 68°C, 1 min, then 25 cycles of 94°C, 30s, 55°C, 30s, 68°C, 1 min, then 68°C, 5 min
798 in a BioRad T100 thermalcycler. PCR products were spin-purified and Sanger sequenced to
799 determine the transposon insertion position relative to the *mScarlet-I* ATG start codon.
800
801 **Tnseq analysis of CRISPRt/CRISPRtOE constructs.**
802 The TnSeq protocol was adapted from Klompe et al(31). Genomic DNA (gDNA) was extracted
803 from the equivalent of 1 ml of cells at OD_{600}=3 (~$2x10^9$ cells) either resuspended from a plate or
804 from liquid culture and was further purified by spot dialysis on a nitrocellulose filter (Millipore
805 VSWP02500) against 0.1 mM Tris, pH 8 buffer for 20 min. 1 µg gDNA was digested with 4U
806 MmeI (NEB) in a 50 µl reaction at 37°C, 12 hrs and heat inactivated at 65°C, 20 min. The digest
807 was purified using 1.8X magnetic beads (Omega) following the manufacturer's protocol, eluting

808 in 20 µl 10 mM Tris, pH 8.0. Adapter oligos oJMP1995 and P-oJMP1996 (phosphorylated) were
809 annealed by mixing equal volume of 100µM oligos in 10mM Tris, pH8 (50 µM each), heating to
810 95°C, 5 min followed by cooling to RT ~15 min, and diluted 1:10 (5 µM each) for use. Annealed
811 oligos were ligated onto MmeI-digested DNA in a 20 µl reaction with 2 µl 10X T4 ligase buffer, 2
812 µl 100 mM DTT, 2 µl 1 mM ATP, 12 µl purified MmeI-digested gDNA (50 ng/µl, 600 ng total), 1 µl
813 5 µM annealed adapter oligos (250 nM final) and 1 µl T4 DNA ligase. Ligations were incubated
814 14 h at 16°C and the enzyme was heat-inactivated for 20 min at 65°C. Ligations were purified
815 using 1.8X magnetic beads, eluting in 22 µl 10 mM Tris, pH 8. Fragments were amplified by
816 PCR with primers containing partial adapters for index PCR with Illumina TruSeq adapters in a
817 100µl reaction containing: 20 µl 5X Q5 buffer, 3 µl GC enhancer, 2 µl 10 mM each dNTPs, 5 µl
818 each forward primer (oJMP1997) and reverse primer (oJMP1998 or indexed primers
819 oJMP2022-2033), 10 µl purified ligation, 1 µl Q5 DNA polymerase, and 54 µl dH_2O with the
820 following program: 98°C, 30s then 18-20 cycles of 98°C, 15s, 66°C, 15s, 72°C, 15s, then 72°C,
821 10 min in a BioRad C1000 thermal cycler. PCR products were spin-purifed (eluted in 15 µl) and
822 quantified fluorometrically. Samples were sequenced by the UWBC NGS Core facility or Azenta
823 Amplicon-EZ service. Briefly, PCR products were amplified with nested primers containing i5
824 and i7 indexes and Illumina TruSeq adapters followed by bead cleanup, quantification, pooling
825 and running on a NovaSeq X Plus (150 bp paired end reads) or MiSeq (250 bp paired end
826 reads). Sequencing analysis of the initial CRISPRt or CRISPRtOE plasmid libraries from which
827 the strain libraries were prepared was by amplification with oJMP2011 and oJMP1998 (or
828 barcoded version of oJMP1998: oJMP2022-2033), followed by spin purification and Illumina
829 sequencing.
830
831 **Analysis of *E. coli mScarlet-I*-targeting CRISPRt libraries.**
832 Two plasmid libraries (pJMP10505 and pJMP10506) were constructed (gen^R and kan^R) and
833 used to create CRISPRtOE libraries (sJMP10519, 10520, 10594, 10595, and 10637-10640) in
834 each of four *E. coli mScarlet-I* reporter strains (sJMP10205, 10269, 10630, 10633). Plasmid
835 DNA from pJMP10505 and pJMP10506 was amplified with oJMP2011 and oJMP1998. gDNA
836 from (sJMP10519, 10520, 10594, 10595, and 10637-10640) was processed by TnSeq as
837 detailed above with oJMP1997 and oJMP2022-2033. Sequencing data was demultiplexed using
838 SplitSamplesSeq.py and guides were quantified using seal.sh from bbmap.
839
840 **MIC assays.**

841 The minimal inhibitory concentration (MIC) of *E. coli folA* and *murA* CRISPRtOE isolates was
842 determined by either growth in a microtiter plate or by disc diffusion assays, respectively. For the
843 broth microdilution assay, CRISPRtOE isolates and WT controls were grown to saturation from
844 an isolated colony and serially diluted to OD600 = 0.003) and the CRISPRtOE library was
845 diluted from a glycerol stock to the same density. Trimethoprim was serially diluted in DMSO at
846 1000X concentration and then diluted to 2X in MHB. *E. coli folA* CRISPRtOE isolates, the *folA*
847 CRISPRtOE library, a *lacZ* CRISPRtOE control, and WT cultures and the media containing
848 antibiotic were mixed in equal proportions and incubated 20 h shaking at 37°C prior to cell
849 density (OD_{600}) determination in a microplate reader. For the MIC strip assays, *E. coli folA* or
850 *murA* CRISPRtOE isolates, a *lacZ* CRISPRtOE control, and WT cultures were diluted to OD_{600} =
851 0.3 and 300 µl was spread on a 100 mm MH agar plate and dried in a laminar flow cabinet.
852 When dry, MIC strips (Liofilchem, Italy; 920371 (TMP 0.002-32 mg/L) and 920791(FOS 0.064-
853 1024 mg/L)) were applied to the plate and 10 µl serially diluted antibiotics were applied to the
854 discs. Plates were incubated at 37°C for 18 h. Broth microdilution assays were repeated 3 times
855 and MIC test strip assays twice.
856
857 **CRISPRtOE data processing and analysis.**
858 All commands and scripts used for processing and analysis of CRISPRtOE data are available at
859 (https://github.com/GLBRC/CtOE_analysis).
860 Paired-end analysis for spacer-insertion site analysis. FASTQ files were separated for each
861 read (R1 and R2) and trimmed to remove transposon-specific sequences using Cutadapt
862 (v5.0)(73). The `--discard-untrimmed` flag was used to remove reads that lacked transposon-
863 specific adapters. R1 reads were filtered to retain only trimmed sequences of length 18-20bp,
864 and R2 reads were filtered to retain only those of length 32bp. Reads were then repaired using
865 BBMap (v39.06) suite's `repair.sh` tool with options to discard unpaired reads (`repair=t
866 tossbrokenreads=t`). This ensured that only properly paired reads with both R1 and R2 passing
867 all quality filters were retained for downstream analysis. The trimmed FASTQ files were
868 separately aligned to the *E. coli* genome (NCBI RefSeq Assembly ID GCF_000005845.2) or the
869 *Z. mobilis* genome (NCBI RefSeq Assembly ID GCF_003054575.1) using Bowtie (v1.3.1) (74) in
870 single-end mode, with flags `-k 1`, `--best`, `--strata`, `--nomaqround`, `-v 0`, and `-m 1` . The
871 alignment SAM file for each sample was converted to BAM using Samtools (v1.13)(75), filtered
872 to retain alignments with MAPQ of >=42 with `samtools view`, then namesorted with `samtools
873 sort –n`, before being parsed to TSV format for downstream analysis. (76) A custom python

874 script was used to annotate the site of Tn insertion, identify unique sites of Tn insertion, and
875 compare these to the predicted sites of Tn insertion from the designed CRISPRtOE library.
876 CRISPRtOE library sequencing analysis (single-end). Prior to analysis of FASTQ reads, a list of
877 expected Tn insertion sites based on the CRISPRtOE library design was created with a custom
878 python script (ctoe_analysis 'guides' pipeline). R1 reads were trimmed and filtered with
879 Cutadapt as in paired-end analysis. Trimmed R1 reads were aligned to reference genome with
880 bowtie, then filtered and sorted with SAMtools as in paired-end analysis. Alignment files were
881 parsed to TSV format, sites of Tn insertion identified and counted with a custom python script.
882 Observed sites of Tn insertion were compared to predicted sites of Tn insertion. Counts of
883 insertions consistent with the target location and orientation of CRISPRtOE library design were
884 retained for downstream analysis in edgeR.
885 Differential abundance analysis**.** Differential abundance analysis was performed using the
886 generalized linear model (GLM) framework in edgeR (v4.4.2). Raw count data were filtered to
887 retain unique Tn insertions with counts per million (CPM) of at least 0.1 in a minimum of half of
888 the samples per comparison set. Normalization factors were calculated using the trimmed mean
889 of M-values method. A negative binomial GLM was fitted using quasi-likelihood (QL) methods
890 with robust dispersion estimation. The model incorporated both treatment and library type
891 factors, modeling each independently as well as their interaction (formula: ~ library * treatment).
892 Differential abundance was assessed for individual insertions. For gene-level analysis, a
893 competitive gene set test was performed using CAMERA, linking Tn insertions to their
894 downstream genes. Separate contrasts were constructed to evaluate treatment effects in
895 promoter and non-promoter contexts, as well as the interaction between library type and
896 treatment. For each gene, median log fold changes were calculated from the insertions mapping
897 to that gene. Multiple testing correction was performed using the Benjamini-Hochberg procedure
898 to control the false discovery rate. Downstream gene-level analyses report the median log fold
899 change calculated from individual insertions and the FDR values calculated using CAMERA.
900 Genes with significant log2FCs between treatment and control conditions were identified from
901 CAMERA analysis, requiring an FDR <= 0.05. Genes with promoter-dependent phenotypes
902 were selected, requiring the median log2FC for the library * treatment interaction factor to be at
903 least 2 (either positive or negative). Genes were then ranked by the log2FC value of the
904 Promoter library, and the top 10 and bottom 10 genes selected for plotting.
905

906 **Data availability**

907 Raw sequencing data is deposited at the Sequence Read Archive
908 (https://www.ncbi.nlm.nih.gov/sra, PRJNA1284861). All other data are available upon request.
909 Plasmids are available from Addgene (https://www.addgene.org, #225832-225871). Guide
910 design script is available at https://github.com/ryandward/CRISPRt_gRNA . Analysis and
911 demultiplexing scripts are available at https://github.com/GLBRC/CtOE_analysis and
912 https://github.com/GLBRC/CtOE_downstream_analysis .
913
914 (Pre-publication SRA reviewer link:
915 https://dataview.ncbi.nlm.nih.gov/object/PRJNA1284861?reviewer=8p8ge077d7g4jthl52a6tuadmv)
916

917 ## Author ORCIDs

918 Amy B. Banta https://orcid.org/0000-0002-1843-5059
919 Ashley N. Hall https://orcid.org/0000-0001-7739-1706
920 Kevin S. Myers https://orcid.org/0000-0003-3302-3877
921 Ryan D. Ward https://orcid.org/0000-0001-9537-2461
922 Bryce C. Davis https://orcid.org/0009-0005-2532-6896
923 Rodrigo A. Cuellar https://orcid.org/0000-0001-7573-3522
924 Michael Place https://orcid.org/0000-0003-2776-7095
925 Claire C. Freeh
926 Emily E. Bacon https://orcid.org/0000-0001-8090-7689
927 Jason M. Peters https://orcid.org/0000-0003-2722-8382

928

929 ## Supplemental Material

930 Supplemental Figures S1-S17
931 Supplemental Tables S1-S12
932

933 ## References

934 1. Jost M, Chen Y, Gilbert LA, Horlbeck MA, Krenning L, Menchon G, Rai A, Cho MY, Stern JJ,
935 Prota AE, Kampmann M, Akhmanova A, Steinmetz MO, Tanenbaum ME, Weissman JS.
936 2017. Combined CRISPRi/a-Based Chemical Genetic Screens Reveal that Rigosertib Is a
937 Microtubule-Destabilizing Agent. Molecular Cell 68:210-223.e6.

938 2. Kampmann M. 2017. Elucidating drug targets and mechanisms of action by genetic screens
939 in mammalian cells. Chem Commun (Camb) 53:7162–7167.

940 3. Kampmann M. 2018. CRISPRi and CRISPRa Screens in Mammalian Cells for Precision
941 Biology and Medicine. ACS Chem Biol 13:406–416.

942 4. Cámara E, Lenitz I, Nygård Y. 2020. A CRISPR activation and interference toolkit for
943 industrial Saccharomyces cerevisiae strain KE6-12. Sci Rep 10:14605.

944 5. Dominguez AA, Lim WA, Qi LS. 2016. Beyond editing: repurposing CRISPR-Cas9 for
945 precision genome regulation and interrogation. Nat Rev Mol Cell Biol 17:5–15.

946 6. Jost M, Weissman JS. 2018. CRISPR Approaches to Small Molecule Target Identification.
947 ACS Chem Biol 13:366–375.

948 7. Lian J, Schultz C, Cao M, HamediRad M, Zhao H. 2019. Multi-functional genome-wide
949 CRISPR system for high throughput genotype-phenotype mapping. Nat Commun 10:5794.

950 8. Santiago M, Matano LM, Moussa SH, Gilmore MS, Walker S, Meredith TC. 2015. A new
951 platform for ultra-high density Staphylococcus aureus transposon libraries. BMC Genomics
952 16:252.

953 9. Kitagawa M, Ara T, Arifuzzaman M, Ioka-Nakamichi T, Inamoto E, Toyonaga H, Mori H. 2005.
954 Complete set of ORF clones of Escherichia coli ASKA library (a complete set of E. coli K-
955 12 ORF archive): unique resources for biological research. DNA Res 12:291–299.

956 10. Tal S, Paulsson J. 2012. Evaluating quantitative methods for measuring plasmid copy
957 numbers in single cells. Plasmid 67:167–173.

958 11. Freed EF, Winkler JD, Weiss SJ, Garst AD, Mutalik VK, Arkin AP, Knight R, Gill RT. 2015.
959 Genome-Wide Tuning of Protein Expression Levels to Rapidly Engineer Microbial Traits.
960 ACS Synth Biol 4:1244–1253.

961 12. Warner JR, Reeder PJ, Karimpour-Fard A, Woodruff LBA, Gill RT. 2010. Rapid profiling of
962 a microbial genome using mixtures of barcoded oligonucleotides. 8. Nat Biotechnol
963 28:856–862.

964 13. Mutalik VK, Novichkov PS, Price MN, Owens TK, Callaghan M, Carim S, Deutschbauer
965 AM, Arkin AP. 2019. Dual-barcoded shotgun expression library sequencing for high-
966 throughput characterization of functional traits in bacteria. Nat Commun 10:308.

967 14. Huang YY, Price MN, Hung A, Gal-Oz O, Ho D, Carion H, Deutschbauer AM, Arkin AP.
968 2023. Barcoded overexpression screens in gut Bacteroidales identify genes with new roles
969 in carbon utilization and stress resistance. bioRxiv
970 https://doi.org/10.1101/2022.10.10.511384.

971 15. Mali P, Aach J, Stranges PB, Esvelt KM, Moosburner M, Kosuri S, Yang L, Church GM.
972 2013. CAS9 transcriptional activators for target specificity screening and paired nickases
973 for cooperative genome engineering. Nat Biotechnol 31:833–838.

974 16. Lee DJ, Minchin SD, Busby SJW. 2012. Activating transcription in bacteria. Annu Rev
975 Microbiol 66:125–152.

976 17. Bikard D, Jiang W, Samai P, Hochschild A, Zhang F, Marraffini LA. 2013. Programmable
977 repression and activation of bacterial gene expression using an engineered CRISPR-Cas
978 system. Nucl Acids Res gkt520.

979 18. Kiattisewee C, Karanjia AV, Legut M, Daniloski Z, Koplik SE, Nelson J, Kleinstiver BP,
980 Sanjana NE, Carothers JM, Zalatan JG. 2022. Expanding the Scope of Bacterial CRISPR
981 Activation with PAM-Flexible dCas9 Variants. ACS Synth Biol 11:4103–4112.

982 19. Ho H-I, Fang JR, Cheung J, Wang HH. 2020. Programmable CRISPR-Cas transcriptional
983 activation in bacteria. Mol Syst Biol 16:e9427.

984 20. Peters JE, Makarova KS, Shmakov S, Koonin EV. 2017. Recruitment of CRISPR-Cas
985 systems by Tn7-like transposons. PNAS 114:E7358–E7366.

986 21. Vo PLH, Ronda C, Klompe SE, Chen EE, Acree C, Wang HH, Sternberg SH. 2021.
987 CRISPR RNA-guided integrases for high-efficiency, multiplexed bacterial genome
988 engineering. Nat Biotechnol 39:480–489.

989 22. Rubin BE, Diamond S, Cress BF, Crits-Christoph A, Lou YC, Borges AL, Shivram H, He C,
990 Xu M, Zhou Z, Smith SJ, Rovinsky R, Smock DCJ, Tang K, Owens TK, Krishnappa N,
991 Sachdeva R, Barrangou R, Deutschbauer AM, Banfield JF, Doudna JA. 2022. Species-
992 and site-specific genome editing in complex bacterial communities. Nat Microbiol 7:34–47.

993 23. Chen W, Ren Z-H, Tang N, Chai G, Zhang H, Zhang Y, Ma J, Wu Z, Shen X, Huang X, Luo
994 G-Z, Ji Q. 2021. Targeted genetic screening in bacteria with a Cas12k-guided transposase.
995 Cell Rep 36:109635.

996 24. Trujillo Rodríguez L, Ellington AJ, Reisch CR, Chevrette MG. 2023. CRISPR-Associated
997 Transposase for Targeted Mutagenesis in Diverse Proteobacteria. ACS Synth Biol
998 12:1989–2003.

999 25. Roberts A, Nethery MA, Barrangou R. 2022. Functional characterization of diverse type I-F
1000 CRISPR-associated transposons. Nucleic Acids Res 50:11670–11681.

1001 26. Hsieh S-C, Peters JE. 2023. Discovery and characterization of novel type I-D CRISPR-
1002 guided transposons identified among diverse Tn7-like elements in cyanobacteria. Nucleic
1003 Acids Res 51:765–782.

1004 27. Walker MWG, Klompe SE, Zhang DJ, Sternberg SH. 2023. Novel molecular requirements
1005 for CRISPR RNA-guided transposition. Nucleic Acids Res 51:4519–4535.

1006 28. Gelsinger DR, Vo PLH, Klompe SE, Ronda C, Wang H, Sternberg SH. 2023. Bacterial
1007 genome engineering using CRISPR RNA-guided transposases. bioRxiv
1008 2023.03.18.533263.

1009 29. Hoffmann FT, Kim M, Beh LY, Wang J, Vo PLH, Gelsinger DR, George JT, Acree C,
1010 Mohabir JT, Fernández IS, Sternberg SH. 2022. Selective TnsC recruitment enhances the
1011 fidelity of RNA-guided transposition. Nature 609:384–393.

1012 30. Halpin-Healy TS, Klompe SE, Sternberg SH, Fernández IS. 2020. Structural basis of DNA
1013 targeting by a transposon-encoded CRISPR-Cas system. Nature 577:271–274.

1014 31. Klompe SE, Vo PLH, Halpin-Healy TS, Sternberg SH. 2019. Transposon-encoded
1015 CRISPR–Cas systems direct RNA-guided DNA integration. Nature 571:219.

1016 32. Garza Elizondo AM, Chappell J. 2024. Targeted Transcriptional Activation Using a
1017 CRISPR-Associated Transposon System. ACS Synth Biol 13:328–336.

1018 33. Cain AK, Barquist L, Goodman AL, Paulsen IT, Parkhill J, van Opijnen T. 2020. A decade of
1019 advances in transposon-insertion sequencing. Nat Rev Genet 21:526–540.

1020 34. Petassi MT, Hsieh S-C, Peters JE. 2020. Guide RNA Categorization Enables Target Site
1021 Choice in Tn7-CRISPR-Cas Transposons. Cell 183:1757-1771.e18.

1022 35. Banta AB, Enright AL, Siletti C, Peters JM. 2020. A High-efficacy CRISPRi System for
1023 Gene Function Discovery in Zymomonas mobilis. Appl Environ Microbiol
1024 https://doi.org/10.1128/AEM.01621-20.

1025 36. Hall AN, Hall BW, Kinney KJ, Olsen GG, Banta AB, Noguera DR, Donohue TJ, Peters JM.
1026 2023. Tools for Genetic Engineering and Gene Expression Control in Novosphingobium
1027 aromaticivorans and Rhodobacter sphaeroides. bioRxiv 2023.08.25.554875.

1028 37. Enright AL, Banta AB, Ward RD, Rivera Vazquez J, Felczak MM, Wolfe MB, TerAvest MA,
1029 Amador-Noguez D, Peters JM. 2023. The genetics of aerotolerant growth in an
1030 alphaproteobacterium with a naturally reduced genome. mBio e0148723.

1031 38. Rice LB. 2008. Federal funding for the study of antimicrobial resistance in nosocomial
1032 pathogens: no ESKAPE. J Infect Dis 197:1079–1081.

1033 39. Fenster JA, Werner AZ, Tay JW, Gillen M, Schirokauer L, Hill NC, Watson A, Ramirez KJ,
1034 Johnson CW, Beckham GT, Cameron JC, Eckert CA. 2022. Dynamic and single cell
1035 characterization of a CRISPR-interference toolset in Pseudomonas putida KT2440 for β-
1036 ketoadipate production from p-coumarate. Metab Eng Commun 15:e00204.

1037 40. Hau HH, Gralnick JA. 2007. Ecology and biotechnology of the genus Shewanella. Annu
1038 Rev Microbiol 61:237–258.

1039 41. Prasad NK, Seiple IB, Cirz RT, Rosenberg OS. 2022. Leaks in the Pipeline: a Failure
1040 Analysis of Gram-Negative Antibiotic Development from 2010 to 2020. Antimicrobial
1041 Agents and Chemotherapy 66:e00054-22.

1042 42. Palmer AC, Kishony R. 2014. Opposing effects of target overexpression reveal drug
1043 mechanisms. Nat Commun 5:4296.

1044 43. Couce A, Briales A, Rodríguez-Rojas A, Costas C, Pascual A, Blázquez J. 2012.
1045 Genomewide overexpression screen for fosfomycin resistance in Escherichia coli: MurA
1046 confers clinical resistance at low fitness cost. Antimicrob Agents Chemother 56:2767–
1047 2769.

1048 44. Ason B, Reznikoff WS. 2004. DNA sequence bias during Tn5 transposition. J Mol Biol
1049 335:1213–1225.

1050 45. Lee J-H, Lee K-L, Yeo W-S, Park S-J, Roe J-H. 2009. SoxRS-mediated lipopolysaccharide
1051 modification enhances resistance against multiple drugs in Escherichia coli. J Bacteriol
1052 191:4441–4450.

1053 46. Seo SW, Kim D, Szubin R, Palsson BO. 2015. Genome-wide Reconstruction of OxyR and
1054 SoxRS Transcriptional Regulatory Networks under Oxidative Stress in Escherichia coli K-
1055 12 MG1655. Cell Rep 12:1289–1299.

1056 47. Jones KM, Guest JR, Woods DD. 1961. Folic acid and the synthesis of methionine by
1057 extracts of Escherichia coli. Biochem J 79:566–574.

1058 48. Weissbach H, Brot N. 1991. Regulation of methionine synthesis in Escherichia coli. Mol
1059 Microbiol 5:1593–1597.

1060 49. Saint-Girons I, Duchange N, Zakin MM, Park I, Margarita D, Ferrara P, Cohen GN. 1983.
1061 Nucleotide sequence of metF, the E. coli structural gene for 5-10 methylene
1062 tetrahydrofolate reductase and of its control region. Nucleic Acids Res 11:6723–6732.

1063 50. Girgis HS, Hottes AK, Tavazoie S. 2009. Genetic architecture of intrinsic antibiotic
1064 susceptibility. PLoS One 4:e5629.

1065 51. Nichols RJ, Sen S, Choo YJ, Beltrao P, Zietek M, Chaba R, Lee S, Kazmierczak KM, Lee
1066 KJ, Wong A, Shales M, Lovett S, Winkler ME, Krogan NJ, Typas A, Gross CA. 2011.
1067 Phenotypic landscape of a bacterial cell. Cell 144:143–156.

1068 52. Giladi M, Altman-Price N, Levin I, Levy L, Mevarech M. 2003. FolM, a new chromosomally
1069 encoded dihydrofolate reductase in Escherichia coli. J Bacteriol 185:7015–7018.

1070 53. Rao TVP, Kuzminov A. 2020. Exopolysaccharide defects cause hyper-thymineless death in
1071 Escherichia coli via massive loss of chromosomal DNA and cell lysis. Proc Natl Acad Sci U
1072 S A 117:33549–33560.

1073 54. Metcalf WW, Wanner BL. 1991. Involvement of the Escherichia coli phn (psiD) gene cluster
1074 in assimilation of phosphorus in the form of phosphonates, phosphite, Pi esters, and Pi. J
1075 Bacteriol 173:587–600.

1076 55. Turner AK, Yasir M, Bastkowski S, Telatin A, Page AJ, Charles IG, Webber MA. 2020. A
1077 genome-wide analysis of Escherichia coli responses to fosfomycin using TraDIS-Xpress
1078 reveals novel roles for phosphonate degradation and phosphate transport systems. J
1079 Antimicrob Chemother 75:3144–3151.

1080 56. Yethon JA, Heinrichs DE, Monteiro MA, Perry MB, Whitfield C. 1998. Involvement of waaY,
1081 waaQ, and waaP in the modification of Escherichia coli lipopolysaccharide and their role in
1082 the formation of a stable outer membrane. J Biol Chem 273:26310–26316.

1083 57. Jacobson TB, Adamczyk PA, Stevenson DM, Regner M, Ralph J, Reed JL, Amador-
1084 Noguez D. 2019. 2H and 13C metabolic flux analysis elucidates in vivo thermodynamics of
1085 the ED pathway in Zymomonas mobilis. Metabolic Engineering 54:301–316.

1086 58. Erickson JW, Gross CA. 1989. Identification of the sigma E subunit of Escherichia coli RNA
1087 polymerase: a second alternate sigma factor involved in high-temperature gene
1088 expression. Genes Dev 3:1462–1471.

1089 59. Newman JD, Falkowski MJ, Schilke BA, Anthony LC, Donohue TJ. 1999. The Rhodobacter
1090 sphaeroides ECF sigma factor, sigma(E), and the target promoters cycA P3 and rpoE P1. J
1091 Mol Biol 294:307–320.

1092 60. Partridge SR, Kwong SM, Firth N, Jensen SO. 2018. Mobile Genetic Elements Associated
1093 with Antimicrobial Resistance. Clin Microbiol Rev 31:e00088-17.

1094 61. Martínez-García E, Aparicio T, de Lorenzo V, Nikel PI. 2014. New transposon tools tailored
1095 for metabolic engineering of gram-negative microbial cell factories. Front Bioeng
1096 Biotechnol 2:46.

1097 62. Yang Q, Yang Y, Tang Y, Wang X, Chen Y, Shen W, Zhan Y, Gao J, Wu B, He M, Chen S,
1098 Yang S. 2020. Development and characterization of acidic-pH-tolerant mutants of
1099 Zymomonas mobilis through adaptation and next-generation sequencing-based genome
1100 resequencing and RNA-Seq. Biotechnol Biofuels 13:144.

1101 63. Dubois L, Vettiger A, Buss JA, Bernhardt TG. 2025. Using fluorescently labeled wheat
1102 germ agglutinin to track lipopolysaccharide transport to the outer membrane in Escherichia
1103 coli. mBio 16:e0395024.

1104 64. Kamat SS, Williams HJ, Raushel FM. 2011. Intermediates in the transformation of
1105 phosphonates to phosphate by bacteria. Nature 480:570–573.

1106 65. Amstrup SK, Ong SC, Sofos N, Karlsen JL, Skjerning RB, Boesen T, Enghild JJ, Hove-
1107 Jensen B, Brodersen DE. 2023. Structural remodelling of the carbon-phosphorus lyase
1108 machinery by a dual ABC ATPase. Nat Commun 14:1001.

1109 66. Tenaillon O, Rodríguez-Verdugo A, Gaut RL, McDonald P, Bennett AF, Long AD, Gaut BS.
1110 2012. The molecular diversity of adaptive convergence. Science 335:457–461.

1111 67. Banta AB, Ward RD, Tran JS, Bacon EE, Peters JM. 2020. Programmable Gene
1112 Knockdown in Diverse Bacteria Using Mobile-CRISPRi. Curr Protoc Microbiol 59:e130.

1113 68. Sharan SK, Thomason LC, Kuznetsov SG, Court DL. 2009. Recombineering: a
1114 homologous recombination-based method of genetic engineering. Nat Protoc 4:206–223.

1115 69. Thomason LC, Costantino N, Court DL. 2007. E. coli genome manipulation by P1
1116 transduction. Curr Protoc Mol Biol Chapter 1:1.17.1-1.17.8.

1117 70. Cherepanov PP, Wackernagel W. 1995. Gene disruption in Escherichia coli: TcR and KmR
1118 cassettes with the option of Flp-catalyzed excision of the antibiotic-resistance determinant.
1119 Gene 158:9–14.

1120 71. Peters JM, Koo B-M, Patino R, Heussler GE, Hearne CC, Qu J, Inclan YF, Hawkins JS, Lu
1121 CHS, Silvis MR, Harden MM, Osadnik H, Peters JE, Engel JN, Dutton RJ, Grossman AD,
1122 Gross CA, Rosenberg OS. 2019. Enabling genetic analysis of diverse bacteria with Mobile-
1123 CRISPRi. Nature Microbiology 4:244–250.

1124 72. Livak KJ, Schmittgen TD. 2001. Analysis of relative gene expression data using real-time
1125 quantitative PCR and the 2(-Delta Delta C(T)) Method. Methods 25:402–408.

1126 73. Martin M. 2011. Cutadapt removes adapter sequences from high-throughput sequencing
1127 reads. 1. EMBnet.journal 17:10–12.

1128 74. Langmead B, Trapnell C, Pop M, Salzberg SL. 2009. Ultrafast and memory-efficient
1129 alignment of short DNA sequences to the human genome. Genome Biology 10:R25.

75. Li H, Handsaker B, Wysoker A, Fennell T, Ruan J, Homer N, Marth G, Abecasis G, Durbin R, 1000 Genome Project Data Processing Subgroup. 2009. The Sequence Alignment/Map format and SAMtools. Bioinformatics 25:2078–2079.

76. Bushnell B. 2014. BBMap: A Fast, Accurate, Splice-Aware Aligner.

Acknowledgements

We thank members of the Peters lab and Michael Thomas for helpful discussions, Joshua Hyman and the University of Wisconsin-Madison Biotechnology Center for technical assistance with Illumina sequencing, and Samuel Sternberg for plasmids. This material is based upon work supported by the Great Lakes Bioenergy Research Center, U.S. Department of Energy, Office of Science, Biological and Environmental Research Program under Award Number DE-SC0018409. This work was also supported by the National Institutes of Health 1R35GM150487-01 to J.M.P. and by the Advanced Research Projects Agency for Health, under award number 1AYSAX000005-01 to J.M.P.

Author contributions

A.B.B. and J.M.P. designed, performed, and interpreted the experiments and wrote the manuscript with input from all authors. K.S.M. and A.N.H. developed the data analysis pipeline and performed data analysis. R.D.W. and M.P. developed code. B.C.D, R.A.C., C.C.F., and E.E.B performed experiments.

Competing interests

The authors declare no competing interests.

Figure legends

Figure 1. A CRISPR-associated transposition (CAST) system for targeted, genome-scale overexpression in Proteobacteria called “CRISPRtOE” (CRISPR transposition and OverExpression). CRISPRtOE precisely delivers a transposon with an outward facing promoter upstream of genes to facilitate overexpression. CRISPRtOE can upregulate gene expression in medically and industrially-relevant Proteobacterial species. Genome-scale CRISPRtOE screens in model (*E. coli*) and non-model (*Zymomonas mobilis*) Proteobacteria can be used to define genes required for resistance to antibiotics or biofuel production stressors.

1162

1163 **Figure 2.** A mobilizable, selectable, dual-plasmid system for CRISPR-guided transposition**.** (A)
1164 Schematic of mechanism of *Vibrio cholera* Type I-F CRISPR-associated transposon (VcCAST)
1165 system(20, 21)**.** (B) Schematic of strain construction using the CRISPRt targeted transposition
1166 system. Plasmids have pir-dependent origins of replication preventing replication in the bacterial
1167 recipient. One plasmid encodes the minimal Type I-F CRISPR-Cas (Cas678) and Tn*7*-like
1168 transposase (TnsABC and TniQ) machinery, and a second plasmid contains a transposon
1169 carrying the guide RNA and antibiotic resistance expression cassettes (see Figure S1 for
1170 details). These plasmids are transferred by co-conjugation to a recipient bacterium by *E. coli*
1171 donor strains with a chromosomal copy of the RP4 transfer machinery. Inside the recipient cell,
1172 the transposon (flanked in yellow) is inserted onto the chromosome at a site determined by the
1173 sequence of the guide RNA. Selection on antibiotic plates lacking diaminopimelic acid (DAP)
1174 selects for transconjugants and against the *E. coli* donor strains. (C) Specificity of CRISPRt
1175 disruption of *gfp* in *E. coli* measured by Tnseq. Mapping of location of transposon insertion sites
1176 to the *E. coli* genome after CRISPRt targeted transposition with the *gfp1* guide (226,671 reads).
1177 (D) Transposition efficiency of 3 individual CRISPRt guides (T03, T09, T21) targeting *mScarlet-I*
1178 cassettes in the *E. coli att*$_{Tn7}$ site either with a promoter (+ transcription) or without a promoter (-
1179 transcription) measured by plating efficiency with and without selection (+/- kanamycin) in
1180 triplicate. Red arrows indicate fold change in efficiency without and with transcription. Error
1181 represents the average of n=3 assays, * indicates $p<0.05$, two-tailed t-test.
1182

1183 **Figure 3.** Tunable overexpression of chromosomally located genes using CRISPRtOE**.** (A)
1184 Schematic of the CRISPRtOE targeted overexpression system. The test chromosomal target is
1185 an *mScarlet-I* gene preceded by a 'Landing Pad' (LP) with no promoter, a PAM, and the *LZ1*
1186 protospacer (see Figure S6C). The CRISPRtOE construct has a transposon carrying guide RNA
1187 and antibiotic resistance expression cassettes and an outward facing promoter (see Figure S6B
1188 for details). Co-conjugation of strains carrying the CRISPRtOE construct and the CRISPRt-H
1189 plasmid (harboring the VcCAST machinery) with a promoterless 'LP' *mScarlet-I* reporter
1190 recipient strain results in a CRISPRtOE test strain. (B) mScarlet-I fluorescence analysis of *E.*
1191 *coli* CRISPRtOE isolates (no promoter or synthetic promoters A, V, and H) compared to the
1192 parent (promoterless 'LP' *mScarlet-I*) strain. CRISPRtOE transposon insertion position and
1193 fluorescence measurements were determined for twelve isolates. Fluorescence measurements
1194 were normalized to cell density (OD_{600}). On target, RL orientation isolates are shown here, see
1195 Figure S7B for all orientations and Table S6 for values. Error is expressed for the median value

1196 of 8-12 isolates in n=3 assays. (C) Fold effect of CRISPRtOE mScarlet-I overexpression using
1197 synthetic promoter H in eight Alpha- and Gammaprotebacteria (*E. coli* (*Eco*), *Enterobacter*
1198 *cloacae* (*Ecl*), *Klebsiella pneumoniae* (*Kpn*), *Acinetobacter baumannii* (*Aba*), *Pseudomonas*
1199 *aeruginosa* (*Pae*), *Pseudomonas putida* (*Ppu*), *Zymomonas mobilis* (*Zmo*), and *Shewanella*
1200 *oneidensis* (*Son*)). CRISPRtOE transposon insertion position and fluorescence measurements
1201 were determined for twelve isolates. Fluorescence measurements were normalized to cell
1202 density (OD_{600}). Values are shown for isolates with on-target, RL orientation CRISPRtOE
1203 insertions and fold changes for on-target and RL orientation CRISPRtOE isolates compared to a
1204 strain with promoterless *mScarlet-I* (see Table S6 for details). Error is expressed for the median
1205 value of 8-12 isolates in n=3 (*Eco* and *Zmo*) or n=2 (*Ecl*, *Kpn*, *Aba*, *Pae*, *Ppu*, and *Son*) assays.
1206
1207 **Figure 4.** Genome-scale CRISPRtOE**.** (A) Schematic of genome-scale CRISPRtOE experiment
1208 including design and construction of libraries, experimental screen, bioinformatic data
1209 processing, and validation. Bioinformatic steps are in purple and experimental steps are in blue.
1210 Ten gRNAs were designed to guide insertion of the Tn6677 transposon (with or without a
1211 promoter) upstream of all genes. Pooled CRISPRtOE libraries grown in the presence of sub-
1212 lethal concentrations of ihibitors (e.g. *E. coli*: trimethoprim and fosfomycin antibiotics; *Z. mobilis*:
1213 switchgrass hydrolysate) and were screened for fitness by Tn-seq before and after treatment.
1214 Data were analyzed by counting reads that were in the R-L orientation upstream of genes to
1215 discover fitness phenotypes dependent on gene overexpression. Individual strains
1216 overexpressing genes with CRISPRtOE or from a plasmid were constructed to validate
1217 phenotypes outside of the pooled context. (B) Positions of CRISPRtOE insertions upstream of
1218 all genes in the genome. Insertion site distance d was calculated based on the distance in bp
1219 from the 3′ end of the Tn to the 5′ end of the gene. CRISPRtOE Tn insertions shown in red. For
1220 comparison, random/untargeted insertions from a Tn*5* library are shown in green. (C)
1221 CRISPRtOE insertions into the *E. coli lac* locus showing precise placement upstream of genes
1222 compared to a library constructed with Tn*5* random transposition. The scale is capped at 20
1223 reads for visual clarity.
1224
1225 **Figure 5.** *E. coli* genome scale CRISPRtOE screen with trimethoprim. (A) Volcano plot of gRNA
1226 spacer counts in trimethoprim (TMP) versus dimethylsulfoxide (DMSO) control. Each dot
1227 represents a strain with a spacer targeting upstream of a gene. Those that are not statistically
1228 significant (false discovery rate (FDR) > 0.05) are shown in light grey and significant hits (FDR $\leq$
1229 0.05) are shown in dark gray. Several outliers are colored: e.g. *folA* (red), *metF* (blue),

1230 *rffM/wecG* (green). (B) Top 10 gene hits with increased fitness in TMP treatment. Genes must
1231 have at least a 4-fold change in the CRISPRtOE-Promoter H data and show a 4-fold difference
1232 in a comparison between Promoter H (red bars) and no promoter (blue bars) to be considered.
1233 Dots represent unique insertions. Error bars represent standard deviation (SD). (C) Liquid MIC
1234 assay showing resistance of strains overexpressing *metF* from a plasmid to TMP. Error bars
1235 represent SD of triplicate assays. Significance was determined by a t test ($\leq$0.05(*), $\leq$0.01(**),
1236 $\leq$0.001(***)). (D) *E. coli* Enterobacterial Common Antigen (ECA) biosynthesis (*rff*/*wec*) operon.
1237 (E) Liquid MIC assay showing resistance of strains overexpressing *rffM* from a plasmid to TMP.
1238 Error bars represent SD of triplicate assays. Significance was determined by a t test ($\leq$0.05(*),
1239 $\leq$0.01(**), $\leq$0.001(***)). (F) Growth assay of strains overexpressing *rffM* from a plasmid in
1240 additional chemical conditions (Biolog phenotypic array plate PM16 comprised of 24
1241 compounds). Two concentrations of CRISPRtOE screen chemicals FOS (no response
1242 expected) and TMP (response expected), and of two additional chemical that had a significant
1243 response (diamide and rifamycin) are shown. Duplicate assays are shown (Rep1 and Rep2).
1244 Significance was determined by a t test ($\leq$0.05(*), $\leq$0.01(**). See figure S14 for additional
1245 details.
1246
1247 **Figure 6.** *E. coli* genome scale CRISPRtOE screen with fosfomycin. (A) Top gene hits with
1248 increased fitness in fosfomycin (FOS) treatment. Genes must have at least a 4-fold change in
1249 the CRISPRtOE-Promoter H data and show a 4-fold difference in a comparison between
1250 Promoter H (red bars) and no promoter (blue bars) to be considered. Dots represent unique
1251 insertions. sError bars represent standard deviation (SD). (B) CRISPRtOE-Promoter H
1252 insertions with increased fitness in FOS in the *E. coli* phosphonate utilization (*phn*) operon
1253 represented by arrows. (C) Quantification of MIC test strip (Liofilchem) assay showing
1254 resistance to FOS of individual CRISPRtOE-Promoter H strains overexpressing *phnC* or *phnH*.
1255 Error bars represent SD of triplicate assays (also see figure S15B). (D) Schematic of *phnMNOP*
1256 chromosomal deletion and *phnM* complementation experiment. (E) Quantification of FOS MIC
1257 test strip (Liofilchem) assays in WT, Δ*phnMNOP* deletion, or CRISPRtOE-Promoter H-*phnC* plus
1258 Δ*phnMNOP* deletion strains that are overexpressing *phnM* from a plasmid (or empty vector
1259 control). Error bars represent SD of triplicate assays (also see figure S15D).
1260
1261 **Figure 7.** *Z. mobilis* genome scale CRISPRtOE screen with plant hydrolysate. (A) Volcano plot
1262 of gRNA spacer counts in 65% hydrolysate versus *Zymomonas* rich defined medium (ZRDM)
1263 control. Each dot represents a strain with a spacer targeting upstream of a gene. Those that are

1264 not statistically significant (false discovery rate (FDR) > 0.05) are shown in light grey and
1265 significant hits (FDR ≤ 0.05) are shown in dark gray. Several outliers are colored: *fumA* (green),
1266 *rpoE* (orange). (B) Top gene hits with increased fitness in 65% hydrolysate. Genes must have at
1267 least a 4-fold change in the CRISPRtOE-Promoter H data and show a 4-fold difference in a
1268 comparison between Promoter H (red bars) and no promoter (blue bars) to be considered. Dots
1269 represent unique insertions. Error bars represent standard deviation (SD). (C) Growth assay of
1270 individually constructed CRISPRtOE-Promoter H *rpoE* strains versus the parent strain in 65%
1271 hydrolysate or ZRDM control. Error bars represent standard deviation (SD) of three independant
1272 cultures. (D) Relative fitness of strains shown in panel (C). Growth was quantified by calculating
1273 the area under the curve (auc_e) using GrowthCurver. Fitness was normalized to control
1274 condition (parent strain in ZRDM). Significance was determined by a t test (≤0.005(***). See
1275 also Figure S16C and S16D.
1276
1277 **Figure S1.** Details of CRISPRt plasmids and *E. coli* GFP reporter strain. (A) Plasmid maps of
1278 CRISPRt-H helper and CRISPRt-T transposon plasmids. Both plasmids in the dual plasmid
1279 system have backbones with an R6K pir-dependent replication origin, an ampicillan resistance
1280 cassette, and conjugative transfer origin. The CRISPRt-H helper plasmid has expression
1281 cassettes for the minimal Vch CRISPR (Cas678) and Transposase (TnsABC, TniQ) machinery
1282 derived from pSpin-R(21). The CRISPRt-T transposon plasmid encodes a modified VchINT
1283 transposon derived from pSpin-R(21) which includes a guide RNA expression cassette with a
1284 modified BsaI cloning site and an antibiotic expression cassette and transcription terminators
1285 derived from CRISPRi plasmids(71). The antibiotic resistance cassette is flanked by XhoI sites
1286 to facilitate modification, six variants are shown. (B) Sequence of CRISPRt targeted
1287 transposition system guide RNA expression cassette including the BsaI cloning site for new
1288 guide RNAs. (C) Efficiency of obtaining CRISPRt transconjugants in *E. coli* using the *LZ1* and
1289 *gfp1* guides. Serial dilutions of three technical replicates of *LZ1* and *gfp1* CRISPRt assays were
1290 plated with and without selection (LB-kan or LB, respectively) and CFUs were compared;
1291 Efficiency of CRISPRt targeted transposition in *E. coli* with the *LZ1* guide was ~1 in 100 and
1292 with the *gfp1* guide was ~1 in 1000. **(**D) Position of the P_{veg}-*sfgfp* expression cassette inserted
1293 between *yjaA* and *yjaB* on the *E. coli* chromosome.
1294
1295 **Figure S2.** CRISPRt disruption efficiency in *E. coli*. (A) Specificity of CRISPRt disruption of *lacZ*
1296 in *E. coli* measured by Tnseq. Mapping of location of transposon insertion sites to the *E. coli*
1297 genome after CRISPRt targeted transposition the *LZ1* guide (216,801 reads). (B) Insertion

1298 position (bp downstream of protospacer) frequency of CRISPRt disruption of *gfp* and (C) *lacZ* in
1299 *E. coli* (RL orientation). Percentage of on-target, RL orientation insertions for all positions with >
1300 0.01%. (D) Efficiency of CRISPRt disruption of *sfgfp* in *E. coli* using a fluorescence phenotypic
1301 assay. The *E. coli yjaA-sfgfp-yjaB* strain (sJMP2688) is green fluorescent whereas the *E. coli*
1302 WT strain (sJMP163) is not. Isolates from CRISPRt targeted transposition of *E. coli yjaA-sfgfp-*
1303 *yjaB* with the *gfp1* guide (selection for transconjugants on LB-kan plates) were assayed for
1304 fluorescence; 82/84 (97.6%) were white indicating disruption of *sfgfp*. (E) Efficiency of CRISPRt
1305 disruption of *lacZ* in *E. coli* using an X-gal phenotypic assay. The *E. coli* WT strain (sJMP163)
1306 can metabolize X-gal resulting in a blue colony color whereas the *E. coli lacZYA* deletion strain
1307 (sJMP3272) cannot metabolize X-gal resulting in a white colony color. Isolates from CRISPRt
1308 targeted transposition of *E. coli* WT with the *LZ1* guide (selection for transconjugants on LB-kan
1309 plates) were assayed for colony color; 90/90 (100%) were white indicating disruption of *lacZ*. (F)
1310 Frequency of co-integration of transposon-containing plasmid versus transposition of
1311 transposon only. *E. coli* CRISPRtOE libraries (sJMP10705 and sJMP10706) were serially
1312 diluted and plated on LB, LB-kan, and LB-carb in triplicate to determine total CFU, CFU with
1313 selection for transposon, CFU with selection for insertion of entire transposon-containing
1314 plasmid.
1315
1316 **Figure S3.** Transcription impacts efficacy of CRISPRt guides**.** (A) Schematic of guides in pooled
1317 *mScarlet-I* disruption experiment. Twenty-three guides matching protospacers located on top
1318 (T1-24) or bottom (B1-24) strand of the mScarlet-I encoding gene with a range of CN guides
1319 (see Table S5 for details). (B) Relative efficacy of CRISPRt *mScarlet-I* guides in a pooled screen
1320 targeting *mScarlet-I* expressed from a transposon in the att_{Tn7} site on the *E. coli* chromosome.
1321 Relative efficacy is expressed as the $\log_2$-fold change of the frequency in the CRISPRt libraries
1322 (sJMP10519 and sJMP10520) vs. the frequency in the original plasmid construct libraries
1323 (sJMP10505 and sJMP10506). Average and standard deviation of two separate CRISPRt
1324 libraries (gentamicin^R and kanamycin^R) containing all 46 guides. (C) Relative efficacy data
1325 ordered by guide position rather than efficacy shows no correlation between position and
1326 efficacy. (D) No correlation between PAM sequence (CA, CC, CG, CT) and efficacy (frequency
1327 of insertion) for 46 *mScarlet-I* targeting guides.
1328
1329 **Figure S4**. Transcription impacts efficacy of CRISPRt guides. (A) Schematic of *mScarlet-I*
1330 cassettes +/- promoter on the *E. coli* chromosome. The *mScarlet-I* expression cassette (red)
1331 with and without a promoter (orange) along with a spectinomycin resistance cassette (spt^R,

1332 brown) are located on the *E. coli* chromosome just downstream of *glmS* and upstream of *pstS*.
1333 The *mScarlet-I* expression cassette is inserted in one of two orientations so that the direction of
1334 transcription is either in the same or the opposite direction of the leading strand of chromosomal
1335 DNA replication. (B) Relative efficacy of CRISPRt *mScarlet-I* guides in a pooled screen targeting
1336 *mScarlet-I* expressed on the *E. coli* chromosome in different orientations with and without
1337 transcription. Relative efficacy is expressed as the log2-fold change of the frequency in the
1338 CRISPRt libraries (sJMP10519-10520, sJMP10594-10595, sJMP10637-10640) vs. the
1339 frequency in the original plasmid construct libraries (sJMP10505 and sJMP10506) with average
1340 and standard deviation of two separate CRISPRt libraries (gentamicin^R and kanamycin^R)
1341 containing all 46 guides shown.
1342
1343 **Figure S5.** Transcription impacts efficacy of CRISPRt guides, continued. (A) Relative efficacy of
1344 CRISPRt gRNAs in a pooled screen targeting *mScarlet-I* as in Figure S4 with average and
1345 standard deviation of two separate CRISPRt libraries (gentamicin^R and kanamycin^R) containing
1346 all 46 guides shown on scatter plots. (B) Fluorescent phenotypes of 80 isolates from each of the
1347 *E. coli* CRISPRt *mScarlet-I* individual guide libraries (sJMP10641-10646) compared to *E. coli*
1348 strains with no *mScarlet-I* gene ((-) mScar, sJMP6999) or expressing *mScarlet-I* ((+) mScar,
1349 sJMP10205). Only 4/480 (0.83%) retained *mScarlet-I* levels equal to the parent strain indicating
1350 an off-target rate of <1% overall.
1351
1352 **Figure S6.** CRISPRtOE construct details. (A) Sequence alignment of CRISPRtOE promoters A,
1353 H, and V compared to a consensus *E. coli* σ^{70} promoter. Promoter A is based on the *lacUV5*
1354 promoter. Promoter H and V are synthetic promoters. Promoter H has an UP element
1355 highlighted in yellow. (B) Schematics of CRISPRtOE Tn*7*-like transposon constructs with four
1356 different outward facing promoter sequences (no promoter, and constitutive promoters A, H, and
1357 V; see Table S3 for plasmid details). Plasmids have been submitted to Addgene (ID 225832-
1358 225871). (C) Schematic of the chromosomally-encoded promoterless *mScarlet-I* reporter
1359 contained on a Tn*7* transposon inserted into the att_{Tn7} site of *E. coli*.
1360
1361 **Figure S7.** Tunable overexpression of chromosomally located genes using CRISPRtOE.
1362 (A) Quantification by qPCR of the *E. coli* CRISPRtOE-P_H-*mScarlet-I* strain versus the
1363 promoterless 'Landing Pad' parent strain. Assay was repeated twice each with three biological
1364 replicates. *mScarlet-I* expression was normalized to expression of *rho*. (B) mScarlet-I
1365 fluorescence analysis of *E. coli* CRISPRtOE isolates (no promoter or synthetic promoters A, V,

1366 and H) compared to the parent (promoterless *mScarlet-I*) strain. As in Figure 2B except values
1367 are shown for all CRISPRtOE isolates (both RL and LR insertion orientations with RL shown in
1368 black and LR (flipped) shown in red). Error is expressed for the median value of 12 isolates in
1369 three replicate assays. (C) mScarlet-I fluorescence analysis of CRISPRtOE isolates of the
1370 Alphaproteobacterium *Zymomonas mobilis* (no promoter or synthetic promoters A, V, and H)
1371 compared to the parent (promoterless *mScarlet-I*) strain. Values are shown for isolates with on-
1372 target, RL orientation CRISPRtOE insertions. Error is expressed for the median value of 8-12
1373 isolates in three replicate assays. (D) Schematic showing insertion of CRISPRtOE transposon
1374 into the 'Landing Pad' upstream of *mScarlet-I*. Insertion position is variable (~45-55bp
1375 downstream of protospacer) resulting in a variable amount of the Landing Pad (containing the
1376 RBS) remaining upstream of the *mScarlet-I* coding sequence. Insertion positions and orientation
1377 of CRISPRtOE isolates in the eight species shown in Figure 2C. Insertion position is expressed
1378 relative to start of *mScarlet-I* coding sequence (equal to the remaining LP sequence).
1379
1380 **Figure S8.** CRISPRtOE *folA* and *murA* pooled library screen and MIC assays inform antibiotic
1381 mode of action. (A) Schematic of CRISPRtOE competitive growth assay. A pooled CRISPRtOE
1382 strain library was constructed by amplification of spacer sequences from a pooled oligo library
1383 and transfer onto the chromosome of a recipient strain. Insertion of the CRISPRtOE transposon
1384 is either upstream of genes of interest (12 guides/gene) or within the *lacZ* gene as a control
1385 gene (4 guides/gene) in *E. coli*. A CRISPRtOE pooled library was screened by culturing a
1386 CRISPRtOE pooled library and control library together for multiple generations in the presence
1387 or absence of a chemical of interest (trimethoprim (TMP) for the *folA* library and fosfomycin
1388 (FOS) for the *murA* library). The change in the composition of the pooled library before and after
1389 treatment was measured by amplification and NGS sequencing of the spacer sequences. (B)
1390 CRISPRtOE *folA* pooled library screen in TMP. Fitness of pooled strains overexpressing *folA*
1391 compared to the *lacZ* control strains in the absence or presence of TMP. (C) CRISPRtOE *murA*
1392 pooled library screen in FOS. (D) Schematic of insertion position for CRISPRtOE isolates. (E)
1393 MIC broth microdilution assay of four individual CRISPRtOE *folA* strains compared to WT, a
1394 CRISPRtOE *lacZ* isolate, and the CRISPRtOE *folA* pooled library in the presence of TMP (0.04-
1395 20 µg/ml). Error is expressed for 3 separate assays. (F) MIC test strip assays (trimethoprim,
1396 0.002-32 µg/ml) comparing WT and four distinct CRISPRtOE *folA* isolates quantified as average
1397 and standard deviation of two assays. (G) MIC test strip assays (fosfomycin, 0.064-1024 µg/ml)
1398 comparing WT and four distinct CRISPRtOE *murA* isolates quantified as average and standard
1399 deviation of two assays.

1400

1401 **Figure S9.** Multiplexed CRISPRtOE strain construction. (A) Schematic of two methods of
1402 multiplexed CRISPRtOE strain construction in *E. coli*. Method 1 utilizes quad-parental mating
1403 with two CRISPRtOE transposon donors with different antibiotic resistance genes while Method
1404 2 utilizes tri-parental mating with a single transposon donor with a single antibiotic resistance
1405 gene and a CRISPR array encoding multiple guides. Guides upstream of *folA* or *murA* that were
1406 previously shown to be effective at conferring TMP or FOS resistance (see Figure S8) were
1407 used to simultaneously guide the CRISPRtOE-promoter H Tn insertion into the genome of *E.*
1408 *coli*. (B) Efficiency of multiplexed insertion of CRISPRtOE-promoter H-*folA* and CRISPRtOE-
1409 promoter H-*murA* as determined by PCR of 32 isolates. Increased TMP and FOS resistance of
1410 4 PCR-confirmed isolates was confirmed by disc diffusion assays. (C) TMP resistance of 1
1411 sequence-confirmed isolate from each of the two methods was compared to WT and previously
1412 isolated single isolates (either CRISPRtOE-promoter H-*folA* or CRISPRtOE-promoter H-*murA*.
1413 (D) FOS resistance of 1 sequence-confirmed isolate from each of the two methods was
1414 compared to WT and previously obtained single isolates (either CRISPRtOE-promoter H-*folA* or
1415 CRISPRtOE-promoter H-*murA*.

1416

1417 **Figure S10.** Tn insertion in *E.coli* and *Z. mobilis* CRISPRtOE genome-scale libraries. (A)
1418 Schematic of two possible transposon insertion positions: intergenic/entirely between genes or
1419 Tn inserted in front of a gene disrupts the end of the gene upstream of it. (B) Percentage of
1420 insertions in the *E. coli* and *Z. mobilis* genome-scale CRISPRtOE libraries that are intergenic
1421 versus in an upstream gene. (C) Percentage of Tn insertions that are on- (orange) or off- (white)
1422 target and percentage on on-target Tn insertions whose position corresponds to the encoded
1423 spacer (medium gray) or is instead near the predicted insertion position based on another
1424 'hijacked' spacer (light gray). (D) Multiplex CRISPRtOE experiment to estimate number of
1425 strains that may have multiple Tn insertions. Quad-parental mating was performed with two
1426 CRISPRtOE transposon donors with different antibiotic resistance genes (kan^R or gen^R) that
1427 were previously shown to effectively target insertion upstream of *folA* or *murA* in *E. coli.*
1428 Transconjugants selected on kan, gen, or kan and gen were quantified in three technical
1429 replicates and the difference between the number of transconjugants with a single antibiotic
1430 resistance phenotype vs. a dual antibiotic resistance phenotype was calculated.

1431

1432 **Figure S11.** Genome-scale CRISPRtOE reproducibility. (A) Comparison of two biological
1433 replicates of CRISPRtOE screen data at the gene level (CPM = counts per million). Either

1434 CRISPRtOE library with Promoter H or no promoter with either TMP or DMSO control treatment
1435 showing correlation (R^2 = ~0.9).(B) Comparison of two biological replicates of the log2FC (FC =
1436 fold change) of TMP versus DMSO control treatment for either the CRISPRtOE library with
1437 Promoter H or no promoter showing correlation (R^2 = ~0.8). (C) Comparison of the median LFC
1438 (Log Fold Change) of TMP versus DMSO control treatment for the CRISPRtOE Promoter H
1439 versus no promoter libraries showing no correlation (R^2 = ~0.007).
1440
1441 **Figure S12.** Robustness of CRISPRtOE with fewer analyzed guides. Scatterplots comparing all
1442 spacers measured in our study to subsets of 5, 4, 3, or 2 randomly selected spacers per gene.
1443
1444 **Figure S13.** *E. coli* CRISPRtOE TMP screen top positive outlier genes considering only the first
1445 gene in the operon. Genes must have at least a 4-fold change in the CRISPRtOE Promoter H
1446 data and show a 4-fold difference in a comparison between Promoter H (red) and no promoter
1447 (blue) to be considered. Dots represent unique insertions. Error bars represent standard
1448 deviation (SD).
1449
1450 **Figure S14.** Growth assay of strains overexpressing *rffM* from a plasmid in additional chemical
1451 conditions using a Biolog phenotypic array plate PM16 comprised of 24 chemicals with 4
1452 concentrations each. (A) Growth curves of are shown for CRISPRtOE screen chemicals FOS
1453 (no response expected) and TMP (response expected), and of two additional chemicals that had
1454 a significant response (diamide and rifamycin) for 3 concentrations. Error bars represent SD of
1455 duplicate assays. (B) Quantification of area under the curve (auc_e) of growth assays shown in
1456 panel (A) using GrowthCurver. Duplicate assays are shown (Rep1 and Rep2). Three
1457 concentrations are shown. Significance was determined by a t test ($\leq$0.05(*), $\leq$0.01(**). Biolog
1458 PM16 compounds tested: cefotaxime, phosphomycin, 5-chloro-7-iodo-8-hydroxyquinoline,
1459 norfloxacin, sulfanilamide, trimethoprim, dichlofluanid, protamine sulphate, cetylpyridinium
1460 chloride, 1-chloro-2,4-dinitrobenzene, diamide, cinoxacin, streptomycin, 5-azacytidine, rifamycin
1461 SV, potassium tellurite, sodium selenite, aluminum sulphate, chromium chloride, ferric chloride,
1462 L-glutamic-g-hydroxamate, glycine hydroxamate, chloroxylenol, sorbic acid.
1463
1464 **Figure S15.** *E. coli* genome scale CRISPRtOE screen with fosfomycin. (A) Volcano plot of
1465 gRNA spacer counts in fosfomycin (FOS) versus water control. Each dot represents a strain
1466 with a spacer targeting upstream of a gene. Those that are not statistically significant (false
1467 discovery rate (FDR) > 0.05) are shown in light grey and significant hits (FDR $\leq$ 0.05) are shown

1468 in dark gray. Several outliers are colored: *murA* (red), *ibaG* (yellow), *phnC-M* (blue), *waaY*
1469 (green). (B) MIC test strip (Liofilchem) assay (3 technical replicates) showing resistance to FOS
1470 of individual CRISPRtOE-Promoter H strains overexpressing *phnC* or *phnH* compared to WT.
1471 (C) MIC test strip (Liofilchem) assay (3 technical replicates) showing resistance to FOS of
1472 strains overexpressing *phnMNOP* from a plasmid with an IPTG-inducible promoter in WT or a
1473 Δ*phnMNOP* deletion strain. (D) MIC test strip (Liofilchem) assay (3 technical replicates) showing
1474 resistance to FOS of strains overexpressing *phnM* from a plasmid with an IPTG-inducible
1475 promoter in WT, Δ*phnMNOP* deletion, or Δ*phnMNOP* deletion plus CRISPRtOE-Promoter H-
1476 *phnC* overexpression strain. (E) MIC test strip (Liofilchem) assay (2 technical replicates)
1477 showing resistance to FOS of strains overexpressing *waaY* using CRISPRtOE-Promoter H (left)
1478 or from a plasmid with an IPTG-inducible promoter (right).
1479
1480 **Figure S16.** Fitness of *Z. mobilis* CRISPRtOE-Promoter H *fumA* and *rpoE* strains. (A) Growth
1481 assay of individually constructed CRISPRtOE-Promoter H *fumA* strains versus the parent strain
1482 in 65% hydrolysate or ZRDM control. Error bars represent standard deviation (SD) of three
1483 independant cultures. (B) Relative fitness of strains shown in panel (A). Growth was quantified
1484 by calculating the area under the curve (auc_e) using GrowthCurver. Fitness was normalized to
1485 control condition (parent strain in ZRDM). Significance was determined by a t test (≤0.005(***).
1486 (C) Growth assay of individually constructed CRISPRtOE-Promoter H *rpoE* strains versus the
1487 parent strain in 65% hydrolysate or ZRDM control. Error bars represent standard deviation (SD)
1488 of three independant cultures. (D) Relative fitness of strains shown in panel (C). Growth was
1489 quantified by calculating the area under the curve (auc_e) using GrowthCurver. Fitness was
1490 normalized to control condition (parent strain in ZRDM). Significance was determined by a t test
1491 (≤0.005(***).
1492
1493 **Figure S17.** Fitness of *Z. mobilis* strains overexpressing *fumA* and *rpoE* from a plasmid. (A)
1494 Growth assay of *fumA* plasmid overexpression strains versus a strain with an empty plasmid in
1495 65% hydrolysate or ZRDM control. Error bars represent standard deviation (SD) of three
1496 independant cultures. (B) Relative fitness of strains shown in panel (A). Growth was quantified
1497 by calculating the area under the curve (auc_e) using GrowthCurver. Fitness was normalized to
1498 control condition (parent strain in ZRDM). Significance was determined by a t test (<0.01(**),
1499 ≤0.005(***). (C) Growth assay of *rpoE* plasmid overexpression strains versus a strain with an
1500 empty plasmid in 65% hydrolysate or ZRDM control. Error bars represent standard deviation
1501 (SD) of three independant cultures. (D) Relative fitness of strains shown in panel (C). Growth

1502 was quantified by calculating the area under the curve (auc_e) using GrowthCurver. Fitness was
1503 normalized to control condition (parent strain in ZRDM). Significance was determined by a t test
1504 (<0.01(**), ≤0.005(***).

Figure 1

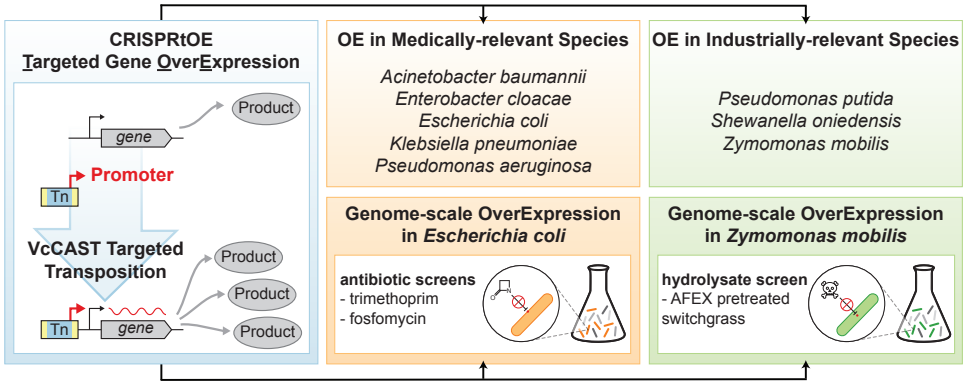
CRISPRtOE
Targeted Gene OverExpression
gene
Product
Promoter
Tn
VcCAST Targeted
Transposition
Product
Product
Product
Tn
gene
OE in Medically-relevant Species
Acinetobacter baumannii
Enterobacter cloacae
Escherichia coli
Klebsiella pneumoniae
Pseudomonas aeruginosa
OE in Industrially-relevant Species
Pseudomonas putida
Shewanella oniedensis
Zymomonas mobilis
Genome-scale OverExpression
in Escherichia coli
antibiotic screens
- trimethoprim
- fosfomycin
Genome-scale OverExpression
in Zymomonas mobilis
hydrolysate screen
- AFEX pretreated
switchgrass

Figure 2

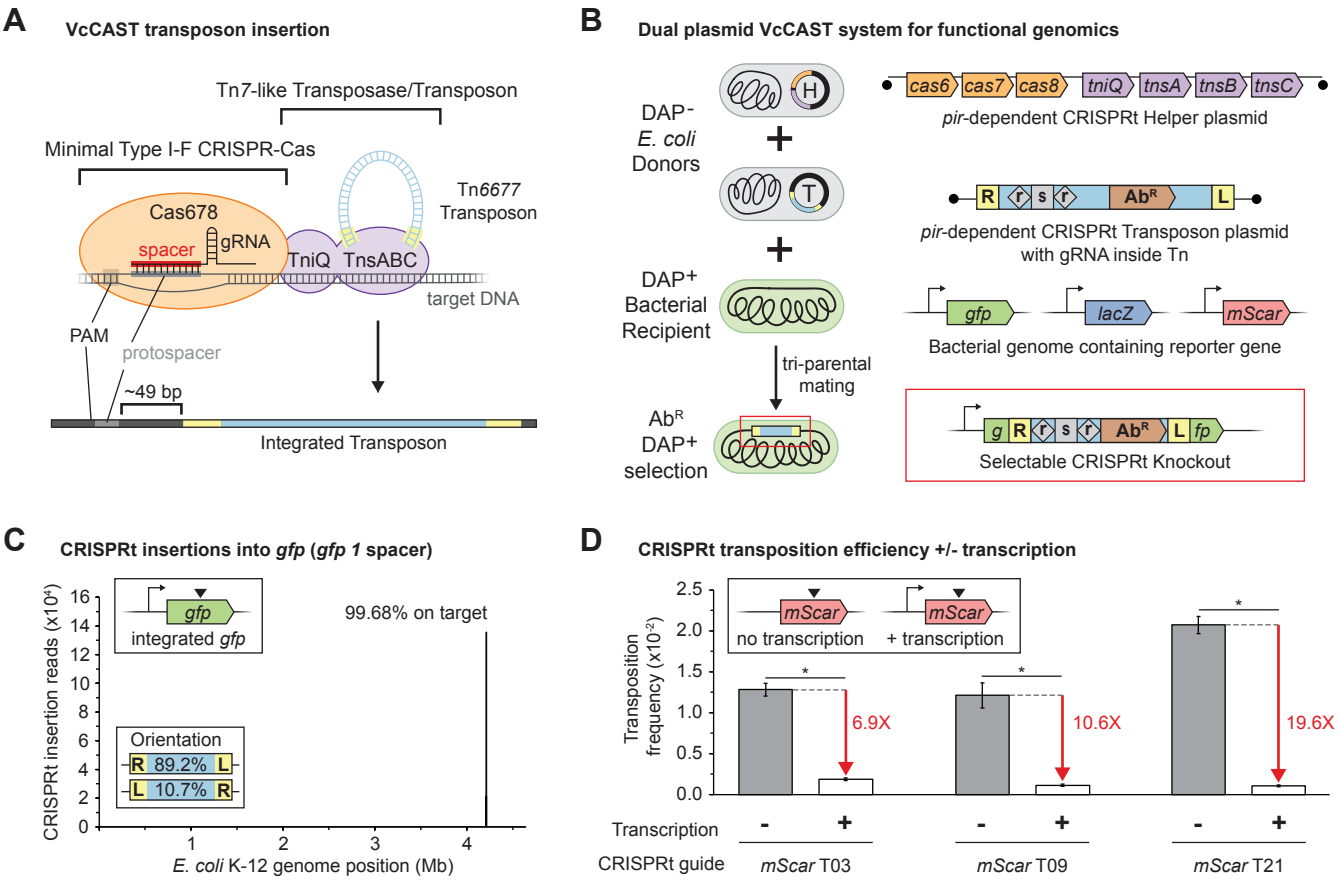
A
VcCAST transposon insertion
Tn7-like Transposase/Transposon
Minimal Type I-F CRISPR-Cas
Cas678
spacer
gRNA
TniQ
TnsABC
Tn6677 Transposon
target DNA
PAM
protospacer
~49 bp
Integrated Transposon
B
Dual plasmid VcCAST system for functional genomics
DAP⁻ E. coli Donors
H
T
cas6
cas7
cas8
tniQ
tnsA
tnsB
tnsC
pir-dependent CRISPRt Helper plasmid
R
r
s
r
AbR
L
pir-dependent CRISPRt Transposon plasmid with gRNA inside Tn
DAP⁺ Bacterial Recipient
gfp
lacZ
mScar
Bacterial genome containing reporter gene
tri-parental mating
AbR DAP⁺ selection
g
fp
Selectable CRISPRt Knockout
C
CRISPRt insertions into gfp (gfp 1 spacer)
integrated gfp
99.68% on target
Orientation
R 89.2% L
L 10.7% R
CRISPRt insertion reads (x10⁴)
E. coli K-12 genome position (Mb)
D
CRISPRt transposition efficiency +/- transcription
no transcription
+ transcription
Transposition frequency (x10⁻²)
6.9X
10.6X
19.6X
Transcription
CRISPRt guide
mScar T03
mScar T09
mScar T21

Figure 3

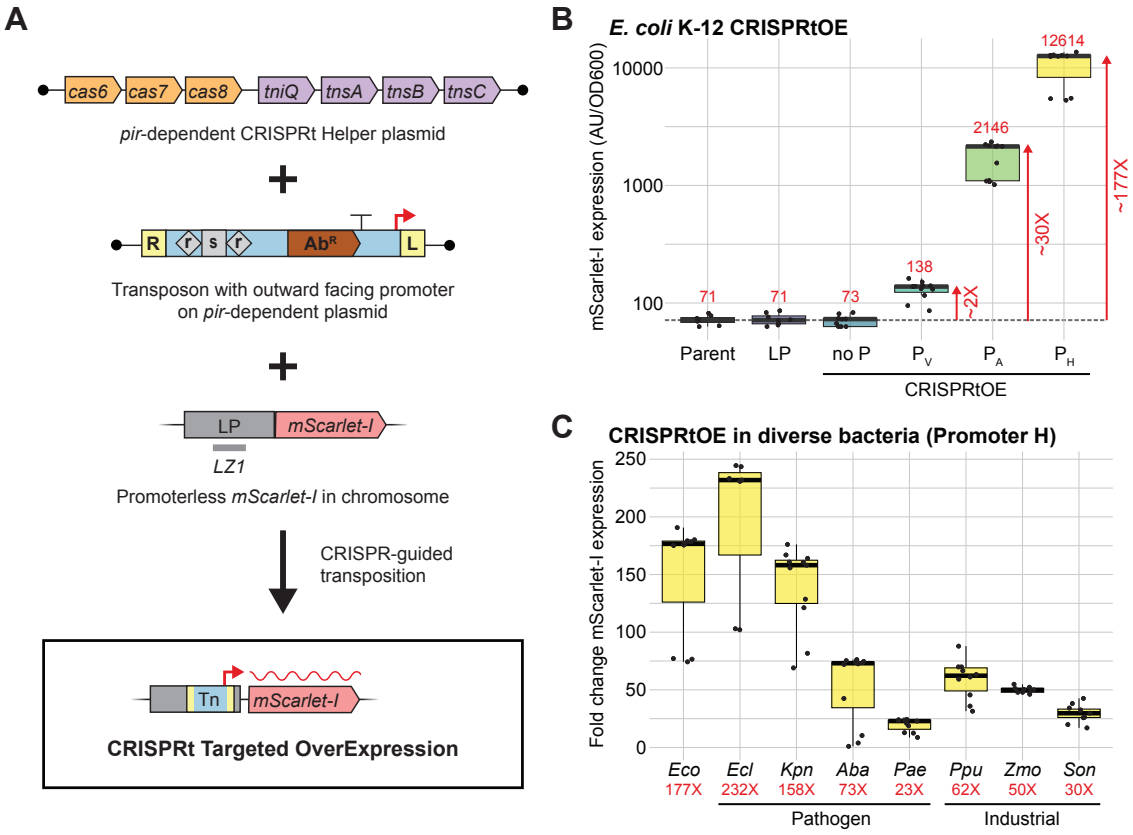
A
cas6
cas7
cas8
tniQ
tnsA
tnsB
tnsC
pir-dependent CRISPRt Helper plasmid
R
r
s
r
AbR
L
Transposon with outward facing promoter on pir-dependent plasmid
LP
mScarlet-I
LZ1
Promoterless mScarlet-I in chromosome
CRISPR-guided transposition
Tn
mScarlet-I
CRISPRt Targeted OverExpression
B
E. coli K-12 CRISPRtOE
mScarlet-I expression (AU/OD600)
10000
1000
100
71
71
73
138
2146
12614
~2X
~30X
~177X
Parent
LP
no P
PV
PA
PH
CRISPRtOE
C
CRISPRtOE in diverse bacteria (Promoter H)
Fold change mScarlet-I expression
250
200
150
100
50
0
Eco
177X
Ecl
232X
Kpn
158X
Aba
73X
Pae
23X
Ppu
62X
Zmo
50X
Son
30X
Pathogen
Industrial

Figure 4

A Genome-scale CRISPRtOE

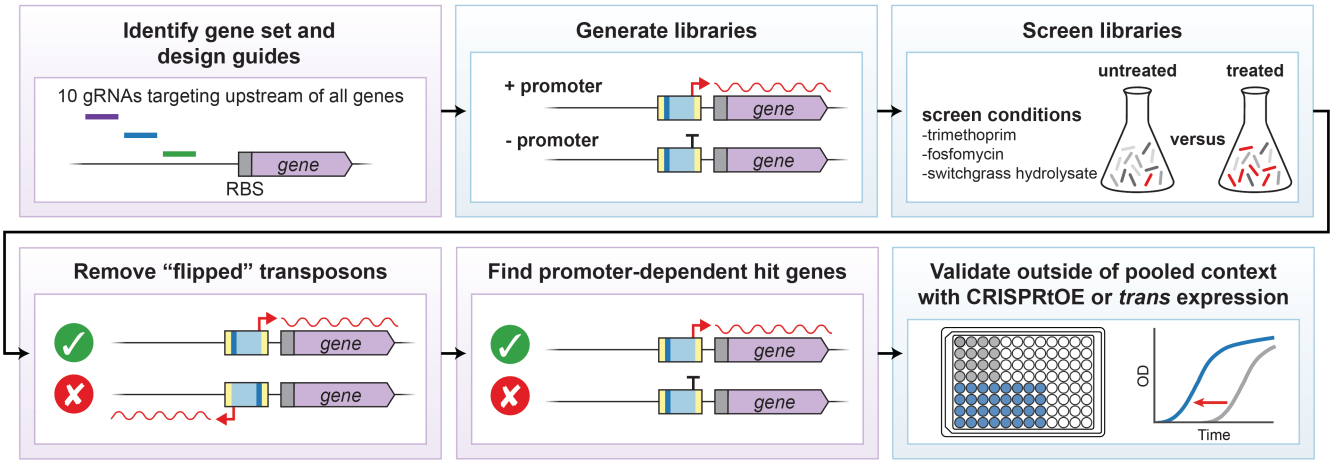

B CRISPRtOE insertions upstream of genes

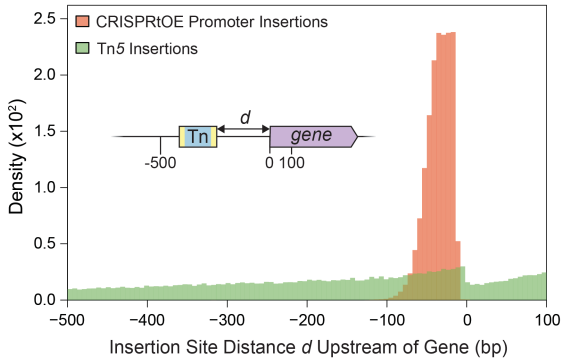

C Genome-scale CRISPRtOE in *E. coli* K-12: *lac* locus

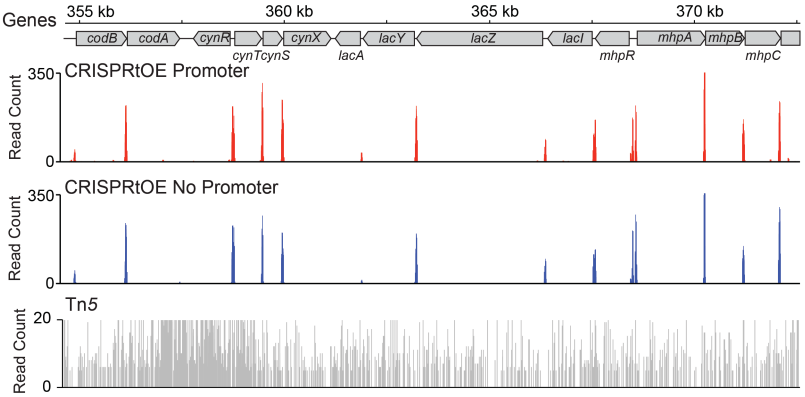

Figure 5

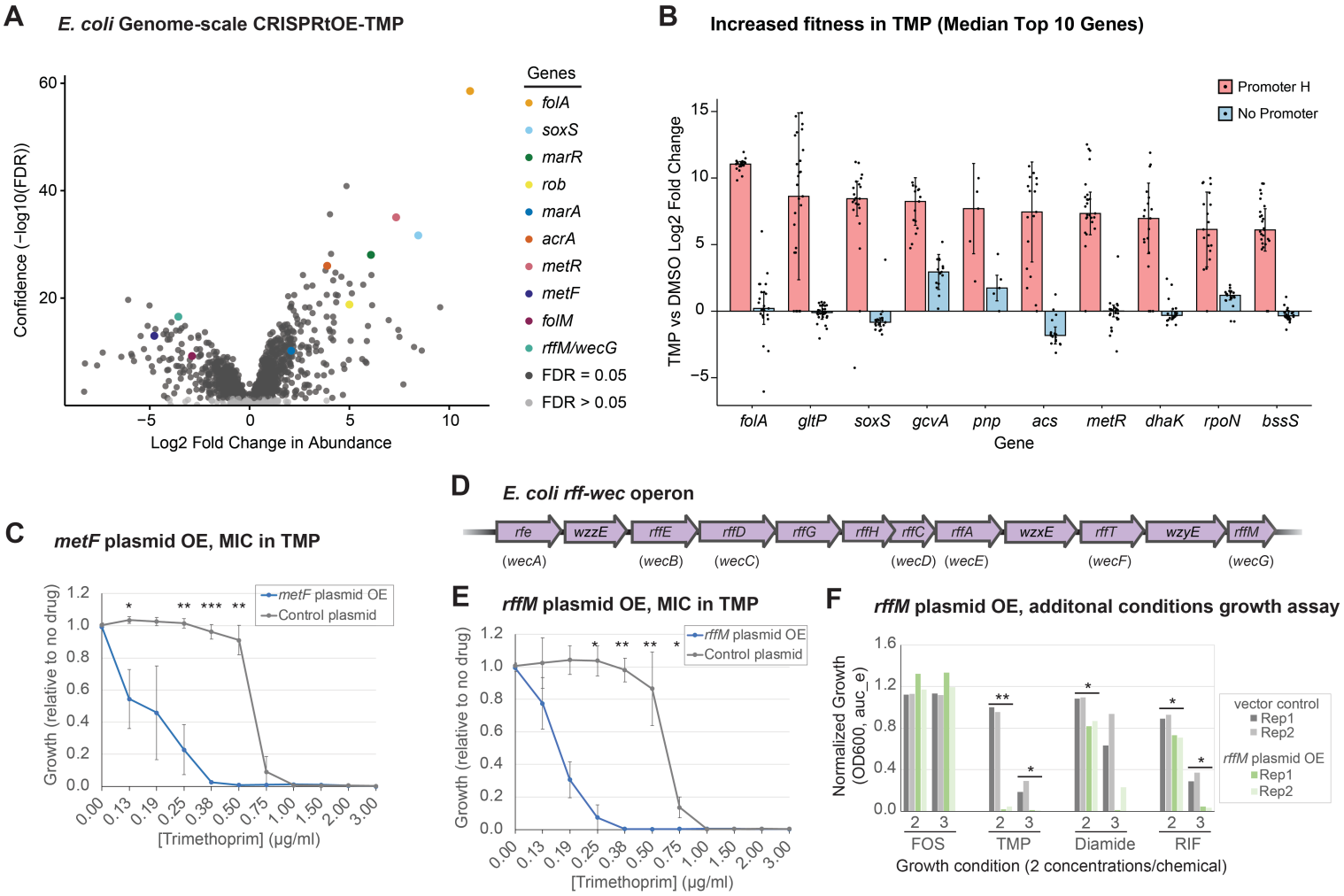
A
E. coli Genome-scale CRISPRtOE-TMP
Confidence (−log10(FDR))
Log2 Fold Change in Abundance
Genes
folA
soxS
marR
rob
marA
acrA
metR
metF
folM
rffM/wecG
FDR = 0.05
FDR > 0.05
B
Increased fitness in TMP (Median Top 10 Genes)
Promoter H
No Promoter
TMP vs DMSO Log2 Fold Change
folA gltP soxS gcvA pnp acs metR dhaK rpoN bssS
Gene
C
metF plasmid OE, MIC in TMP
metF plasmid OE
Control plasmid
Growth (relative to no drug)
[Trimethoprim] (µg/ml)
D
E. coli rff-wec operon
rfe wzzE rffE rffD rffG rffH rffC rffA wzxE rffT wzyE rffM
(wecA) (wecB) (wecC) (wecD) (wecE) (wecF) (wecG)
E
rffM plasmid OE, MIC in TMP
rffM plasmid OE
Control plasmid
Growth (relative to no drug)
[Trimethoprim] (µg/ml)
F
rffM plasmid OE, additonal conditions growth assay
Normalized Growth (OD600, auc_e)
vector control
Rep1
Rep2
rffM plasmid OE
Rep1
Rep2
FOS TMP Diamide RIF
Growth condition (2 concentrations/chemical)

Figure 6

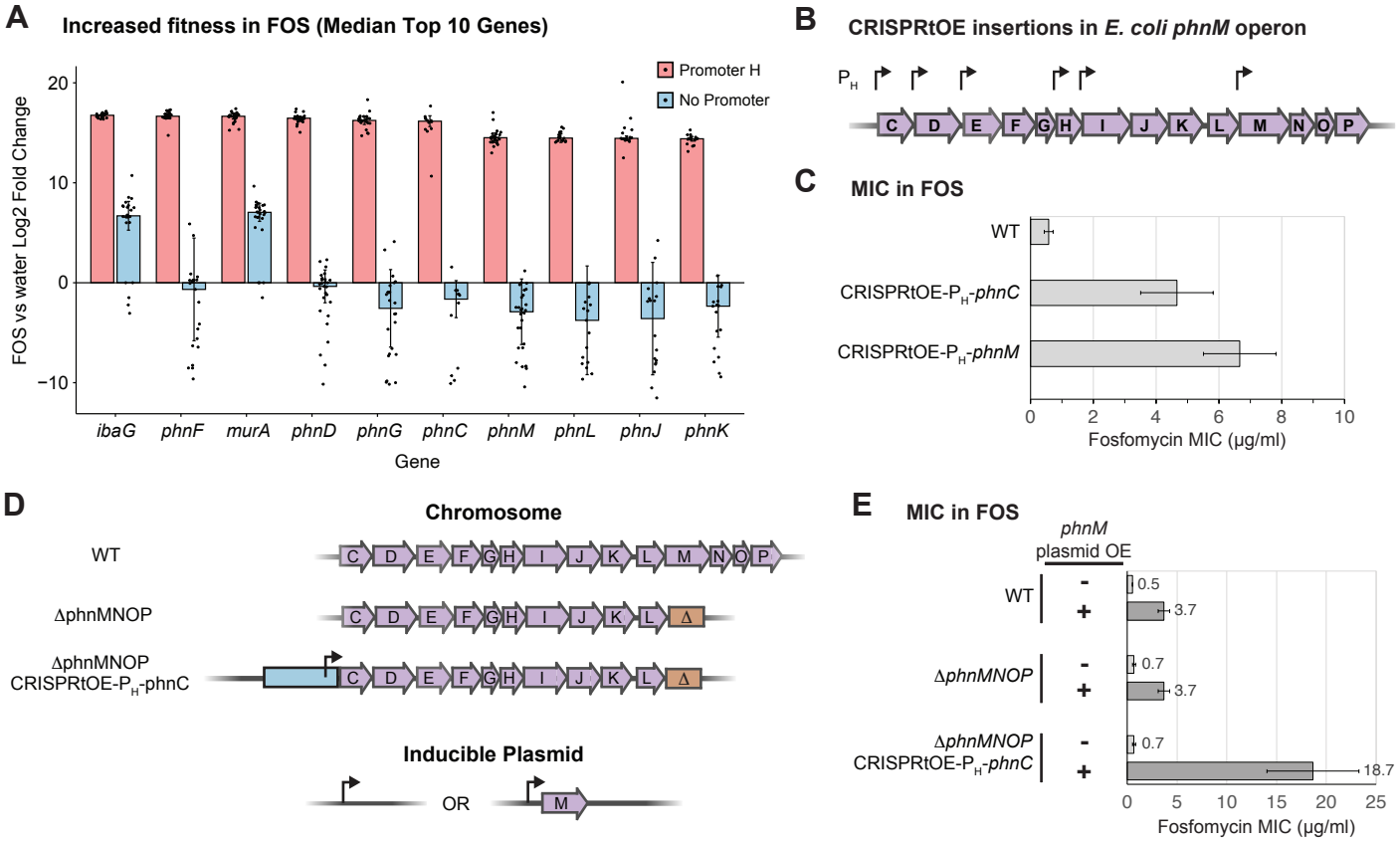
A
Increased fitness in FOS (Median Top 10 Genes)
Promoter H
No Promoter
FOS vs water Log2 Fold Change
20
10
0
−10
ibaG
phnF
murA
phnD
phnG
phnC
phnM
phnL
phnJ
phnK
Gene
B
CRISPRtOE insertions in E. coli phnM operon
P_H
C D E F G H I J K L M N O P
C
MIC in FOS
WT
CRISPRtOE-P_H-phnC
CRISPRtOE-P_H-phnM
0 2 4 6 8 10
Fosfomycin MIC (µg/ml)
D
Chromosome
WT
C D E F G H I J K L M N O P
ΔphnMNOP
C D E F G H I J K L Δ
ΔphnMNOP
CRISPRtOE-P_H-phnC
C D E F G H I J K L Δ
Inducible Plasmid
OR
M
E
MIC in FOS
phnM
plasmid OE
WT
-
+
0.5
3.7
ΔphnMNOP
-
+
0.7
3.7
ΔphnMNOP
CRISPRtOE-P_H-phnC
-
+
0.7
18.7
0 5 10 15 20 25
Fosfomycin MIC (µg/ml)

Figure 7

A ***Z. mobilis* Genome-scale CRISPRtOE-hydrolysate**

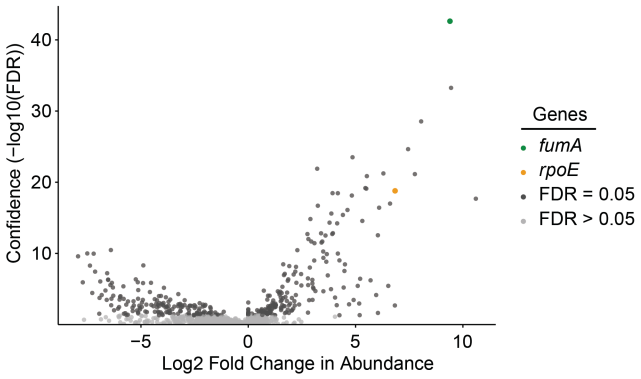

B **Increased fitness in hydrolysate (Median Top 10 Genes)**

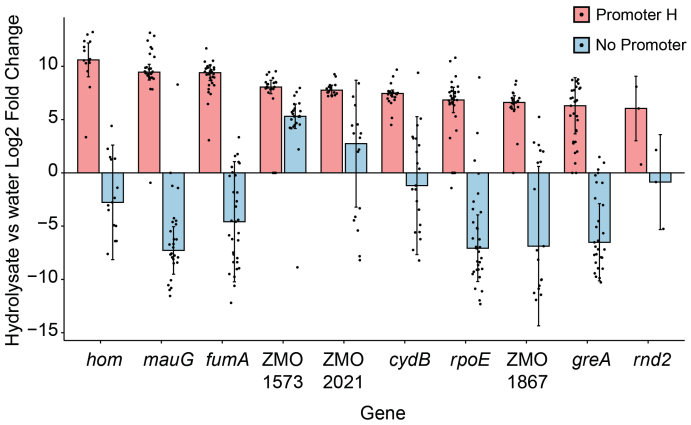

C **CRISPRtOE-*rpoE* Growth curve**

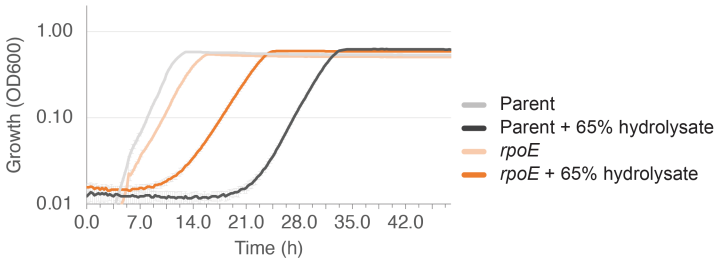

D **CRISPRtOE-*rpoE* Fitness**

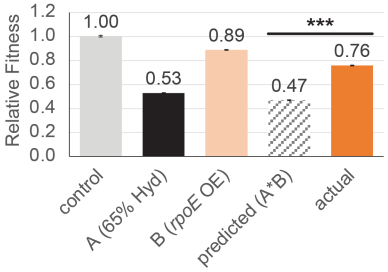

Figure S1

A CRISPRt plasmids

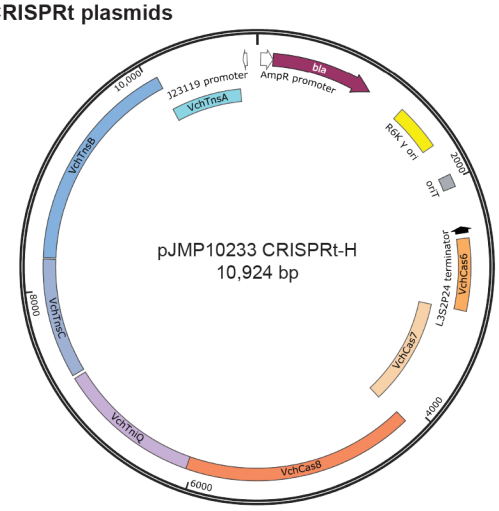

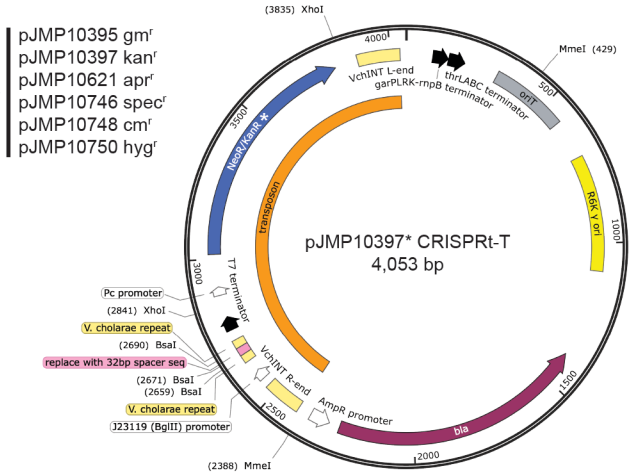

B CRISPRt guide RNA cloning site

C *E. coli* efficiency of transposition

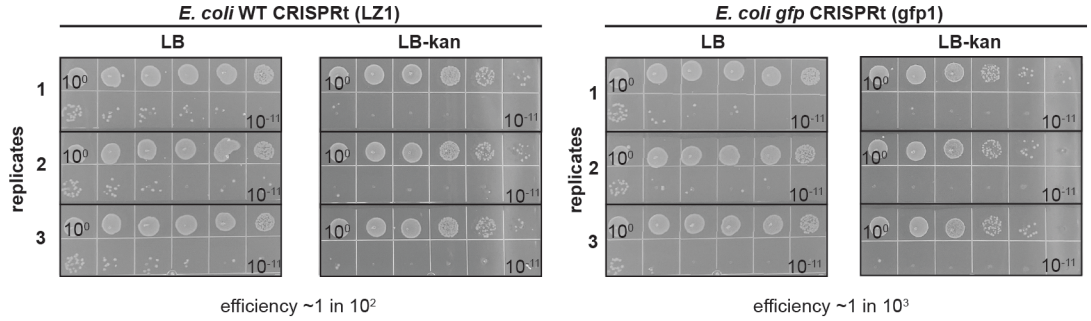

D *E. coli* chromosomal *gfp* reporter

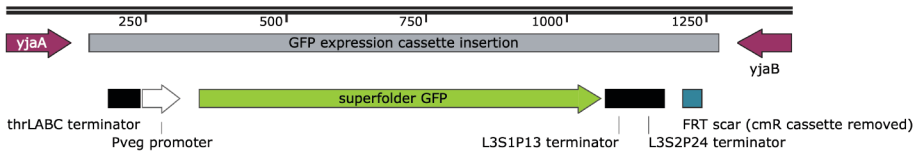

Figure S2

A CRISPRt insertions into *lacZ* (*LZ1* spacer)

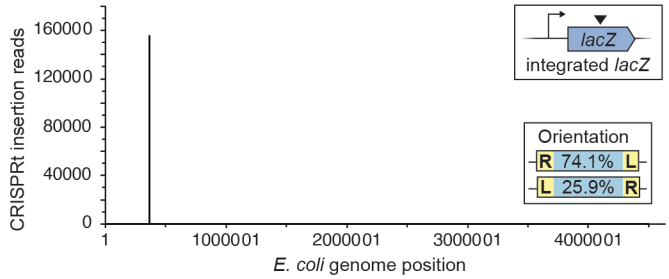

B *gfp1* insertion position (on target, RL orientation)

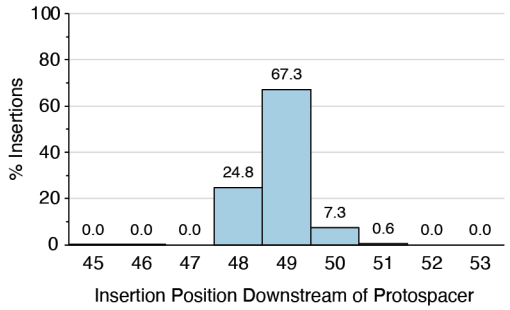

C *LZ1* insertion position (on target, RL orientation)

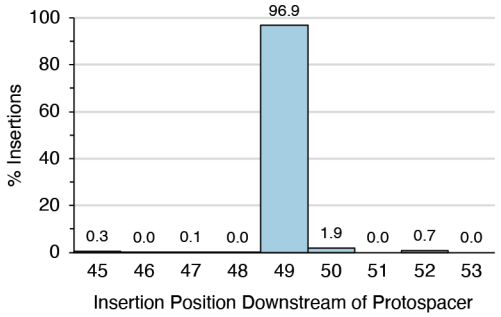

D *gfp* insertion phenotype

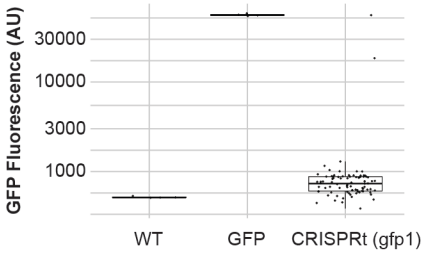

Strain	Parent Strain genotype	CRISPRt guide	Fluorescence phenotype
sJMP163	*E. coli* MG1655 WT	na	white
sJMP2688	*E. coli* MG1655 *gfp*	na	green
isolates	*E. coli* MG1655 *gfp*	gfp1	82/84 white (97.6%)

E *lacZ* insertion phenotype

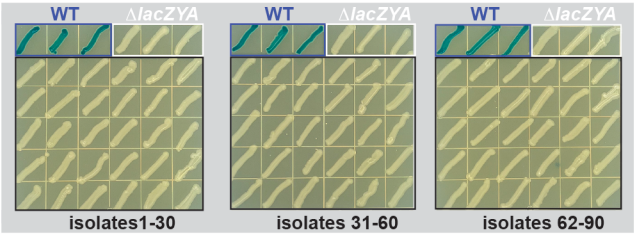

Strain	Parent Strain genotype	CRISPRt guide	X-gal phenotype
sJMP163	*E. coli* MG1655 WT	na	blue
sJMP3272	*E. coli* MG1655 DlacZYA	na	white
isolates	*E. coli* MG1655 WT	LZ1	90/90 white (100%)

F Frequency of insertion of entire transposon vs transposition only

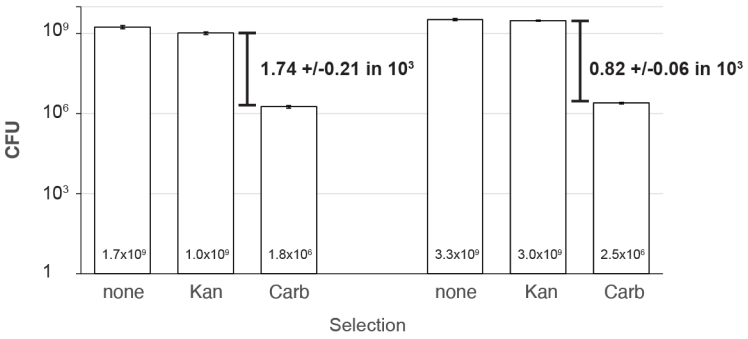

Figure S3

A CRISPRt *mScarlet-I* spacer library

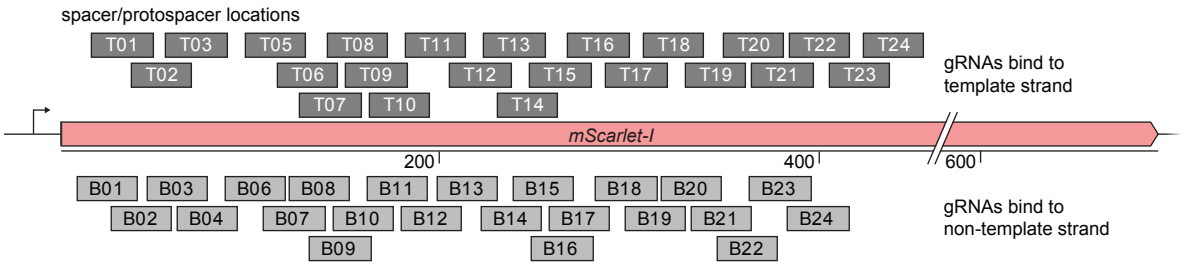

B CRISPRt *mScarlet-I* guide relative efficacy

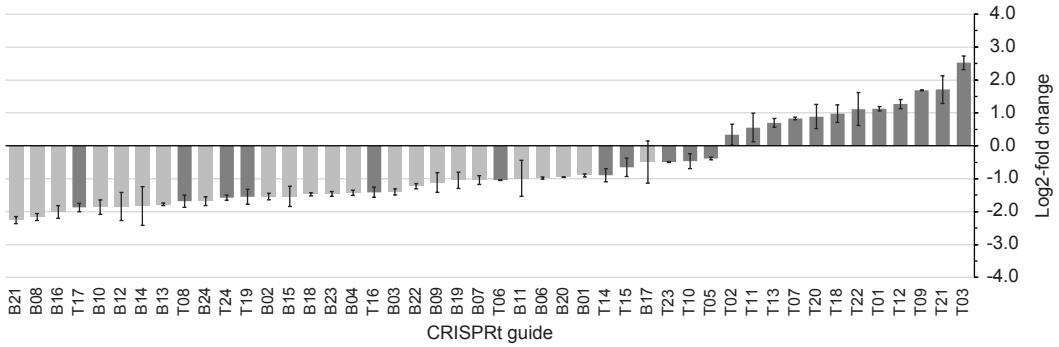

C CRISPRt guide efficacy by position

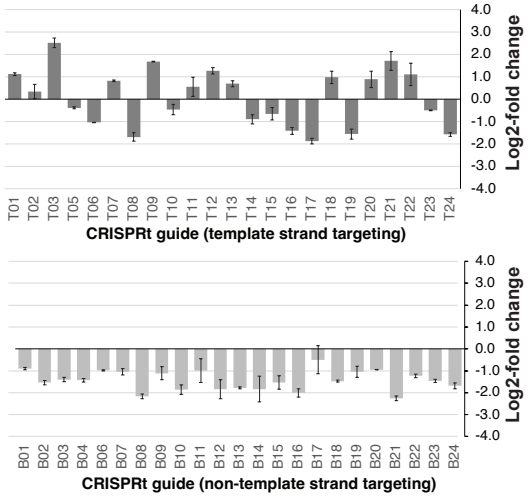

D Frequency of insertion vs. PAM

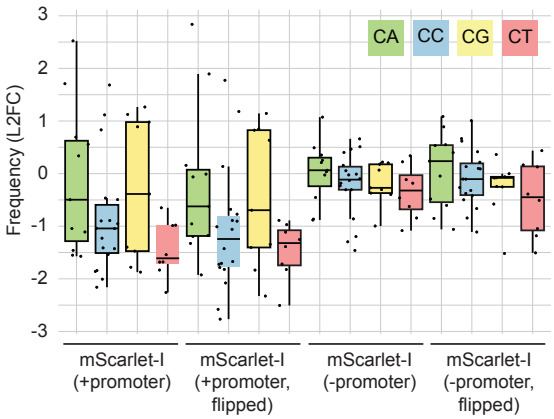

Figure S4

A

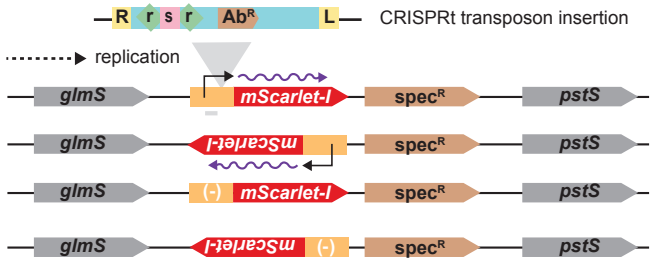

DNA strand	Promoter
leading	+
lagging	+
leading	-
lagging	-

B

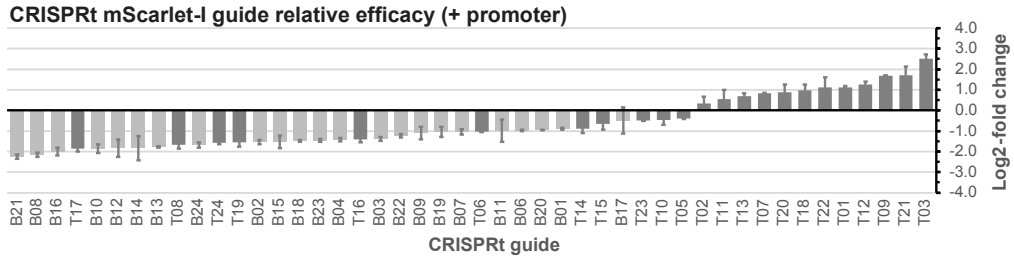

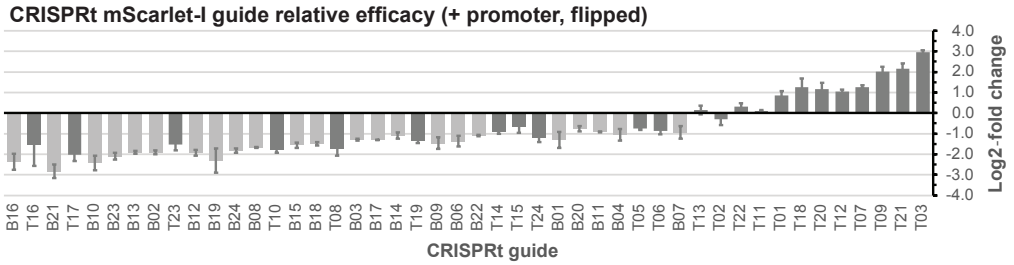

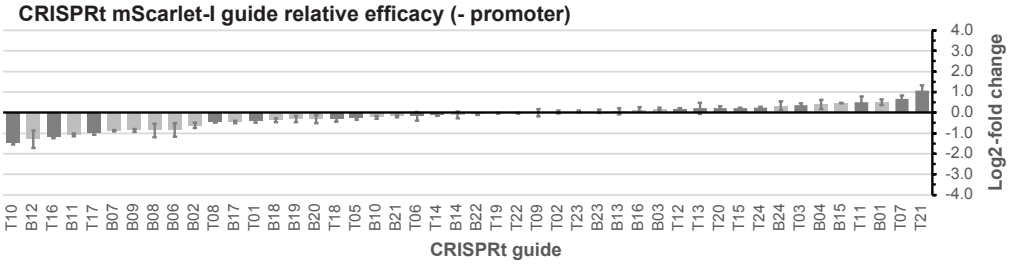

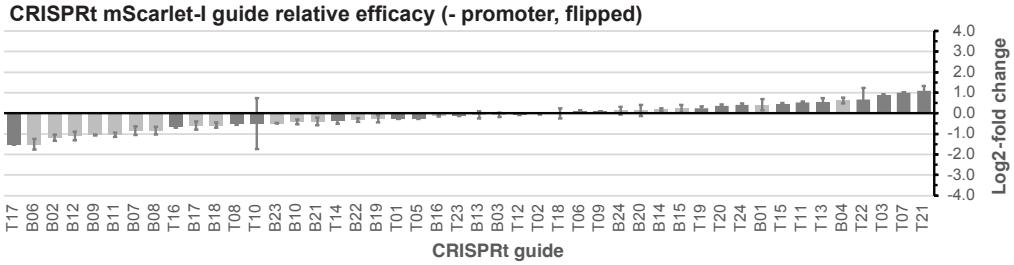

Figure S5

A

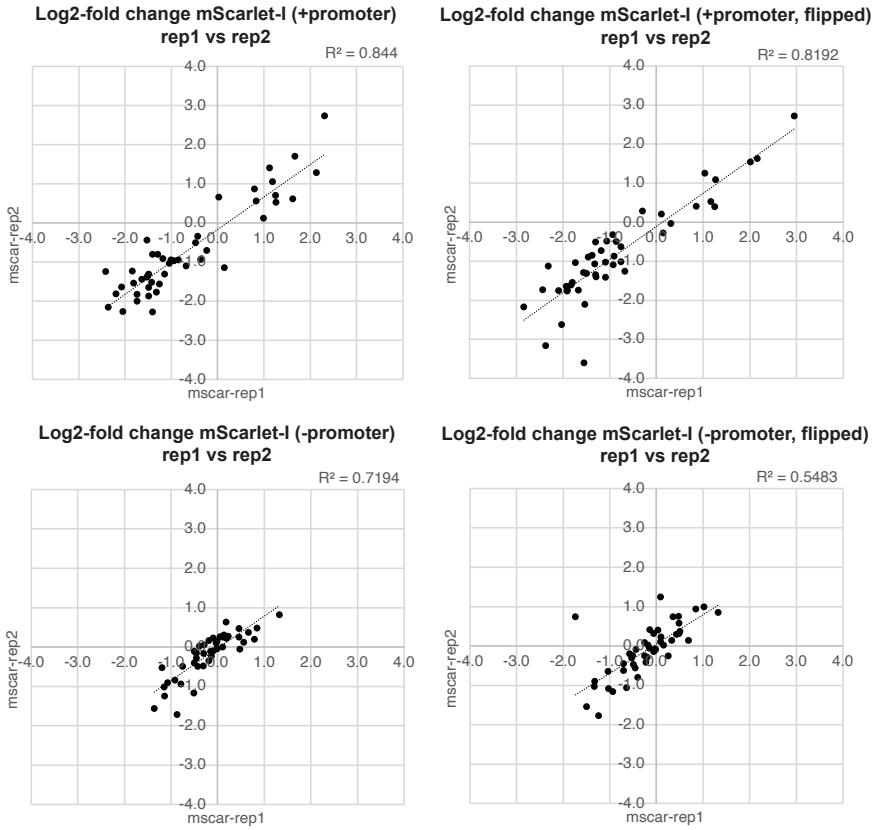
Log2-fold change mScarlet-I (+promoter) rep1 vs rep2
R² = 0.844
Log2-fold change mScarlet-I (+promoter, flipped) rep1 vs rep2
R² = 0.8192
Log2-fold change mScarlet-I (-promoter) rep1 vs rep2
R² = 0.7194
Log2-fold change mScarlet-I (-promoter, flipped) rep1 vs rep2
R² = 0.5483
mscar-rep1
mscar-rep2
4.0
3.0
2.0
1.0
0.0
-1.0
-2.0
-3.0
-4.0

B

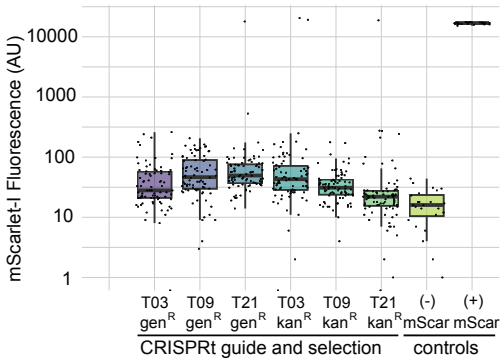
mScarlet-I Fluorescence (AU)
10000
1000
100
10
1
T03 genR
T09 genR
T21 genR
T03 kanR
T09 kanR
T21 kanR
(-) mScar
(+) mScar
CRISPRt guide and selection
controls

Figure S6

A CRISPRtOE Promoter Sequences

```
A   CTCACTCATTAGGCACCCCAGGCTTTACACTTTATGCTTCCGGCTCGTATAATGTCTAG
H   GGAAAATTTTTTTTCAAAAGTACTTGAAAATTAATCA•TCCGGCTCGTATAATTCTAGT
V   CACCAAGCCAGTTACCTCGGTTCTTTAATCTTTATGC•TCCGGCTCGTATAGTGCTAGC
    nnnnnnnnnnnnnnnnnnnnnnnTTGACAnnnnnnnn•nnnnnnnnnTATAATnnnnnn
                            -35        spacer        -10
```

B Transposons with outward facing promoters (or no promoter control)

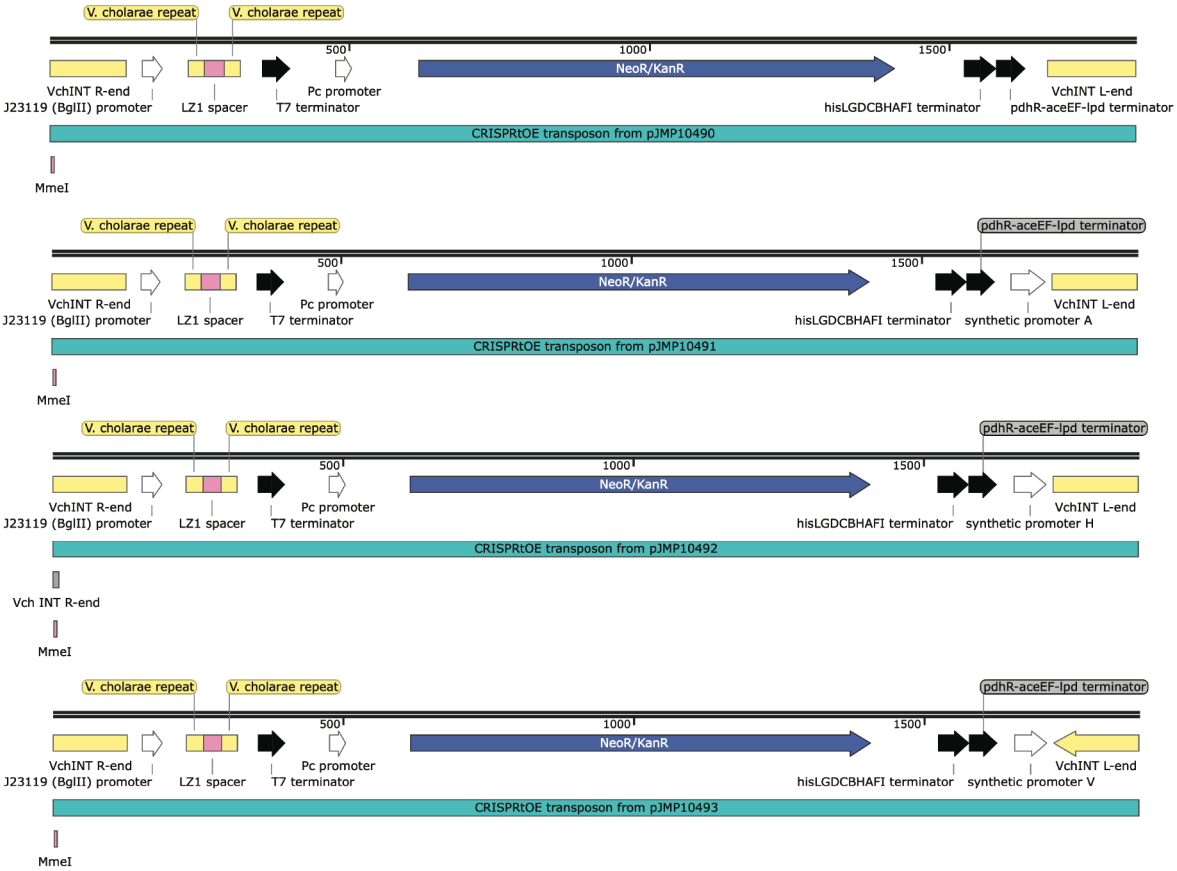

C Chromosomal promoterless mScarlet-I reporter

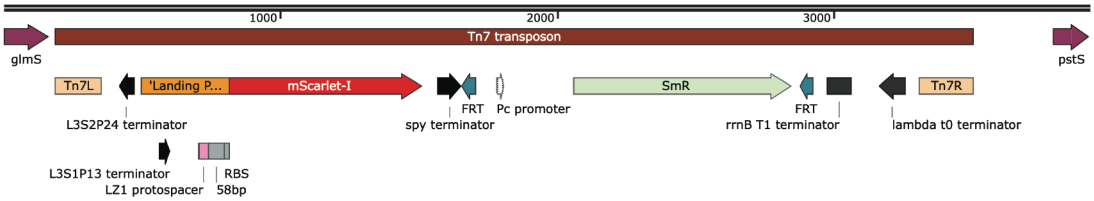

Figure S7

A *mScarlet-I* expression (qPCR)
CRISPRtOE-P_H vs LP/parent strain

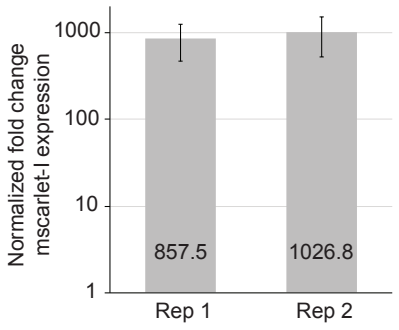

B *E. coli* CRISPRtOE mScarlet-I overexpression (all orientations)

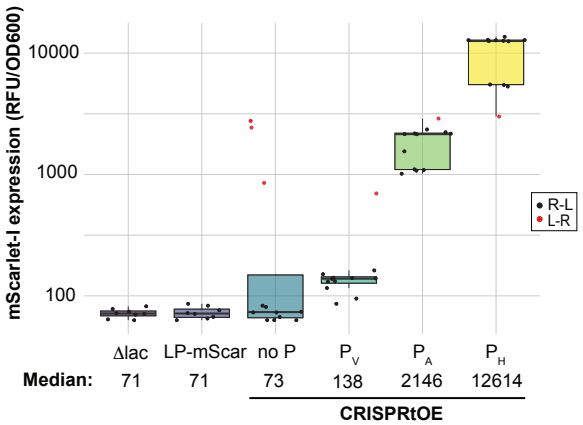

C *Z. mobilis* CRISPRtOE

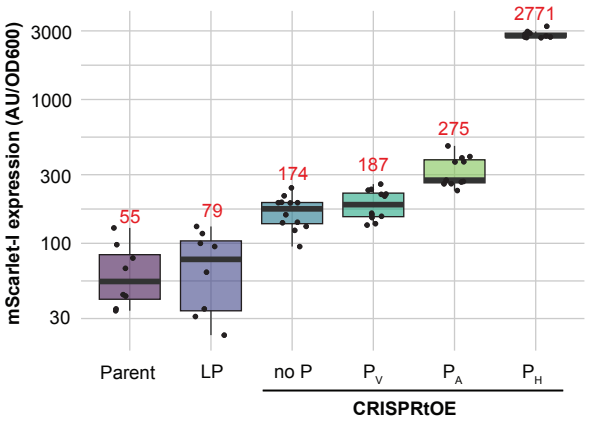

D

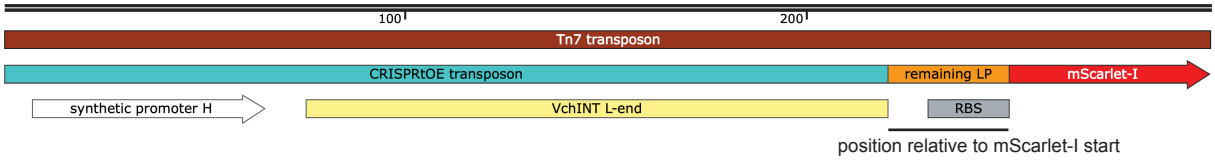

Position of CRISPRtOE transposon in Landing Pad relative to mScarlet-I start (LZ1 guide)

	# insertions analyzed	RL vs LR orientation		Position relative to ATG start (% of total RL insertions)									
	total RL and LR	%RL	%LR	-35	-34	-33	-32	-31	-30	-13	-2	+19	+108
Eco	48	87.5	12.5	21.4	2.4	71.4	0.0	0.0	4.8	0.0	0.0	0.0	0.0
Aba	12	100.0	0.0	0.0	0.0	66.7	0.0	0.0	0.0	8.3	8.3	8.3	8.3
Ecl	8	87.5	12.5	28.6	0.0	71.4	0.0	0.0	0.0	0.0	0.0	0.0	0.0
Kpn	10	90.0	10.0	22.2	0.0	77.8	0.0	0.0	0.0	0.0	0.0	0.0	0.0
Pae	12	91.7	8.3	36.4	0.0	63.6	0.0	0.0	0.0	0.0	0.0	0.0	0.0
Ppu	12	83.3	16.7	10.0	10.0	80.0	0.0	0.0	0.0	0.0	0.0	0.0	0.0
Son	11	100.0	0.0	36.4	9.1	45.5	0.0	0.0	9.1	0.0	0.0	0.0	0.0
Zmo	48	91.7	8.3	0.0	2.3	95.5	2.3	0.0	0.0	0.0	0.0	0.0	0.0

Figure S8

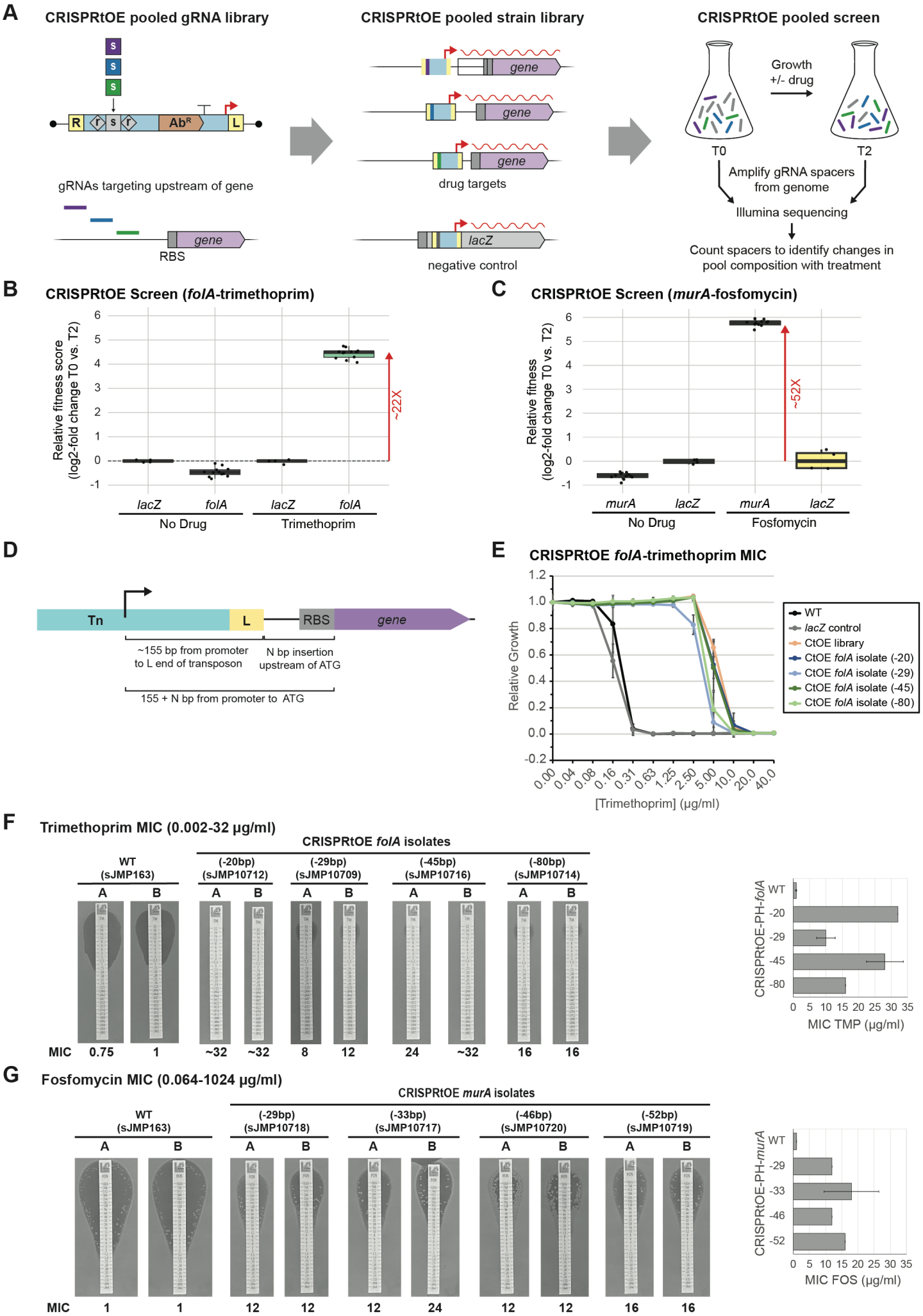
A
CRISPRtOE pooled gRNA library
CRISPRtOE pooled strain library
CRISPRtOE pooled screen
gRNAs targeting upstream of gene
RBS
drug targets
negative control
Growth
+/- drug
T0
T2
Amplify gRNA spacers from genome
Illumina sequencing
Count spacers to identify changes in pool composition with treatment
B
CRISPRtOE Screen (folA-trimethoprim)
Relative fitness score (log2-fold change T0 vs. T2)
~22X
No Drug
Trimethoprim
C
CRISPRtOE Screen (murA-fosfomycin)
Relative fitness (log2-fold change T0 vs. T2)
~52X
No Drug
Fosfomycin
D
Tn
L
RBS
gene
~155 bp from promoter to L end of transposon
N bp insertion upstream of ATG
155 + N bp from promoter to ATG
E
CRISPRtOE folA-trimethoprim MIC
Relative Growth
[Trimethoprim] (µg/ml)
WT
lacZ control
CtOE library
CtOE folA isolate (-20)
CtOE folA isolate (-29)
CtOE folA isolate (-45)
CtOE folA isolate (-80)
F
Trimethoprim MIC (0.002-32 µg/ml)
CRISPRtOE folA isolates
WT (sJMP163)
(-20bp) (sJMP10712)
(-29bp) (sJMP10709)
(-45bp) (sJMP10716)
(-80bp) (sJMP10714)
MIC 0.75 1 ~32 ~32 8 12 24 ~32 16 16
CRISPRtOE-PH-folA
MIC TMP (µg/ml)
G
Fosfomycin MIC (0.064-1024 µg/ml)
CRISPRtOE murA isolates
WT (sJMP163)
(-29bp) (sJMP10718)
(-33bp) (sJMP10717)
(-46bp) (sJMP10720)
(-52bp) (sJMP10719)
MIC 1 1 12 12 12 24 12 12 16 16
CRISPRtOE-PH-murA
MIC FOS (µg/ml)

Figure S9

A Multiplex strain construction

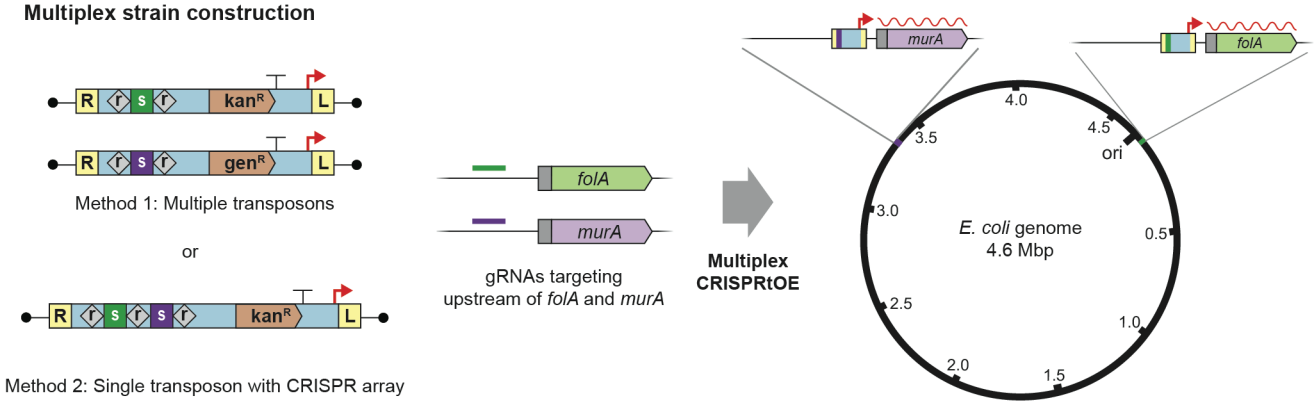

B Multiplex efficiency (*E. coli*)

Method	Transposon donor	crRNA	Conjugation	Selection	Insertion/genotype confirmed by PCR	Resistance phenotypes confirmed
1	Dual	1/donor	quad-parental	kan and gen	31/32 (97%)	4/4
2	Single	2/donor (array)	Tri-parental	kan	4/32 (12.5%)	4/4

C Trimethoprim MIC (0.002-32 µg/ml)

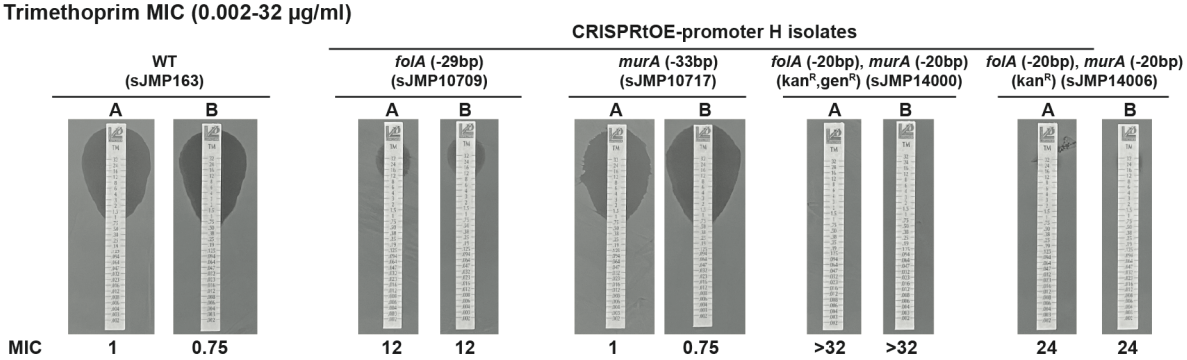

D Fosfomycin MIC (0.064-1024 µg/ml)

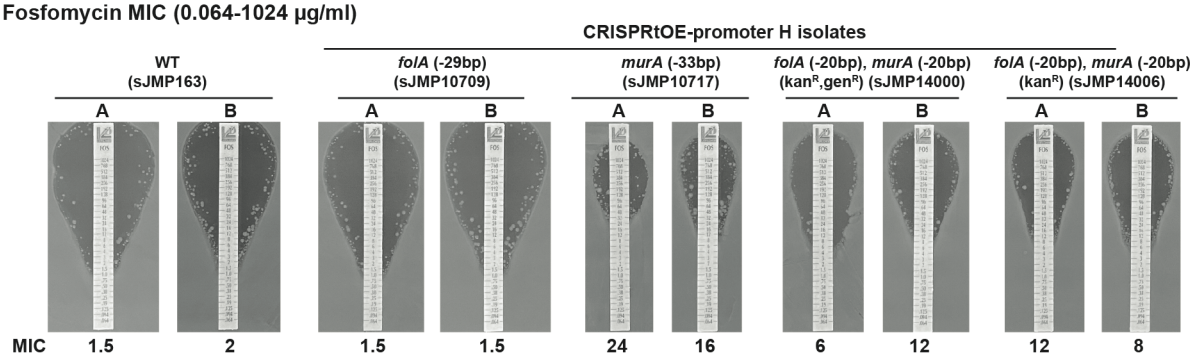

Figure S10

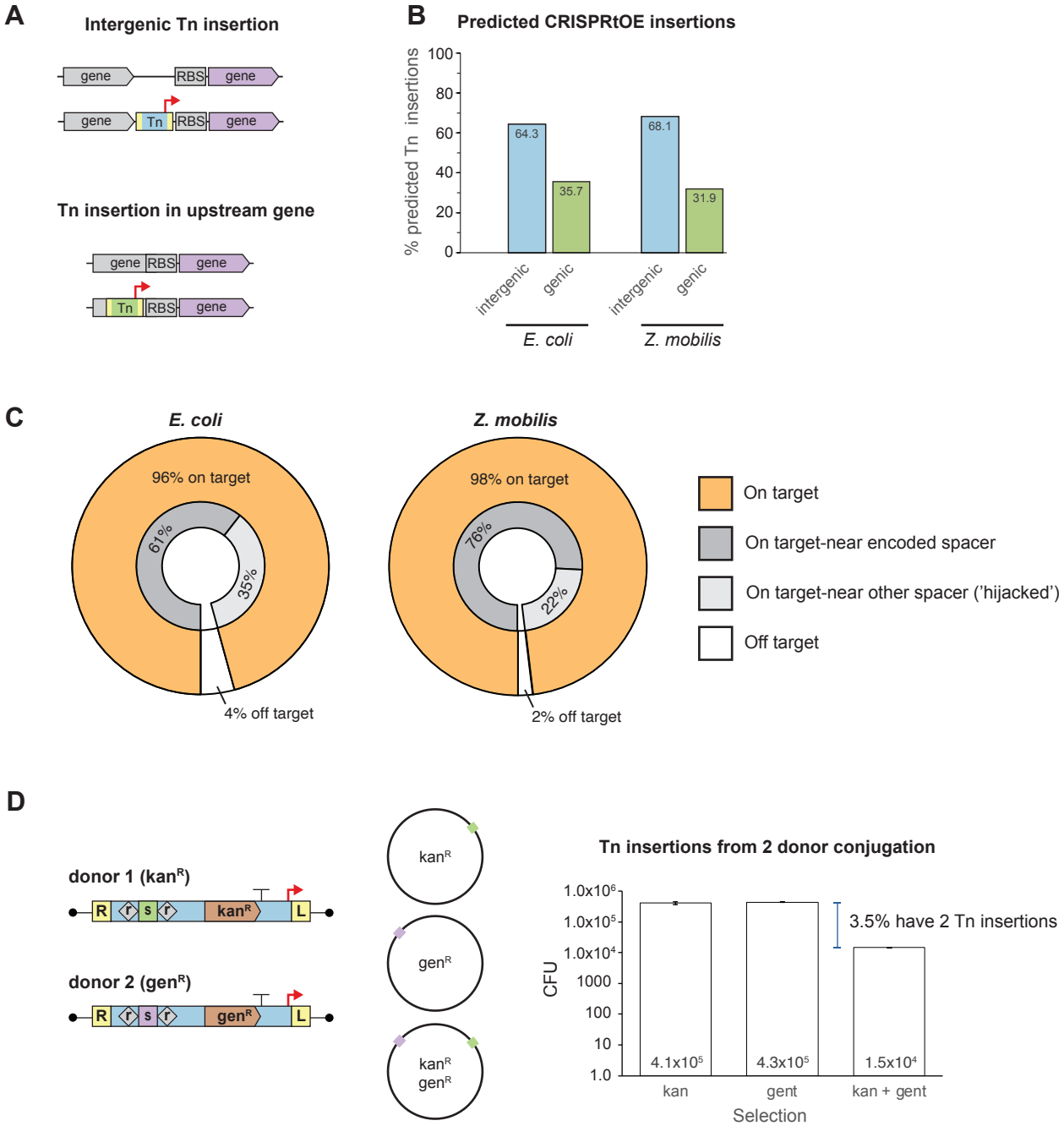
A
Intergenic Tn insertion
gene
RBS
gene
gene
Tn
RBS
gene
Tn insertion in upstream gene
gene
RBS
gene
Tn
RBS
gene
B
Predicted CRISPRtOE insertions
% predicted Tn insertions
100
80
60
40
20
0
64.3
35.7
68.1
31.9
intergenic
genic
intergenic
genic
E. coli
Z. mobilis
C
E. coli
96% on target
61%
35%
4% off target
Z. mobilis
98% on target
76%
22%
2% off target
On target
On target-near encoded spacer
On target-near other spacer ('hijacked')
Off target
D
donor 1 (kanR)
R
r
s
r
kanR
L
donor 2 (genR)
R
r
s
r
genR
L
kanR
genR
kanR
genR
Tn insertions from 2 donor conjugation
CFU
1.0x10^6
1.0x10^5
1.0x10^4
1000
100
10
1.0
4.1x10^5
4.3x10^5
1.5x10^4
3.5% have 2 Tn insertions
kan
gent
kan + gent
Selection

Figure S11

A Comparing Replicates With or Without Promoter H − Gene Medians

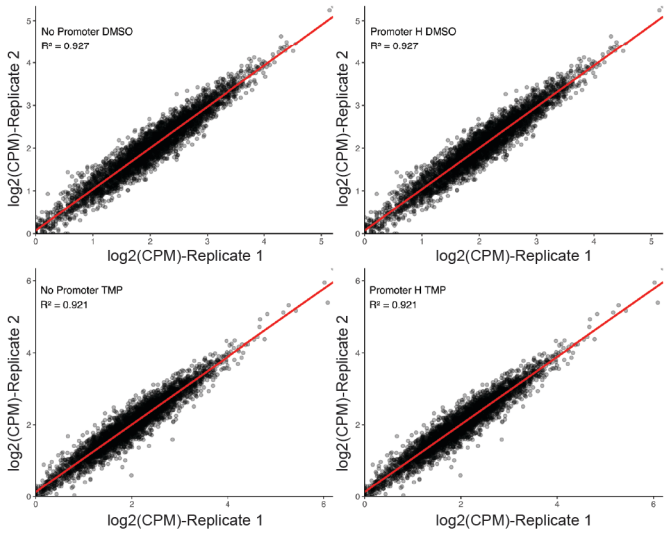

B Comparing TMP vs DMSO With or Without Promoter H − Gene Medians

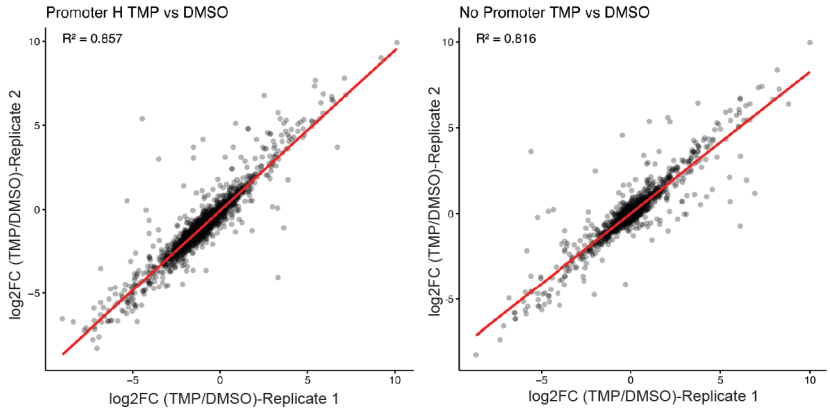

C Comparing LFC TMP vs DMSO Gene Medians for CRISPRtOE With and Without Promoter

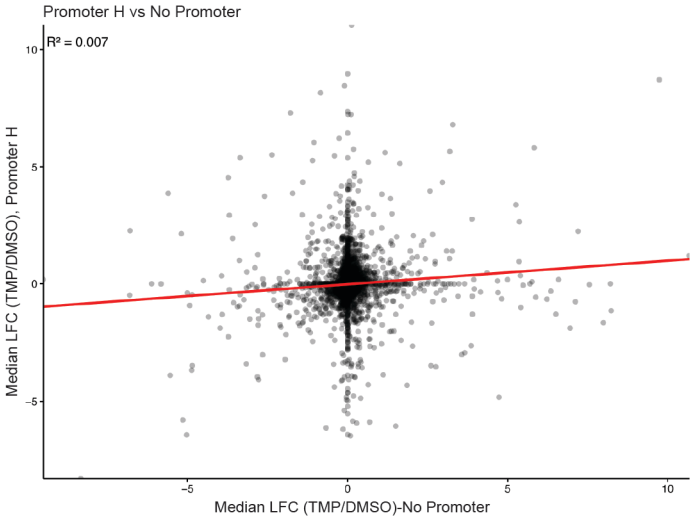

Figure S12

A

Log2 FC Gene Median TMP vs. DMSO treatment CRISPRtOE-Promoter H
Subset Number of Spacers vs All Spacers

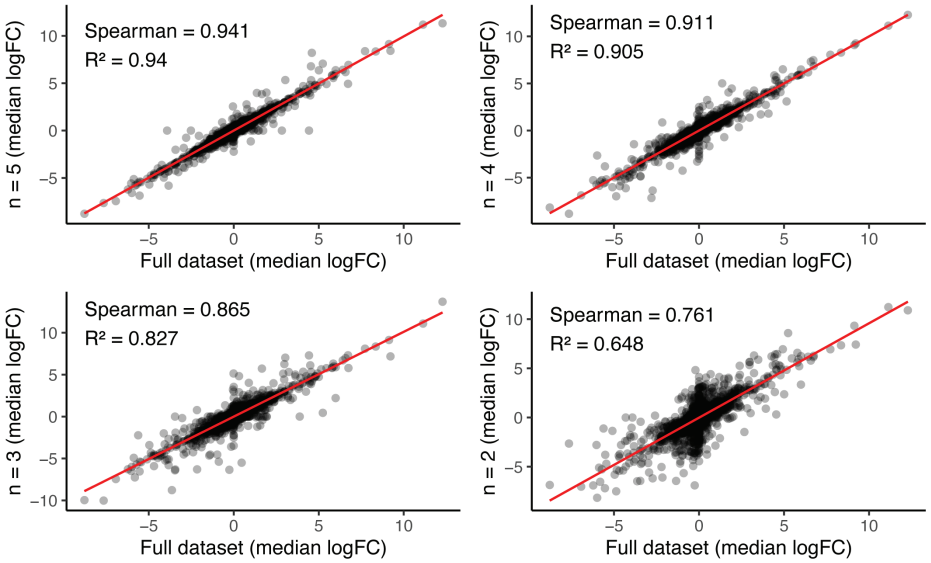

Figure S13

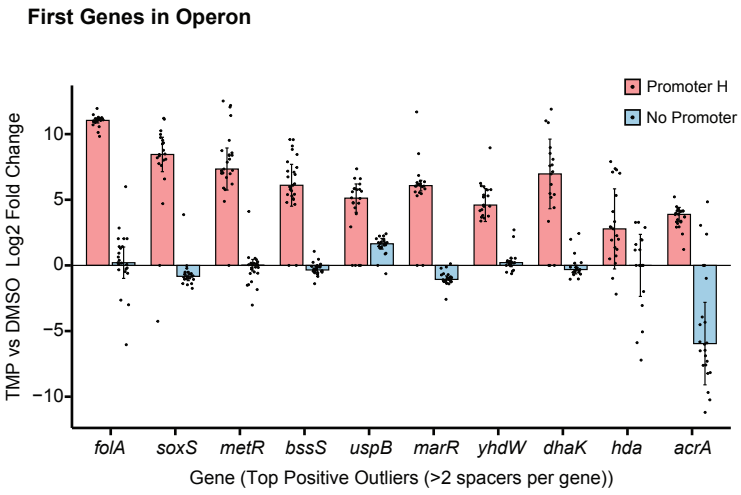
First Genes in Operon
Promoter H
No Promoter
TMP vs DMSO Log2 Fold Change
10
5
0
−5
−10
folA
soxS
metR
bssS
uspB
marR
yhdW
dhaK
hda
acrA
Gene (Top Positive Outliers (>2 spacers per gene))

Figure S14

A

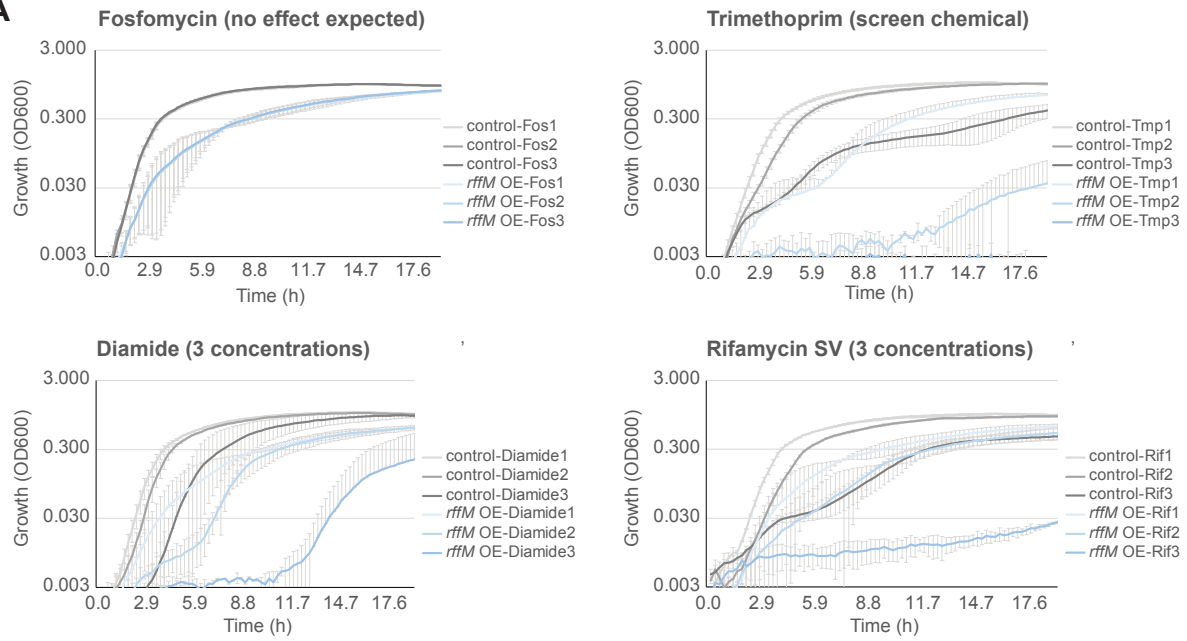

B

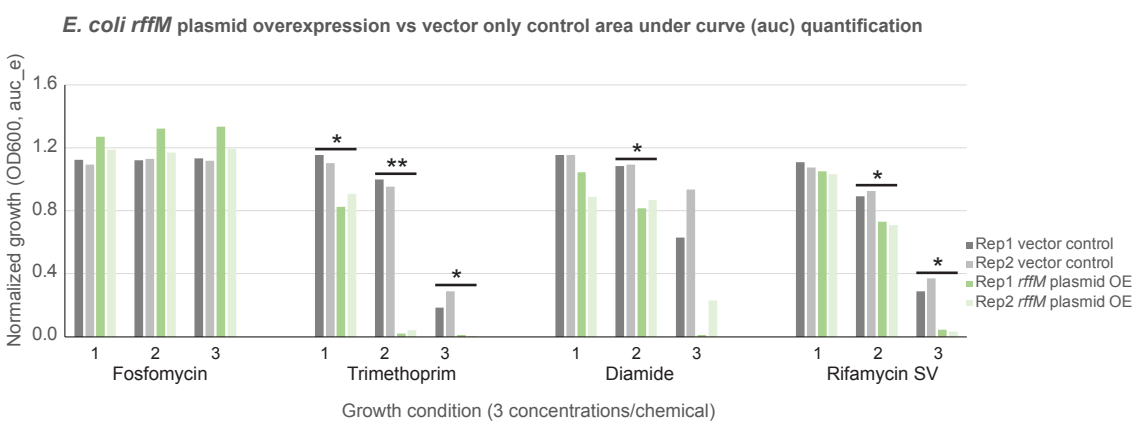

Figure S15

A *E. coli* Genome-scale CRISPRtOE Fosfomycin vs water

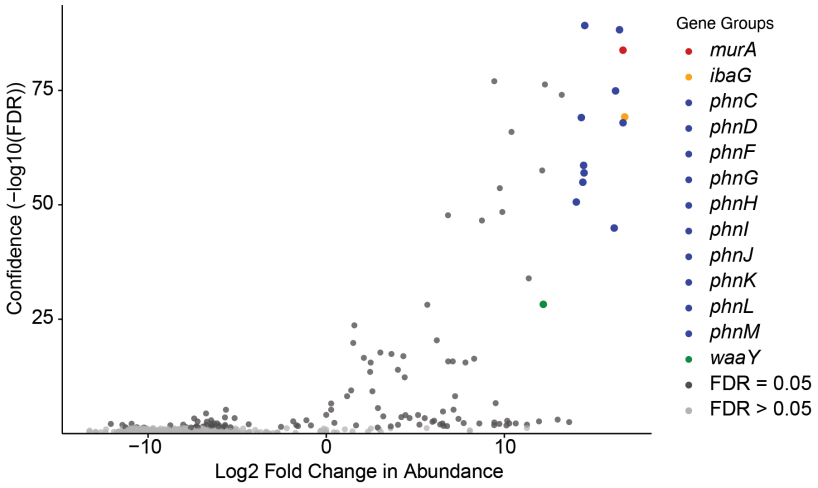

B CRISPRtOE

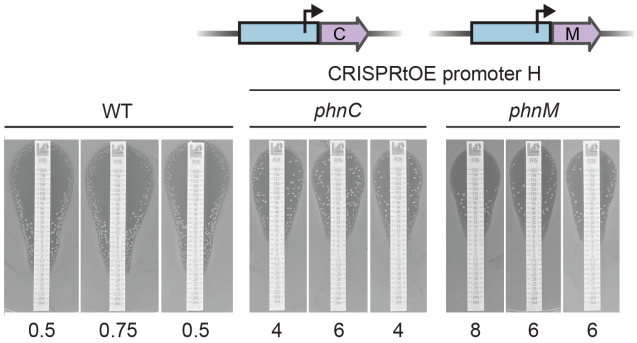

C *phnMNOP* Plasmid OE (100 μM IPTG induction)

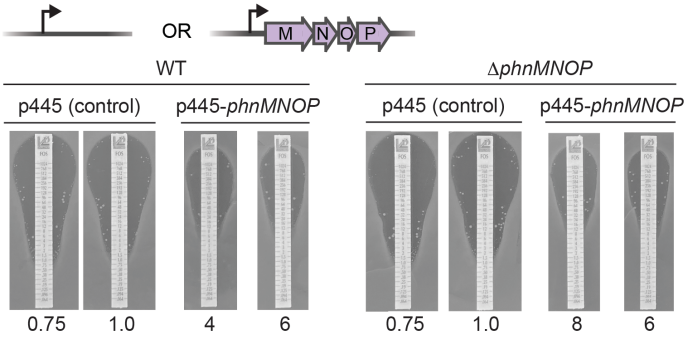

D *phnM* Plasmid OE (30 μM IPTG induction)

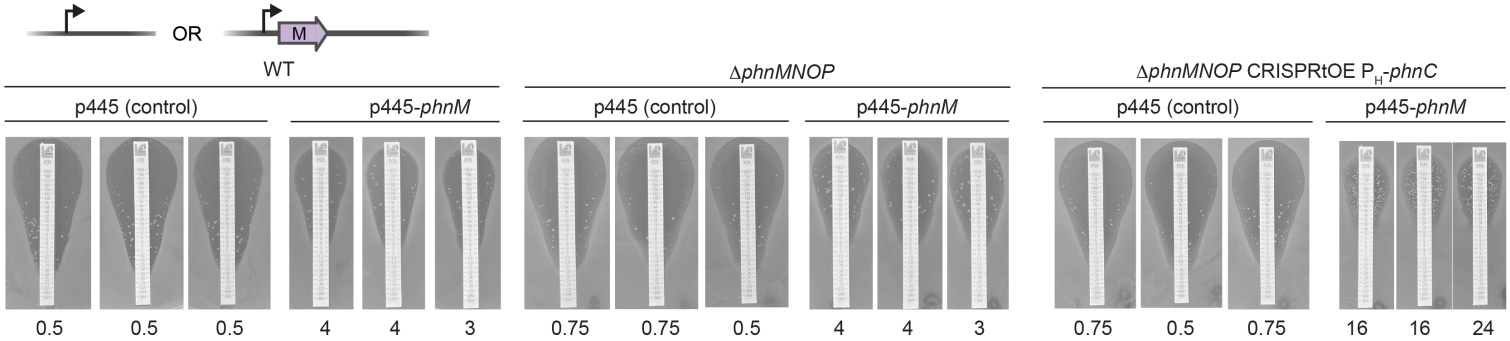

E *waaY* CRISPRtOE or Plasmid OE (100 μM IPTG induction)

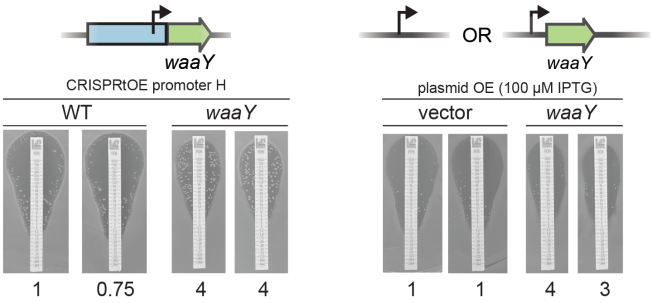

Figure S16

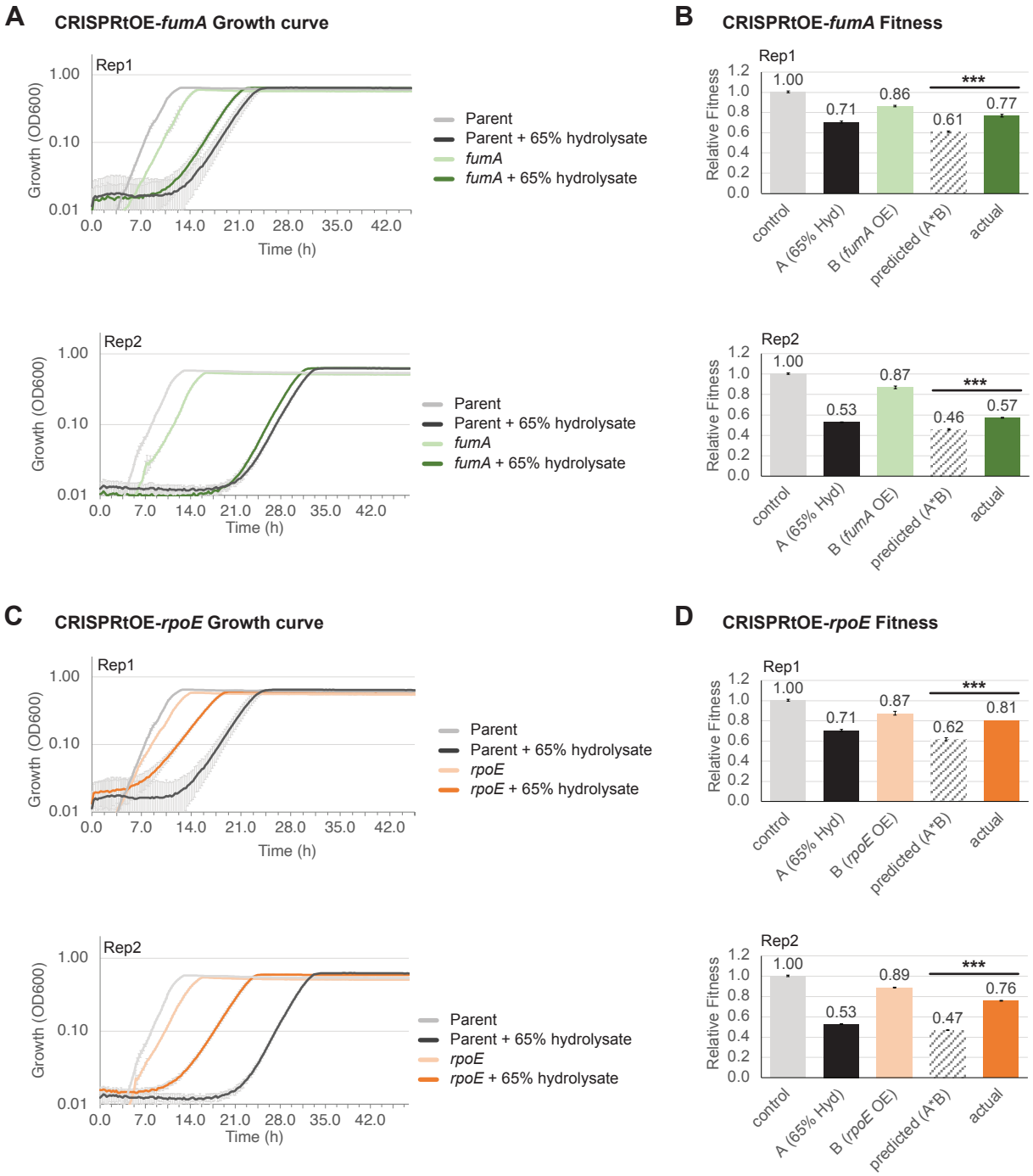
A
CRISPRtOE-fumA Growth curve
Rep1
Growth (OD600)
1.00
0.10
0.01
0.0 7.0 14.0 21.0 28.0 35.0 42.0
Time (h)
Parent
Parent + 65% hydrolysate
fumA
fumA + 65% hydrolysate
Rep2
B
CRISPRtOE-fumA Fitness
Relative Fitness
1.2 1.0 0.8 0.6 0.4 0.2 0.0
1.00
0.71
0.86
0.61
0.77
***
0.53
0.87
0.46
0.57
control
A (65% Hyd)
B (fumA OE)
predicted (A*B)
actual
C
CRISPRtOE-rpoE Growth curve
rpoE
rpoE + 65% hydrolysate
D
CRISPRtOE-rpoE Fitness
0.87
0.62
0.81
0.89
0.47
0.76
B (rpoE OE)

Figure S17

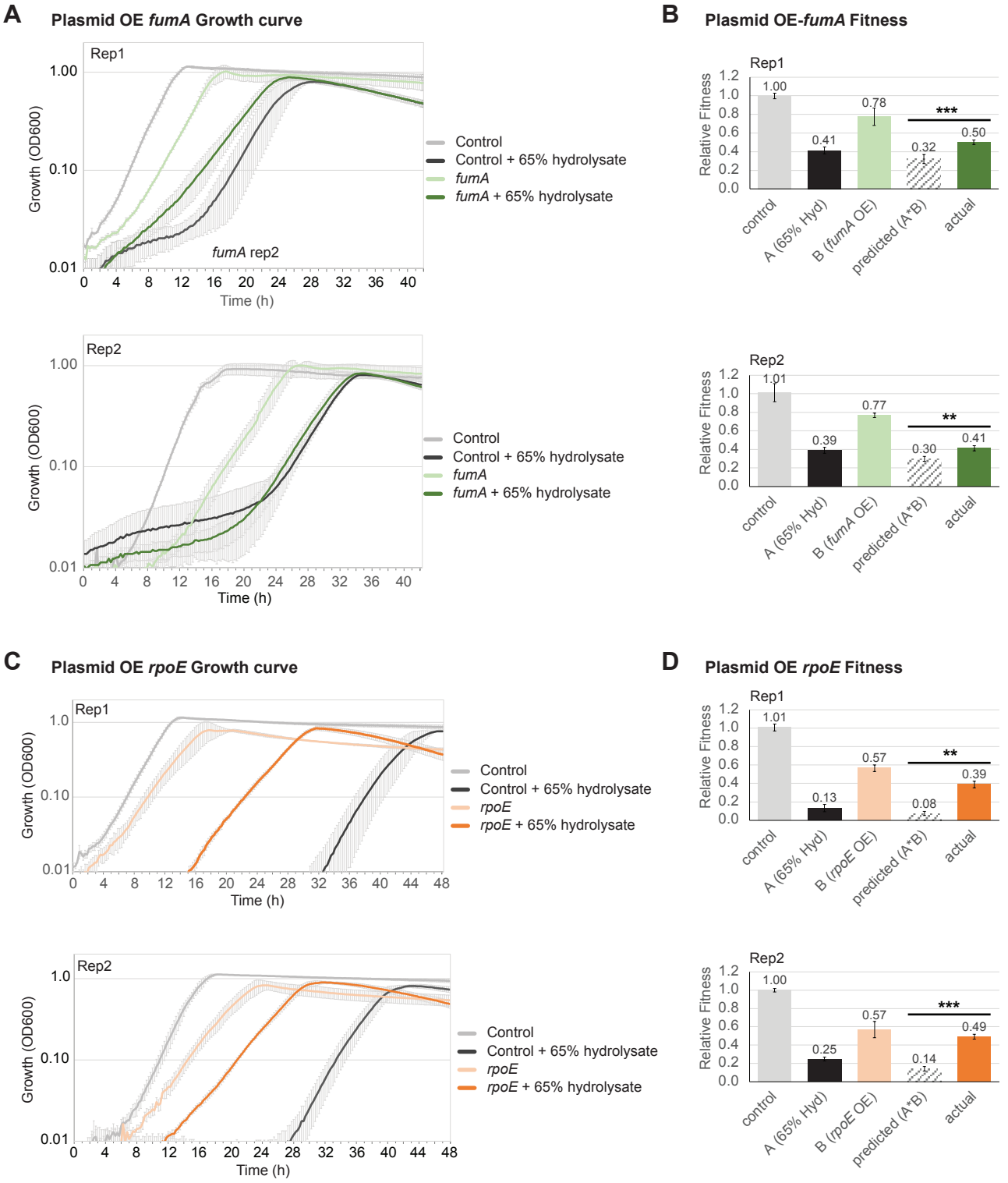
A
Plasmid OE fumA Growth curve
Rep1
Growth (OD600)
Time (h)
fumA rep2
Control
Control + 65% hydrolysate
fumA
fumA + 65% hydrolysate
Rep2
B
Plasmid OE-fumA Fitness
Relative Fitness
control
A (65% Hyd)
B (fumA OE)
predicted (A*B)
actual
C
Plasmid OE rpoE Growth curve
rpoE
rpoE + 65% hydrolysate
D
Plasmid OE rpoE Fitness
B (rpoE OE)